Chemical Exchange Processes in Lanthanide(III), Dioxouranium(VI) and Sodium(I) Complexes

Alex White B.Sc.(Hons.)

This thesis is presented for the degree of Doctor of Philosophy

Department of Physical and Inorganic Chemistry
University of Adelaide

March, 1987

Contents

Summary

Substituted urea complexes of several lanthanide(III) ions and dioxouranium(III) have been prepared and their ligand exchange properties studied in solution using variable temperature ^{1}H NMR and complete lineshape analysis.

Tetramethylurea complexes of Pr(III) and Tb(III) – Yb(III) are found to show a coordination number of six. Where possible, several solutions of different concentrations were studied to determine the mechanism of intermolecular ligand exchange. For example, in $[Tm(tmu)_6](ClO_4)_3$ the rate of intermolecular ligand exchange is found to be independent of [tmu] over a five-fold concentration variation and the mechanism is deduced to be dissociative. The exchange is characterised by the following activation parameters: $k(298.2K) = 145 \pm 1\ s^{-1}$, $\Delta H^{\ddagger} = 29.3 \pm 0.3$ kJ mol^{-1} and $\Delta S^{\ddagger} = -105 \pm 1$ J K^{-1} mol^{-1}. These data are discussed in conjunction with data from related lanthanide, scandium and yttrium systems and the kinetic and mechanistic implications are considered.

Dioxouranium(VI) complexes of 1,1-dimethylurea, 1,3-dimethylurea and 1,1,3-trimethylurea have been studied to assess the effect of the degree of substitution of the urea on the rates of intra- and, where possible, inter-molecular exchange. For example, the kinetic parameters characterising the rotation about the C–NMe_2 and C–NH_2 bonds of 1,1-dimethylurea in $[UO_2(1,1\text{-dmu})_5](ClO_4)_2$ in CD_3CN solution were determined as: $k(265K) = 39.1 \pm 0.4$ and $2960 \pm 60\ s^{-1}$, $\Delta H^{\ddagger} = 49.1 \pm 0.8$ and 61.1 ± 0.5 kJ mol^{-1} and $\Delta S^{\ddagger} = -28.3 \pm 2.7$ and 53.1 ± 2.2 J K^{-1} mol^{-1} respectively. The mechanistic and kinetic data for these complexes are compared with each other and with similar complexes. The isokinetic relationship for dioxouranium(VI) complexes is also discussed.

In the second part of this work, ^{23}Na NMR has been used to study Na^+ exchange on the crown ether complex $Na.18C6^+$ in acetone, methanol and pyridine. The respective decomplexation rate constants thus obtained are $k_d(265K) = 60600 \pm 8800$, 4200 ± 200 and $716 \pm 30\ s^{-1}$. The corresponding activation parameters are $\Delta H^{\ddagger} = 36.7 \pm 0.7$, 53.6 ± 0.8 and 50.5 ± 1.2 kJ mol^{-1} and $\Delta S^{\ddagger} = -14.0 \pm 3.2$, 27.8 ± 2.9 and 1.4 ± 4.2 J K^{-1} mol^{-1}. These data are discussed in conjunction with data from

other NMR and ultrasonic relaxation studies for other host-guest complexes and mechanistic aspects of the complexation of Na^+ by 18C6 are considered in the light of ion, ligand and solvent characteristics.

Statement

This thesis contains no material which has been submitted for any other degree or diploma in any University and to the best of my knowledge and belief, contains no material previously published or written by another person, except where due reference is made in the text of the thesis.

The author consents to the thesis being made available for photocopying and loan if applicable if accepted for the award of the degree.

Alex White

Acknowledgements

I wish to thank my supervisor, Dr. S.F.Lincoln for his help, guidance and encouragement throughout the period of this project. I would like to thank Prof. M.I.Bruce, Dr. T.Kurucsev and Dr. J.H.Coates for making available the facilities of the department, Dr. E.H.Williams for instruction on the operation of the spectrometers and Mrs. A.M.Hounslow for useful discussions and help. I wish to acknowledge the invaluable help and friendship afforded me by associates and other research students within the department.

I also wish to acknowledge the receipt of a Commonwealth Postgraduate Research Award for financial support.

Finally, I wish to express my gratitude to my family and Miss A.Mifsud for their support, understanding and encouragement.

Abbreviations

The following abbreviations have been used in this thesis :

12C4	12-crown-4 (1,4,7,10-tetraoxacyclododecane)
15C5	15-crown-5 (1,4,7,10,13-pentaoxacyclopentadecane)
18C6	18-crown-6 (1,4,7,10,13,16-hexaoxacyclooctadecane)
B*3n*C*n*	benzo-*3n*-crown-*n* (e.g. B12C4 = benzo-12-crown-4)
C*3n*C*n*	cyclohexyl-*3n*-crown-*n* (e.g. C12C4 = cyclohexyl-12-crown-4)
DA*3n*C*n*	diazo-*3n*-crown-*n* (e.g. DA12C4 = diazo-12-crown-4)
DB*3n*C*n*	dibenzo-*3n*-crown-*n* (e.g. DB12C4 = dibenzo-12-crown-4)
DC*3n*C*n*	dicyclohexyl-*3n*-crown-*n* (e.g. DC12C4 = dicyclohexyl-12-crown-4)
dea	N,N-diethylacetamide
def	N,N-diethylformamide
dma	N,N-dimethylacetamide
dmf	N,N-dimethylformamide
dmmp	dimethylmethylphosphonate
dmso	dimethylsulphoxide
1,1-dmu	1,1-dimethylurea
1,3-dmu	1,3-dimethylurea
fpr	N-formylpyrrolidine
hmpa	hexamethylphosphoramide
nipa	nonamethylimidophosphoramide
nma	N-methylacetamide
nmf	N-methylformamide
pc	propylene carbonate
thf	tetrahydrofuran
tmp	trimethylphosphate
t.m.s.	tetramethylsilane
tmu	1,1,3,3-tetramethylurea
trmu	1,1,3-trimethylurea
C.W.	continuous wave

CD_3CN	the D represents deuterium (^2H)
d^n-	n-deuterated-
F.I.D.	free induction decay
F.T.	Fourier transform
Hz	Hertz
[L]	concentration of L
$[L]_{free}$	concentration of free ligand L in solution
nmr	nuclear magnetic resonance
ppm	parts per million
r.f.	radio frequency

Chapter 1

Introduction

1.1 The Solvated Cation

In aqueous solution, a metal ion is situated at the centre of a sphere of water molecules [1] in which the oxygen donor atoms are orientated towards the metal ion (Region A, Figure 1.1). This is termed the first, primary or inner coordination sphere and has been defined by Lincoln [2] in two ways:

time independent: The molecules of the first coordination sphere are those within "contact" or "bonding" distance of the metal ion and such that no other molecules are interposed between them.

time dependent: The molecules of the first coordination sphere are those that have a long residence time in the immediate vicinity of the metal ion compared to its correlation time outside of the first coordination sphere.

The second definition is useful as it implies the dynamic nature of the first coordination sphere but may be of little use for the more labile cations such as Cs^+, Rb^+, K^+ and Ba^{2+} because of the short residence time in these cases. These definitions affect the way in which the coordination number is defined and determined. There exist both time independent (such as X-ray diffraction) and time dependent (such as nmr resonance area integration) methods for determining the coordination number [2].

At a significant distance from the aquated ion, its influence on the water molecules is negligible because the electrostatic field due to the charge on the ion is

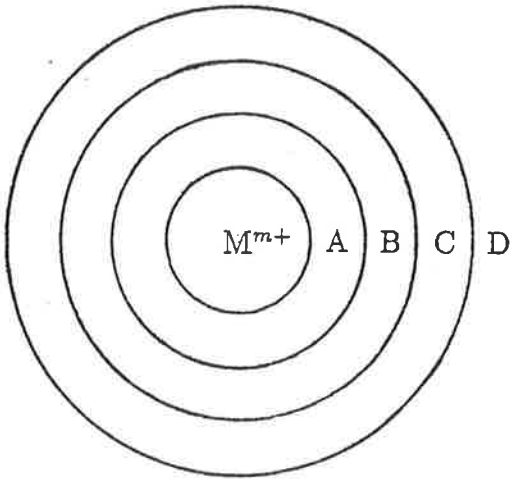

Figure 1.1: Model of a Solvated Metal Cation

virtually zero (in dilute solution). In this region, the normal structure of "bulk" water prevails (Region D, Figure 1.1). In the volume between the first coordination sphere and bulk water there are competing orientational effects on the water molecules from the ionic charge and the bulk water network dipole-dipole forces. Thus the water in this region adopts a compromise structure that is neither completely orientated or disorientated ("region of structure breaking"). This region may be arbitrarily divided into two regions, B and C in Figure 1.1. Region B is the second or outer coordination sphere in which the water molecules are still substantially orientated directly by the ion and indirectly by the dipole-dipole interaction with the orientated water molecules of the first coordination sphere. The water molecules in Region C are randomly orientated due to the competing orientational forces from Regions A and B and from Region D discussed above. The first coordination sphere is well-defined while the boundaries between the other regions are not distinct [3].

In non-aqueous solvents, such as acetonitrile, in which the bulk solvent is less structured than water, Regions B and C become less distinct from the bulk solvent. Regions A and B still experience the orientational effects of the field due to the ionic charge. Now Region B is primarily one of structure enhancement over the

bulk solvent due to the ion-dipole forces rather than a region of structure breaking due to competing orientational forces. Region C is now less important for similar reasons.

In a mixture of solvents, there is competition for the sites in the primary coordination sphere. A solvent of higher coordinating ability is expected to occupy the sites to a greater extent than one of lower coordinating ability and may be the only type of ligand present in the first coordination sphere. This situation is expected to prevail in the ligand exchange studies which follow in which a strongly coordinating ligand (such as 1,1,3,3-tetramethylurea) is present in a solvent of low coordinating ability (such as d^3-acetonitrile). The proportions of the ligands of different coordinating ability in the other regions around the ion will depend on various factors, such as relative coordinating ability and concentrations.

1.2 Mechanisms of Solvent and Ligand Exchange

Langford and Gray [4] have proposed a system of mechanistic classification for ligand substitution reactions:

$$[ML_n]^{m+} + L^* \rightleftharpoons [ML_{n-1}L^*]^{m+} + L \tag{1.1}$$

where M is a metal ion and L and L* are any two monodentate ligands. If the activation energy of the reaction is primarily determined by the dissociation of the ligand (M–L bond breaking) then the activation mode is said to be dissociative (**d**). If the activation mode is primarily determined by the assistance of the entering group then the activation mode is associative (**a**). The ligand *exchange* reaction is a special case of ligand substitution reactions where L = L* and there is no net chemical change. The mechanisms proposed for this reaction are as follows:

*Dissociative (**D**) Mechanism for Ligand Exchange Reactions*

A leaving ligand is lost in the first, rate determining, step to produce an intermediate of reduced coordination number:

$$[ML_n]^{m+} \overset{k_1}{\rightleftharpoons} [ML_{n-1}]^{m+} + L$$
$$\underset{-L}{\overset{+L^*}{\rightleftharpoons}} [ML_{n-1}L^*]^{m+} \quad (1.2)$$

Using the steady state approximation, the rate law for this reaction may be derived and the rate of exchange is found to be independent of the concentration of free ligand:

$$\text{exchange rate} = nk_{ex}[[ML_n]^{m+}] \quad (1.3)$$

where the observed rate constant $k_{ex} = k_1$ (see Equation 6.26) and n is the coordination number of the metal ion M^{m+}. In general, the lifetime of a ligand in the coordinated state, τ_c, is related to the observed first order rate constant k_{ex} by:

$$\tau_c = \frac{\tau_f \chi_c}{\chi_f} = \frac{1}{k_{ex}} = \frac{n[[ML_n]^{m+}]}{\text{exchange rate}} \quad (1.4)$$

where τ_f is the lifetime of a ligand in the free state, χ_f and χ_c are the mole fractions of free and coordinated ligand respectively. For this mechanism, the activation mode is necessarily **d** as M–L bond breaking is the rate determining step and is responsible for the major contribution to the activation energy.

*Associative (**A**) Mechanism for Ligand Exchange Reactions*

An entering ligand is gained in the first, rate determining, step to form an intermediate of increased coordination number:

$$[ML_n]^{m+} + L^* \overset{k_2}{\rightleftharpoons} [ML_nL^*]^{m+}$$
$$\rightarrow [ML_{n-1}L^*]^{m+} + L \quad (1.5)$$

The rate of exchange is directly dependent on the free ligand concentration and the rate law is second order:

$$\text{exchange rate} = nk_{ex}[[ML_n]^{m+}] \quad (1.6)$$

where $k_{ex} = k_2[L]$ and [L] is the free ligand concentration. For the **A** mechanism, the activation mode is necessarily **a** as M–L bond formation is the major determinant of the activation energy.

Interchange ($\mathbf{I}_d$ and $\mathbf{I}_a$) Mechanisms for Ligand Exchange Reactions

An "encounter" or "outer sphere" complex is formed in a diffusion controlled equilibrium in which a ligand enters the second coordination sphere. This then exchanges with a leaving ligand from the first coordination sphere:

$$\begin{aligned} [ML_n]^{m+} + L^* &\overset{K_{ass}}{\rightleftharpoons} [ML_n]^{m+} \ldots L^* \\ &\overset{k_i}{\rightarrow} [ML_{n-1}L^*]^{m+} + L \end{aligned} \tag{1.7}$$

If M–L bond breaking is rate determining, the activation mode is predominantly dissociative (**d**) and the mechanism is dissociative interchange ($\mathbf{I}_d$). If, on the other hand, M–L* bond formation is rate determining, an associative activation mode (**a**) is operational and the mechanism is associative interchange ($\mathbf{I}_a$). Now, regardless of the activation mode, the rate law is:

$$\begin{aligned} \text{exchange rate} &= nk_{ex}[[ML_n]^{m+}] \\ &= \frac{nk_iK_{ass}[[ML_n]^{m+}][L]}{1 + K_{ass}[L]} \end{aligned} \tag{1.8}$$

where K_{ass} is the equilibrium constant for the facile formation of the encounter complex. If $K_{ass}[L] \ll 1$, $k_{ex} \approx k_iK_{ass}[L]$ and the rate is dependent on [L]:

$$\text{exchange rate} \approx nk_iK_{ass}[L][[ML_n]^{m+}] \tag{1.9}$$

If $K_{ass}[L] \gg 1$ then the rate law reduces to:

$$\text{exchange rate} \approx nk_i[[ML_n]^{m+}] \tag{1.10}$$

and $k_{ex} \approx k_i$ so that in a plot of k_{ex} against [L] over a sufficiently large concentration range, k_{ex} will appear virtually linearly dependent on [L] but eventually, at high [L], curves off asymptotically to k_i. For an $\mathbf{I}_d$ mechanism, the rate constant, k_i, is approximately that expected for a **D** mechanism, k_1, as M–L bond breaking is the rate determining step in both.

Thus, if k_{ex} for a series of solutions of varying concentrations of free ligand are obtained then the dependence of k_{ex} on [L] can be measured. If k_{ex} is found to be

dependent on [L] then an **I** mechanism in which $K_{ass} \ll 1$ or an **A** mechanism is indicated. If k_{ex} is independent of [L] then an **I** mechanism in which $K_{ass}[L] \gg 1$ or a **D** mechanism is indicated. K_{ass} can be estimated from the Fuoss equation [5,6] and the upper limit is of the order of 1 for M^{m+} in non-aqueous solutions. Some experimental estimates in ligand substitution studies are significantly higher ($\approx 10^2$ dm^3mol^{-1} [7]) although this is probably a consequence of a specific interaction (possibly charge-transfer) between different ligands [7]. Hence, at the concentrations considered in this work, if k_{ex} is independent of [L], the mechanism is much more likely to be **D** than $\mathbf{I}_d$.

1.3 Objectives of This Research

The aim of this research work was to determine the rates and, if possible, the mechanisms of the chemical exchange processes in several systems using variable temperature nmr and complete lineshape analysis. The systems were chosen because of their poorly understood behaviour when undergoing chemical exchange.

The lanthanide series has only recently received the attention of two systematic and extensive studies of ligand exchange. These were studies of complexes of H_2O [8] and N,N-dimethylformamide [9] and revealed complexes of high coordination number (8 or 9) undergoing fast exchange. It was known that 1,1,3,3-tetramethylurea (tmu) forms six-coordinate complexes with Sc^{3+}, Y^{3+} and Lu^{3+} (see Section 2.1.2) and hence it appeared that the lanthanide complexes of tmu might provide an opportunity to study the ligand exchange of lanthanide(III) complexes of monodentate oxygen donor ligands of unusually low coordination number. These complexes were consequently chosen for study in this work.

The tmu complex of dioxouranium(VI), $[UO_2(tmu)_5](ClO_4)_2$, had been the subject of a previous ligand exchange study [10] and so the complexes of dioxouranium(VI) with several other substituted ureas were investigated for comparison with the results from studies of lanthanide(III) and dioxouranium(VI) complexes of tmu, formamides and acetamides. In this way, it was hoped to ascertain the effects of substitution on the rates of intra- and inter-molecular exchange in the complexes of

substituted ureas.

Finally, the exchange processes of alkali metal ions in macrocyclic ligand complexes were still not fully understood, despite a large amount of study in this area. The recent availability of high field multinuclear nmr spectrometers has made it possible to study previously unobservable metal ion exchange in macrocyclic complexes. Accordingly, alkali metal complexes of crown ethers were also studied to determine the effects of cation, ligand and solvent parameters on the exchange processes.

This thesis is a report of the results from these investigations.

Chapter 2

Ligand Exchange on Lanthanide(III) Complexes

2.1 Introduction

2.1.1 The Lanthanide Series

The term "lanthanides" will be used here to denote all the elements from lanthanum to lutetium inclusive. The elements scandium and yttrium, which have +3 ions with noble gas configurations, also have similar properties to the lanthanides and so will also be included in this discussion. The lanthanides present a unique series of metal ions with which to study the dependence of the rates and mechanisms of ligand exchange on the ionic radius without interference from strong crystal field effects. On traversing the series from La to Lu, successive electrons enter the inner 4f shell (in general — for more detailed electron configurations see Table 2.1) which is not significantly involved in bonding due to shielding by the overlying filled shells ($5s^2$ and $5p^6$) and so the metal ion – ligand bonding is predominantly ion-dipole in nature for all the lanthanides. The radii of the lanthanides decrease monotonically (although not regularly) from La to Lu (Table 2.1) as a result of the very imperfect shielding from the nuclear charge of one electron in the 4f shell by another due to the shape and diffuse nature of the orbitals. This increases the effective nuclear charge experienced by the outer electrons and decreases the radius. It is seen from Table 2.1 that the effective ionic radius of a particular lanthanide(III) ion varies substantially with its coordination number. Thus it is important to establish

Table 2.1: Some Properties of the Lanthanides, Scandium and Yttrium

		Electronic Configuration		$r(M^{3+})^1$ pm		
A.N.[2]	Element	Atom	M^{3+}	CN=6	CN=8	CN=9
21	Sc	$[Ar]3d^14s^2$	[Ar]	74.5	87.0	–
39	Y	$[Kr]4d^15s^2$	[Kr]	90.0	101.9	107.5
57	La	$[Xe]5d^16s^2$	[Xe]	103.2	116.0	121.6
58	Ce	$[Xe]4f^15d^16s^2$	$[Xe]4f^1$	101	114.3	119.6
59	Pr	$[Xe]4f^36s^2$	$[Xe]4f^2$	99	112.6	117.9
60	Nd	$[Xe]4f^46s^2$	$[Xe]4f^3$	98.3	110.9	116.3
61	Pm	$[Xe]4f^56s^2$	$[Xe]4f^4$	97	109.3	114.4
62	Sm	$[Xe]4f^66s^2$	$[Xe]4f^5$	95.8	107.9	113.2
63	Eu	$[Xe]4f^76s^2$	$[Xe]4f^6$	94.7	106.6	112.0
64	Gd	$[Xe]4f^75d^16s^2$	$[Xe]4f^7$	93.8	105.3	110.7
65	Tb	$[Xe]4f^96s^2$	$[Xe]4f^8$	92.3	104.0	109.5
66	Dy	$[Xe]4f^{10}6s^2$	$[Xe]4f^9$	91.2	102.7	108.3
67	Ho	$[Xe]4f^{11}6s^2$	$[Xe]4f^{10}$	90.1	101.5	107.2
68	Er	$[Xe]4f^{12}6s^2$	$[Xe]4f^{11}$	89.0	100.4	106.2
69	Tm	$[Xe]4f^{13}6s^2$	$[Xe]4f^{12}$	88.0	99.4	105.2
70	Yb	$[Xe]4f^{14}6s^2$	$[Xe]4f^{13}$	86.8	98.5	104.2
71	Lu	$[Xe]4f^{14}5d^16s^2$	$[Xe]4f^{14}$	86.1	97.7	103.2

[1] Effective ionic radii [11], CN = coordination number.
[2] atomic number.

coordination numbers when comparing complexes on the basis of their ionic radii.

Lanthanide complexes exhibit a variety of coordination numbers in the solid state and in solution. In the solid state, when the ligand is water, the coordination number is between 6 and 9 depending on the anion [12, and references therein]. In aqueous solution, the coordination number appears to be between 8 and 10 but the actual values are still a matter of debate [12,13]. The balance of evidence seems to lie in favour of a coordination number of nine and that will be assumed in this discussion.

For complexes of ligands other than water, the coordination number appears to be better defined. In the solid state, the lanthanide complexes of N,N-dimethylformamide (dmf), $[Ln(dmf)_8](ClO_4)_3$, (Ln = La – Lu) have been isolated [14,15]. In solution, $[Ln(dmf)_8]^{3+}$ is the major species for Ln = Ce – Nd and the only stable

species for Ln = Tb – Lu [9]. Conductivity [16,17] and ^{35}Cl nmr [15] studies indicate that the perchlorate ion does not enter the first coordination sphere of Ln^{3+} to a detectable extent in dmf solutions of lanthanide perchlorates. Although $Eu(ClO_4)_3$ in pure acetonitrile has one perchlorate anion in the first coordination sphere in about 60% of the ions [18] this is due to the low coordinating ability of acetonitrile. Perchlorate is not expected to coordinate to a significant extent in the presence of a ligand of greater coordinating ability such as 1,1,3,3-tetramethylurea.

When the ligand is N,N-dimethylacetamide (dma), the complexes of the lanthanide ions display various stoichiometries. Complexes of the form $[Ln(dma)_n](ClO_4)_3$ are found with n = 8 when Ln = La – Nd, n = 7 for Ln = Sm – Er, Y and n = 6 for Ln = Tm – Lu [19]. A similar series is observed for complexes of dimethylsulphoxide (dmso) [20] with coordination numbers of 8 for Ln = La, Ce, Pr and Nd, and 7 for Ln = Sm, Gd and Y. Complexes of hexamethylphosphoramide (hmpa) of the form $[Ln(hmpa)_6](ClO_4)_3$ (Ln = Sc, Y, La – Lu) have been prepared [21,22,23]. The complexes $[Ln(hmpa)_4(ClO_4)_2](ClO_4)$ have also been prepared [23] by recrystallisation from ethanol, but convert to the species with six hmpa ligands when recrystallised from acetonitrile with excess hmpa.

With 1,1,3,3-tetramethylurea (tmu) as the ligand, a range of anions have been used to produce complexes of various stoichiometry such as $Ln(tmu)_3Cl_3$ (Ln = La – Sm, Gd, Ho) and $Ln(tmu)_n(NO_3)_3$ (with n = 1 for Ln = La – Sm, Gd, Ho and n = 3 for Ln = La –Lu, Y) [24]. However, when the anion is perchlorate [25] or hexafluoroarsenate [26] only one type of adduct appears to be obtained, $[Ln(tmu)_6]X_3$ (Ln = Y, La – Lu; X = ClO_4, AsF_6), probably as a consequence of the lower coordinating ability of these anions. This stoichiometry has been confirmed by a crystal structure of $[Er(tmu)_6](ClO_4)_3$ [27] and in solution for complexes of lutetium [28], scandium [29] and yttrium [30].

2.1.2 Previous Ligand Exchange Studies on Lanthanide(III) Complexes

The rates of water exchange on several lanthanide ions have been determined [8,31] and some are shown in Table 2.2. Most have been calculated for both 8 and 9 coor-

Table 2.2: Kinetic Parameters Characterising Exchange of Water on Lanthanide Ions

Ln^{3+}	CN[1]	10^{-8}k(298 K) s^{-1}	$\Delta H^{\ddagger}$ kJ mol^{-1}	$\Delta S^{\ddagger}$ J K mol^{-1}	$\Delta V^{\ddagger}$ $cm^3 mol^{-1}$
Gd[2]	9	10.6 ± 0.9	11.99 ± 1.40	−31.9 ± 4.3	–
Tb[3]	8	5.58 ± 0.13	12.08 ± 0.48	−36.9 ± 1.6	−5.7 ± 0.5
	9	4.96 ± 0.12	12.08 ± 0.48	−37.9 ± 1.6	−5.7 ± 0.5
Dy[3]	8	4.34 ± 0.10	16.57 ± 0.47	−24.0 ± 1.5	−6.0 ± 0.4
	9	3.86 ± 0.09	16.57 ± 0.47	−25.0 ± 1.5	−6.0 ± 0.4
Ho[3]	8	2.14 ± 0.04	16.36 ± 0.39	−30.5 ± 1.3	−6.6 ± 0.4
	9	1.91 ± 0.03	16.36 ± 0.39	−31.5 ± 1.3	−6.6 ± 0.4
Er[3]	8	1.33 ± 0.02	18.37 ± 0.34	−27.8 ± 1.1	−6.9 ± 0.4
	9	1.18 ± 0.02	18.37 ± 0.34	−28.8 ± 1.1	−6.9 ± 0.4
Tm[3]	8	0.91 ± 0.02	22.68 ± 0.58	−16.4 ± 1.9	−4.5 ± 0.3
	9	0.81 ± 0.02	22.68 ± 0.58	−17.4 ± 1.9	−4.5 ± 0.3
Yb[3]	8	0.47 ± 0.02	23.29 ± 0.94	−21.0 ± 3.3	–
	9	0.41 ± 0.01	23.29 ± 0.94	−22.0 ± 3.3	–

[1] Coordination Number.
[2] Reference [31].
[3] Reference [8].

dinate species and are all *ca.* 10^8 s^{-1} at 298 K but show a systematic decrease across the series from Gd to Yb as the radius decreases. The enthalpy of activation ($\Delta H^{\ddagger}$), in general, increases across the series from Gd to Yb but the entropy of activation ($\Delta S^{\ddagger}$) does not show a systematic variation. The rates of exchange on the trivalent lanthanides are much higher than those of several other trivalent metal water complexes. For example, the k(298 K) values for $[Ti(H_2O)_6]^{3+}$ and $[In(H_2O)_6]^{3+}$ are 1.81×10^5 s^{-1} [32] and 4.0×10^4 s^{-1} [33] respectively. The effective ionic radii for these six-coordinated ions are 67.0 and 80.0 pm respectively [11]. The greater lability of ligand exchange on $[Ln(H_2O)_n]^{3+}$, where n = 8 or 9, is probably a result of the increased coordination number and consequently decreased Ln–O bond strength. The increase in coordination number also necessitates a change in geometry from octahedral to tricapped trigonal prismatic or capped square antiprismatic (for n = 9) or square antiprismatic (for n = 8) which may also provide a mechanism for increased lability as discussed below.

Theoretically, the most stable 9 coordinate geometry is the tricapped trigonal prism (this structure has been established experimentally in the solid state for $Ln(H_2O)_9(CF_3SO_3)_3$ where Ln = La, Gd, Lu and Y [34]) but the capped square antiprism is only slightly less stable [35,36] so that it is probable that scrambling of all nine waters occurs via this intermediate [12]. The tricapped trigonal prismatic geometry (D_{3h}) can easily interchange with the capped square antiprismatic one (C_{4v}) with only a small distortion (Figure 2.1) [37]. In the capped square antiprismatic geometry, a unique water at a greater distance from the central Ln^{3+} ion can easily dissociate producing an 8 coordinate square antiprism ion, $[Ln(H_2O)_8]^{3+}$, which is probably the most stable geometry for this coordination number [35]. This could provide a mechanism for fast exchange between complexed and uncomplexed ligands via a dissociatively activated pathway. Alternatively, another water molecule can approach one of the uncapped faces of the capped square antiprism or tricapped trigonal prism of $[Ln(H_2O)_9]^{3+}$ and exchange with the capped H_2O via either an A or an I_a mechanism. The observed decrease in the rate constants for H_2O exchange as the radius decreases from Gd to Yb (Table 2.2) could be explained by a dissociatively activated mechanism in the following way. As the radius decreases, the Ln–O bonds become stronger and the breaking of these bonds is the rate determining step (and hence the observed increase in the $\Delta H^{\ddagger}$ values from Gd – Yb). However, the operation of an associatively activated mechanism may also explain the decrease of k with decreasing radius as the increased steric crowding necessary in the activation state would make the approach of the incoming ligand less favourable for the smaller lanthanides.

The volume of activation, $\Delta V^{\ddagger}$, is the difference in volume between the transition state and the initial state. Polar molecules in the first coordination sphere of a metal ion are more closely packed than they would be in the bulk solution and so occupy less volume (hence the term "electrostriction"). For exchange reactions of neutral ligands, the interpretation of $\Delta V^{\ddagger}$ is simplified as there is no change in the number of ions present in solution and hence no significant changes in volume due to changes in electrostriction. For an associatively activated exchange process, $\Delta V^{\ddagger}$, is expected to be negative as the transition state, in which an incoming ligand has penetrated

tctp csap

Figure 2.1:
Interconversion between tricapped trigonal prismatic (tctp) and capped square antiprismatic (csap) geometry. The arrows show the relatively small distortion required [37].

into the first coordination sphere, is expected to occupy less volume than the species in the initial state ($[ML_n]^{3+}$ and L^* in Equation 1.5). On the other hand, for a dissociatively activated process, as shown in Equation 1.2, $\Delta V^{\ddagger}$ is expected to be positive as the transition state occupies more volume than the initial species as a ligand is leaving the first coordination sphere.

Values for $\Delta V^{\ddagger}$ can be determined by observing the variation of the ligand exchange rate (using nmr [9]) with applied pressure. Then $\Delta V^{\ddagger}$ is given by [38]:

$$\Delta V^{\ddagger} = -RT\left(\frac{\delta \ln k}{\delta P}\right)_T \tag{2.1}$$

where R is the gas constant and the other symbols have their usual meanings.

The volumes of activation for exchange of H_2O on $[Ln(H_2O)_n]^{3+}$ (n = 8 or 9) shown in Table 2.2 are all negative as are the values of $\Delta S^{\ddagger}$. This seems to indicate an associative activation mode. As the series is traversed from terbium to thulium, the ionic radius decreases from 109.5 pm to 105.2 pm [11], assuming a coordination number of 9. If an associative mechanism is operating, this is expected to make the penetration of an incoming ligand into the first coordination sphere more difficult and hence make $\Delta V^{\ddagger}$ less negative. This is observed from Er to Tm, but from Tb to Er, the $\Delta V^{\ddagger}$ values become slightly more negative. This must reflect other factors

such as a slight bond lengthening in the transition state.

The only other extensive study to date of solvent or ligand exchange on the lanthanide(III) ions has been the exchange of dmf on $[Ln(dmf)_8](ClO_4)_3$ for Ln = Tb – Yb [9,15,39,40] by nmr using the Swift and Connick method [41]. Some of the results are presented in Table 2.3. The k values are high but are between one and two orders of magnitude less than those characterising water exchange even if the values for a coordination number of eight are used for the latter. This is in agreement with the observation that the rates of nonaqueous solvent exchange are generally lower than those of water exchange [9]. This appears to arise through a combination of the values of $\Delta H^{\ddagger}$ and $\Delta S^{\ddagger}$. For example, compared to the corresponding parameters for water exchange in Table 2.2, $\Delta H^{\ddagger}$ is higher for Tb, Er, Tm and Yb but $\Delta S^{\ddagger}$ is lower for the first two and higher for the latter two. Thus, the effect of the high $\Delta H^{\ddagger}$ values appear to be dominating here. However, for Dy and Ho, the $\Delta H^{\ddagger}$ values are lower but the $\Delta S^{\ddagger}$ values are also much lower, thus decreasing the rates of exchange below those of water, so that the effect of the entropy appears to be dominant in these cases.

For dmf exchange, in general, as the series is traversed from Tb to Yb, the $\Delta H^{\ddagger}$, $\Delta S^{\ddagger}$, $\Delta V^{\ddagger}$ and k(200 K) values all increase. The values of $\Delta V^{\ddagger}$ are positive for all the elements from Tb to Yb indicating the operation of a dissociatively activated mechanism but $\Delta S^{\ddagger}$ changes sign from negative to positive between Er and Tm. These results and those from a study using a diluent, CD_3NO_2, to vary the concentration of dmf, led Pisaniello *et al.* [9] to conclude that the exchange of dmf on $[Ln(dmf)_8](ClO_4)_3$ proceeds via an interchange mechanism for Tb, Dy, Ho and Er while exchange on Tm and Yb proceeds via a **D** mechanism. For dmf exchange on the neodymium complex [39], the values $\Delta H^{\ddagger} = 14.9 \pm 1.3$ kJ mol^{-1}, $\Delta S^{\ddagger} = -69.1 \pm 4.2$ J K^{-1}mol^{-1} and $\Delta V^{\ddagger} = -9.8 \pm 1.1$ cm^{3}mol^{-1} were obtained. Unfortunately, the coordination number could not be established but appeared to be between 8 and 9 with the former being favoured at higher temperatures so that these values cannot be directly compared to those of Table 2.3. However, the value of $\Delta V^{\ddagger}$ is negative indicating that the exchange is primarily associatively activated. This seems to indicate that there is a trend across the lanthanide series from La –

Table 2.3: Kinetic Parameters Characterising Exchange of dmf on $[Ln(dmf)_8]^{3+}$

Ln^{3+}	$10^{-7}k(298\ K)^1$ s^{-1}	$10^{-5}k(200\ K)^1$ s^{-1}	$\Delta H^{\ddagger\ 1}$ kJ mol^{-1}	$\Delta S^{\ddagger\ 1}$ J $K\ mol^{-1}$	$\Delta V^{\ddagger\ 1}$ $cm^3 mol^{-1}$
Tb^2	1.9 ± 0.1	7.9 ± 0.2	14.09 ± 0.4	-58.25 ± 2.1	5.2 ± 0.2
Dy^2	0.63 ± 0.03	2.8 ± 0.1	13.76 ± 0.4	-68.54 ± 1.6	6.1 ± 0.2
Ho^2	0.36 ± 0.06	1.16 ± 0.02	15.31 ± 0.8	-68.13 ± 4.0	5.2 ± 0.5
Er^2	1.3 ± 0.4	0.80 ± 0.03	23.64 ± 1.8	-29.57 ± 8.6	5.4 ± 0.3
Tm^2	3.1 ± 0.3	0.294 ± 0.009	33.18 ± 0.5	9.85 ± 2.4	7.4 ± 0.3
Yb^2	9.9 ± 0.9	0.278 ± 0.009	39.30 ± 0.6	39.95 ± 2.7	11.8 ± 0.4

[1] Quoted errors represent one standard deviation.
[2] Reference [9].

Lu, at least for dmf, for the mechanism to vary in the sequence **A**, $\mathbf{I}_a$, $\mathbf{I}_d$ and **D**. This is similar to the mechanistic changeover from associative to dissociative activation modes observed for the di- and tri-valent ions of the first row transition series [38,42]. In these cases, however, the mechanistic change has been ascribed predominantly to the increase in electronic occupancy of the t_{2g} orbitals while in the lanthanide case this is probably a consequence of the decrease in radius due to the lanthanide contraction.

The ligand exchange of several six-coordinate species of scandium, yttrium and lutetium have been previously investigated. Some of the results obtained in these studies are presented in Table 2.4 with those for several other ions. The general rate law for the ligand exchange on these complexes is:

$$\text{exchange rate} = 6k_{ex}[[ML_6]^{3+}] = 6(k_1 + k_2[L])[[ML_6]^{3+}]. \qquad (2.2)$$

where k_{ex} is related to the lifetime of a coordinated ligand, τ_c, by $k_{ex} = \frac{1}{\tau_c}$ as shown in Equation 1.4. If only k_1 is observed, a **D** mechanism can be assigned because an **I** mechanism only showing k_1 would require a high degree of preferential occupancy of the second coordination sphere such that $K_{ass}[L] \gg 1$ (where K_{ass} is the equilibrium constant for the facile formation of the encounter complex). This is unlikely as discussed in Section 1.2. If only k_2 is observed, then the mechanism may be **A**, or $\mathbf{I}_a$ or $\mathbf{I}_d$ with a small K_{ass} such that it is insufficient to cause curvature of the plot of k_{ex} against [L]. However, the observation that $\Delta V^{\ddagger}$ values for several complexes are

negative and large in magnitude indicates the operation of an **A** mechanism. For example, for the trimethylphosphate (tmp) complexes of scandium, $[Sc(tmp)_6]^{3+}$, and indium, $[In(tmp)_6]^{3+}$, in CD_3NO_2, $\Delta V^{\ddagger}$ for exchange is -18.7 ± 1.1 cm^3mol^{-1} [42] and -22.8 ± 1.1 cm^3mol^{-1} [42]) respectively. Thus, it is probable that for all these complexes, if only a k_2 term is observed, the exchange mechanism is associative (**A**) and this is assumed in this discussion. If both k_1 and k_2 terms are observed, the exchange proceeds via at least two different pathways with intermediates of comparable energy.

From Table 2.4, it is seen that the rates of exchange on these six-coordinate species are much smaller than those for dmf exchange on $[Ln(dmf)_8]^{3+}$ (Table 2.3) or those of H_2O exchange on $[Ln(H_2O)_n]^{3+}$, where n = 8 or 9 (Table 2.2). This decrease in lability appears to be a consequence of the lower coordination number and consequently shorter, and stronger, Ln–O bonds. It can also be seen that the complexes of tmp in CD_3NO_2 undergo exchange via an **A** mechanism when the ion is Sc^{3+} [43,42] or In^{3+} [49,42] while exchange proceeds via a **D** mechanism when the ion is Al^{3+} [47,42] or Ga^{3+} [49,42]. The effective ionic radii [11] for these four ions are 74.5, 80.0, 53.5 and 62.0 pm respectively, so it appears that the mechanism is influenced to a great extent by the radius of the metal ion. The metal ions with radii close to the point where the changeover occurs would be expected to be most susceptible to mechanistic change from changes in environment. It is seen from Table 2.4 that this occurs for several complexes of Sc^{3+} on changing the solvent from CD_3CN to CD_3NO_2. The mechanism is also influenced greatly by the nature of the ligand as observed for the Sc^{3+} and Y^{3+} complexes in Table 2.4. The exchange of nmf (N-methylformamide), dmf (N,N-dimethylformamide) and def (N,N-diethylformamide) on $[ScL_6]^{3+}$ [45] was too rapid to be measured by the nmr methods used for nma (N-methylacetamide), dma (N,N-dimethylacetamide) and dea (N,N-diethylacetamide). The decrease in steric crowding on changing the acetyl methyl group to the formyl proton apparently either causes the coordination number to increase or increases the k_2 term in the rate equation beyond that which can be measured by these techniques.

A study of complexes of lanthanide(III) ions with 1,1,3,3-tetramethylurea (tmu)

Table 2.4: Kinetic Parameters Characterising Ligand Exchange on $[M(L)_6]^{3+}$

M^{3+},L	diluent	k_1(298 K) s^{-1}	k_2(298 K) $dm^3mol^{-1}s^{-1}$	$\Delta H^{\ddagger}$ kJ mol^{-1}	$\Delta S^{\ddagger}$ J K mol^{-1}	Mech.[1]
$\underline{Sc^{3+}}$						
tmp[2]	CD_3NO_2	–	45	26.0 ± 0.9	−126 ± 3	A
tmp[3]	CD_3NO_2	–	39	21.2	−143.5	A
tmp[2]	CD_3CN	59	–	29.8 ± 0.4	−111 ± 2	D
tmp[3]	neat	736	(85)[4]	34.1	−75.6	A
dmmp[5]	CD_3NO_2	–	13.0	29.7 ± 1.1	−124 ± 3	A
dmmp[5]	CD_3CN	286	–	43.5 ± 1.8	−90.3 ± 5.4	D
dmmp[5]	CD_3CN	–	14.2	24.4 ± 1.1	−141 ± 3	A
nma[6]	CD_3CN	79.2	–	27.3 ± 0.9	−117 ± 4	D
nma[6]	CD_3CN	–	380	26.1 ± 1.2	−108 ± 5	A
dma[6,7]	CD_3NO_2	3.88	–	30.8 ± 2.0	−131 ± 6	D
dma[6,7]	CD_3NO_2	–	105	26.0 ± 0.6	−119 ± 2	A
dma[6,7]	CD_3CN	6.1	–	32.2 ± 3.5	−116 ± 12	D
dma[6,7]	CD_3CN	–	190	27.2 ± 1.2	−112 ± 4	A
dea[7]	CD_3NO_2	0.089	–	82 ± 3	10 ± 7	D
dea[7]	CD_3NO_2	–	13.5	28.1 ± 0.6	−129 ± 2	A
dea[7]	CD_3CN	10.7	–	43.9 ± 1.0	−78 ± 3	D
dea[7]	CD_3CN	–	18.1	23.5 ± 0.9	−142 ± 3	A
tmu[6]	CD_3NO_2	2.06	–	91.2 ± 2.3	47.8 ± 6.7	D
tmu[6]	CD_3CN	0.90	–	68.6 ± 1.3	−15.7 ± 3.8	D
$\underline{Y^{3+}}$						
tmu[8]	CD_3CN	253	–	27.1 ± 0.5	−108 ± 2	D
opm[9]	CD_2Cl_2	312 (215 K)	–	31.4 ± 1.4	−48.4 ± 6.6	D
opm[9]	CD_2Cl_2	–	455 (215 K)	35.2 ± 2.8	−27.6 ± 12.6	A
$\underline{Lu^{3+}}$						
tmu[10]	CD_3CN	41.9	–	41.7 ± 0.6	−74 ± 2	D

(Table continues on next page)

Table 2.4: (Cont.)

M^{3+},L	diluent	k_1(298 K) s^{-1}	k_2(298 K) $dm^3mol^{-1}s^{-1}$	$\Delta H^{\ddagger}$ kJ mol^{-1}	$\Delta S^{\ddagger}$ J K mol^{-1}	Mech.[1]
$\underline{Al^{3+}}$						
tmp[11]	CD_3NO_2	0.36	–	98.3	76.1	
tmp[3]	CD_3NO_2	0.78	–	85.1	38.2	**D**
dmmp[12]	CD_3NO_2	5.1	–	79.5	33.0	
dmf[3]	CD_3NO_2	0.05	–	88.3	28.4	**D**
$\underline{Ga^{3+}}$						
tmp[13]	CD_3NO_2	5.0	–	87.9	63.2	**D**
tmp[3]	CD_3NO_2	6.4	–	76.5	27.0	**D**
dmf[3]	CD_3NO_2	1.72	–	85.1	45.1	**D**
$\underline{In^{3+}}$						
tmp[13]	CD_3NO_2	–	7.2	35.6	−109.2	**A**
tmp[3]	CD_3NO_2	–	7.6	32.8	−118	**A**

[1] Assigned Mechanism. [2] Reference [43]. [3] Reference [42].
[4] Calculated with molality of 8.66 for free tmp.
[5] dmmp = dimethylmethylphosphonate, Reference [44].
[6] Reference [29]. [7] Reference [45]. [8] Reference [30].
[9] opm = OPMe(OMe)Ph, Reference [46].
[10] Reference [28]. [11] Reference [47]. [12] Reference [48].
[13] Reference [49].

was undertaken to determine:

(i) if the trend of decreased lability on decreasing coordination number holds for the lanthanides in general and

(ii) if there is a change in coordination number and/or a mechanistic crossover for six-coordinate species on traversing the lanthanide series.

1,1,3,3-tetramethylurea is a monodentate oxygen donor ligand which, because because of its steric bulk, forms six-coordinate complexes with Sc^{3+} [29], Y^{3+} [30] and Lu^{3+} [28]. Thus it presented the possibility of observing ligand exchange on lanthanide complexes of unusually low coordination number and the opportunity to compare the results with complexes of similar ligands of higher coordination number.

Lanthanum, and the elements neodymium to gadolinium, were not studied in this work. The 1,1,3,3-tetramethylurea complex of lanthanum had been previously prepared [50] and was found to be unsuitable for kinetic study as described in Section 2.1.2. The observed behaviour of the praseodymium complex was taken as representative of the behaviour of the lighter lanthanides. The ionic radius of neodymium (98.3 pm) is very similar to that of praseodymium (99 pm) and so was not studied. Promethium is not readily available and is radioactive. For Sm, the energy gap to the first excited J state (and for Eu, the second and third excited states also) is small enough to be appreciably populated at temperatures at which the exchange is in the nmr timescale. The populations change with temperature giving variable magnetic moments and hence are not readily studied by nmr techniques for quantitative kinetic data. The other lanthanide ions have only one single well-defined populated J state giving well-defined and non-temperature dependent values of magnetic moments and susceptibilities. Gadolinium gives small chemical shifts and very large resonance broadening [51] and so is not suitable for study by complete lineshape analysis. The tmu complex of lutetium has been previously studied to obtain the parameters of ligand exchange [28]. Accordingly, the elements considered in detail in this study are praseodymium, terbium, dysprosium, holmium, erbium, thulium and ytterbium. The 1,1,3,3-tetramethylurea complexes of the trivalent ions

of these elements were prepared as perchlorate salts using the method described in Chapter 5. In each case, the solid state stoichiometry was determined as described in Section 5.3. A study of the ligand exchange on each complex was undertaken and the results are described below.

2.2 Ligand Exchange on Hexakis(1,1,3,3-tetramethylurea)praseodymium(III)

The complex $[Pr(tmu)_6](ClO_4)_3$ was found to be very hygroscopic, hydrating within minutes of exposure to the atmosphere. An anhydrous solution of the complex (0.06676 M) and tmu (0.3859 M) in CD_3CN (17.16 M) was studied by 300.13 MHz ^1H nmr. Only one sharp singlet resonance was observed over the entire temperature range (235 – 285 K) indicating that the ligand exchange is in the fast exchange limit of the nmr timescale. This may be a consequence of the large ionic radius of Pr(III) (99 pm) or possibly due to a significant contribution from an associatively activated mechanism. This possibility will be discussed further in Section 2.10. As the coordination number could not be determined in solution, it is unknown whether the observed fast exchange is due to an increase in coordination number. A similarly intractable situation is found to prevail for the lanthanum complex of 1,1,3,3-tetramethylurea [50].

2.3 Ligand Exchange on Hexakis(1,1,3,3-tetramethylurea)terbium(III)

A solution of the complex $[Tb(tmu)_6](ClO_4)_3$ and tmu in CD_3CN showed broad ^1H nmr singlets at low temperature due to slowing of the rate of ligand exchange (Figure 2.2) and consistent with the rate of rotation about the C–N bonds in tmu being in the fast exchange limit. As the small difference in the shift values and the broadness of the resonances would allow only semi-quantitative analysis of the rate of exchange, it was decided that only one solution would be studied in detail. Spectra of a solution of the complex alone in CD_3CN of similar concentration were recorded over the temperature range of coalescence to determine estimates of the

linewidth and shift and of their variation with temperature for the complex in solution with tmu. These parameters for the free tmu could be determined from the spectra of the solution of both free and coordinated tmu at low temperature in the slow exchange limit and extrapolated into the coalescence region.

The 300.13 MHz ^{1}H nmr signal due to coordinated tmu appeared upfield from that of the free ligand as can be seen in Figure 2.2. The sharp resonance between the two tmu peaks is due to the proton impurity of CD_3CN. The two small resonances at low field are due to a small impurity in the tmu which could not be removed by distillation and drying. It does not take part in the the exchange processes (as the peaks do not vary with temperature) and hence can be ignored. The areas of the peaks due to tmu (estimated from lineshaping) are consistent with $[Tb(tmu)_6]^{3+}$ being the predominant terbium species in solution. Complete lineshape analysis of the coalescence of the free and coordinated tmu resonances of a solution of $[Tb(tmu)_6](ClO_4)_3$ (0.03331 M), tmu (0.2228 M) and CD_3CN (17.63 M) yielded the mean site lifetime of a single tmu ligand coordinated to $[Tb(tmu)_6]^{3+}$, $\tau_c = \frac{1}{k_{ex}}$. The following parameters were derived from a linear regression of the data to the Eyring equation (Equation 6.31): $\Delta H^{\ddagger} = 38.2 \pm 0.5$ kJ mol^{-1}, $\Delta S^{\ddagger} = -56.7 \pm 1.8$ J K mol^{-1} and k(298.2 K) = 1377 ± 21 s^{-1}. Representative experimental spectra and best fit calculated lineshapes are shown in Figure 2.2 with the relevant temperatures and τ_c values. A semilogarithmic plot of $T\tau_c$ against $\frac{10^4}{T}$ for the solution is displayed in Figure 2.3. The linear regression line for the fit of the data to the Eyring equation is also shown on the plot. As only one solution was quantitatively studied, the exchange mechanism could not be determined from the variation of k_{ex} with [tmu].

2.4 Ligand Exchange on Hexakis(1,1,3,3-tetramethylurea)dysprosium(III)

A solution of $[Dy(tmu)_6](ClO_4)_3$ and tmu in CD_3CN showed broad ^{1}H nmr singlets in the slow exchange region of the ligand exchange (i.e. at low temperature) as shown in Figure 2.4. This is also consistent with the rate of rotation about the C–N bonds in tmu being in the fast exchange limit. Again, only one solution was

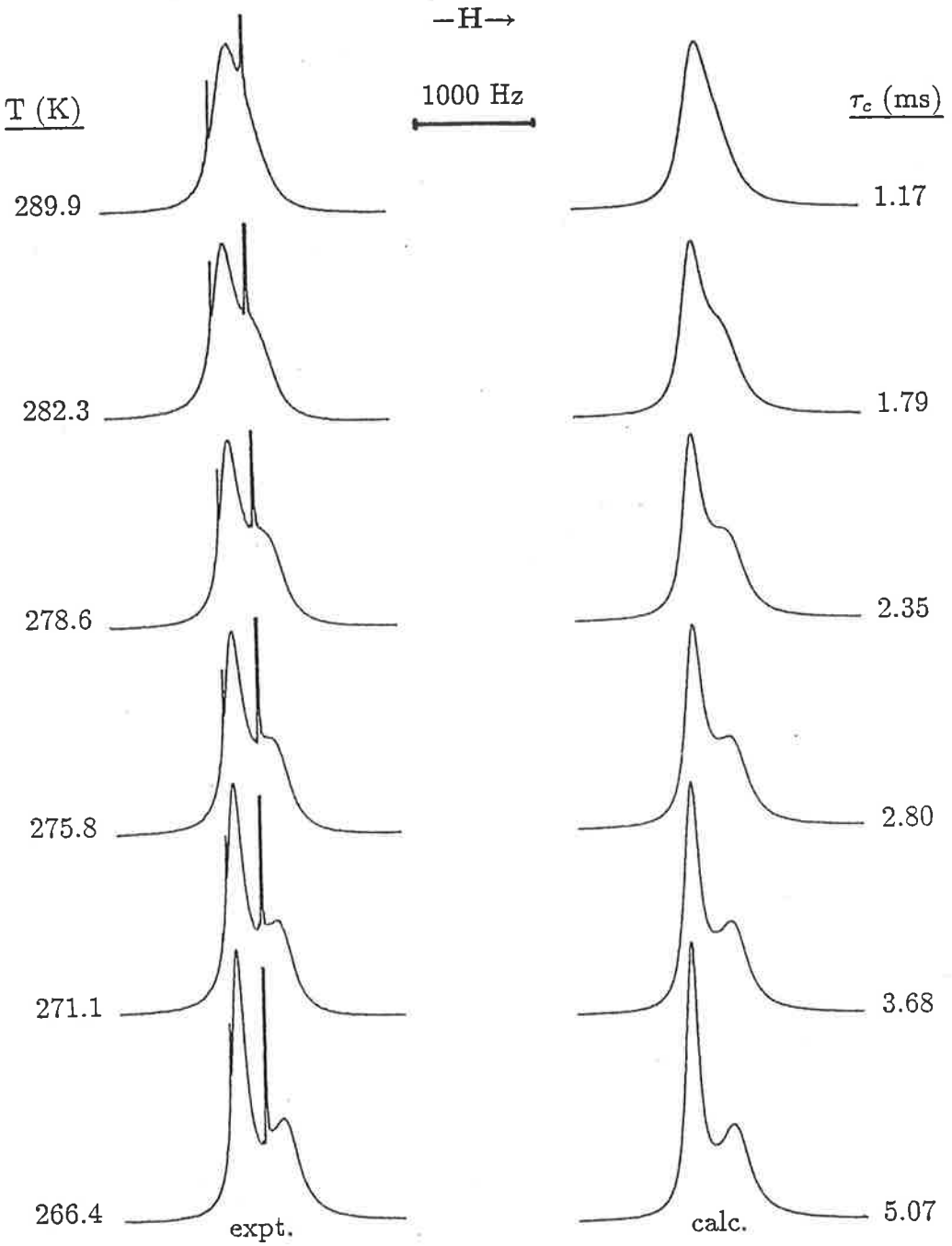

Figure 2.2:
300.13 MHz ^{1}H nmr spectra characterising ligand exchange for a CD_3CN solution (17.63 M) of $[Tb(tmu)_6](ClO_4)_3$ (0.03331 M) and tmu (0.2228 M). The experimental spectra and the corresponding temperatures appear to the left and the best fit calculated lineshapes and corresponding τ_c values appear to the right of the figure. The resonance due to coordinated tmu is upfield and the narrow signal appearing in the middle arises from the CD_3CN proton impurity.

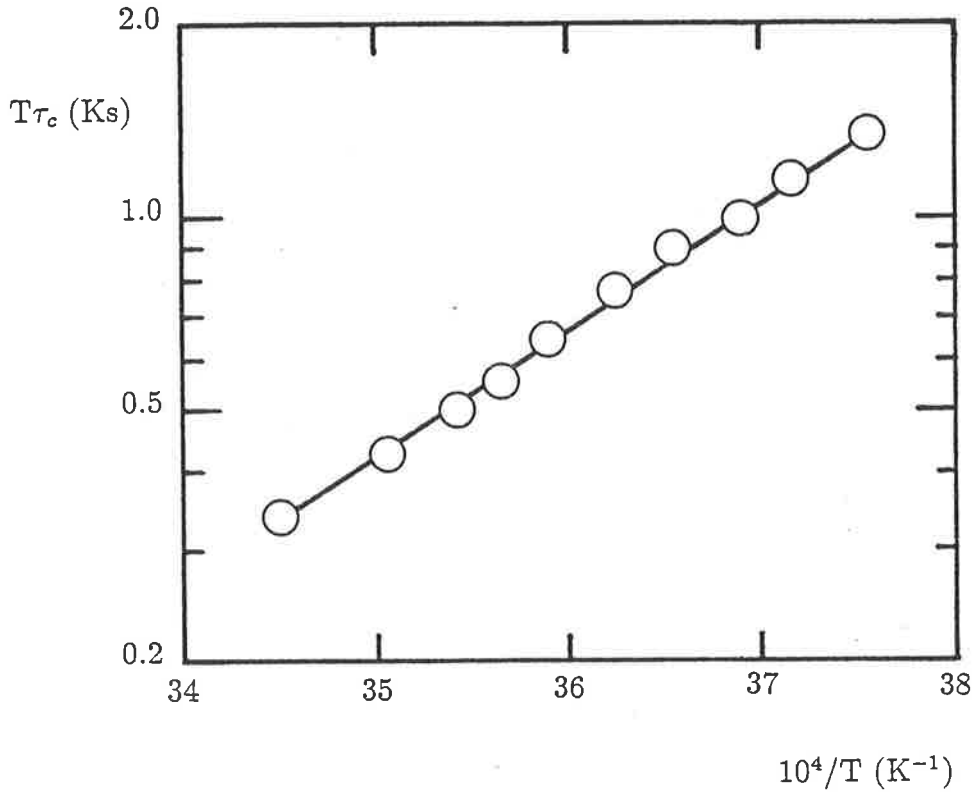

Figure 2.3:
Semilogarithmic plot of $T\tau_c$ against $\frac{10^4}{T}$ for tmu exchange on $[Tb(tmu)_6]^{3+}$ in CD_3CN solution. The solid line represents a linear regression line for the fit of the data set to the Eyring equation (Equation 6.31).

studied quantitatively due to the small shift difference between the resonances and broadness of the resonances. Estimates of the linewidth and shift variation of the complexed tmu resonance over the temperature range of coalescence were obtained by recording spectra of a solution of similar concentration of the complex alone in CD_3CN. These parameters for the free tmu were determined from the spectra of the solution of both free and coordinated tmu at low temperature in the slow exchange limit and extrapolated into the coalescence region.

300.13 MHz ^1H nmr spectra were recorded of a solution of the complex and tmu over the temperature range of coalescence. The signal due to coordinated tmu appeared upfield from that of the free ligand (Figure 2.4). The sharp resonance over the coordinated tmu peak is due to the proton impurity of CD_3CN. The two small resonances at low field are due to the small impurity in the tmu discussed in Section 2.1.2. The relative areas of the peaks due to tmu were estimated from the lineshaping and are consistent with $[Dy(tmu)_6]^{3+}$ being the predominant dysprosium species in solution. A complete lineshape analysis of the coalescence of the free and coordinated tmu resonances of a solution of $[Dy(tmu)_6](ClO_4)_3$, tmu and CD_3CN (0.03069 M, 0.1533 M and 17.60 M respectively) yielded the parameters $\Delta H^{\ddagger} = 38.6 \pm 0.7$ kJ mol^{-1}, $\Delta S^{\ddagger} = -56.0 \pm 2.4$ J K mol^{-1} and k(298.2 K) $= 1285 \pm 33$ s^{-1}. Typical experimental spectra and best fit calculated lineshapes together with the relevant temperatures and τ_c values are shown in Figure 2.4 . A semilogarithmic plot of $T\tau_c$ against $\frac{10^4}{T}$ for the solution is exhibited in Figure 2.5. The linear regression line for the fit of the data to equation 6.31 is also shown. Again, as only one solution was quantitatively studied, the exchange mechanism could not be determined from the variation of k_{ex} with [tmu].

2.5 Ligand Exchange on Hexakis(1,1,3,3-tetramethylurea)holmium(III)

A solution of the complex $[Ho(tmu)_6](ClO_4)_3$ and tmu in CD_3CN showed a broad ^1H nmr singlet which developed a shoulder at low temperature (Figure 2.6) due to slowing of the rate of ligand exchange. As the peaks due to coordinated and free tmu could not be separately distinguished, the errors in the parameters derived from

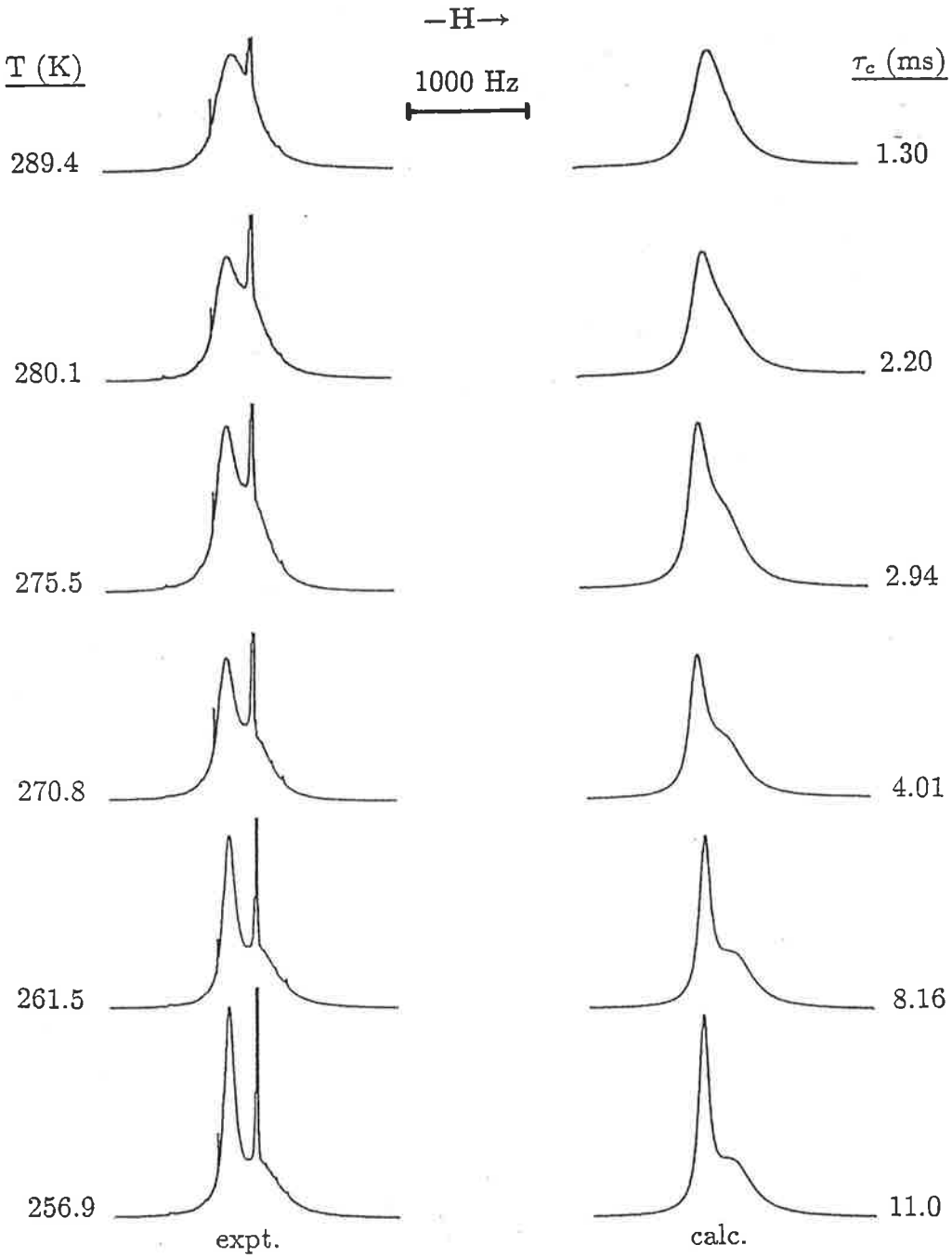

Figure 2.4:
300.13 MHz ^{1}H nmr spectra characterising ligand exchange for a solution of the complex $[Dy(tmu)_6](ClO_4)_3$ (0.03069 M) and tmu (0.1533 M) in CD_3CN (17.60 M). The experimental spectra and the corresponding temperatures appear to the left and the best fit calculated lineshapes and corresponding τ_c values appear to the right of the figure. The resonance due to coordinated tmu is upfield and the narrow signal appearing over the broad coordinated tmu signal arises from the CD_3CN proton impurity.

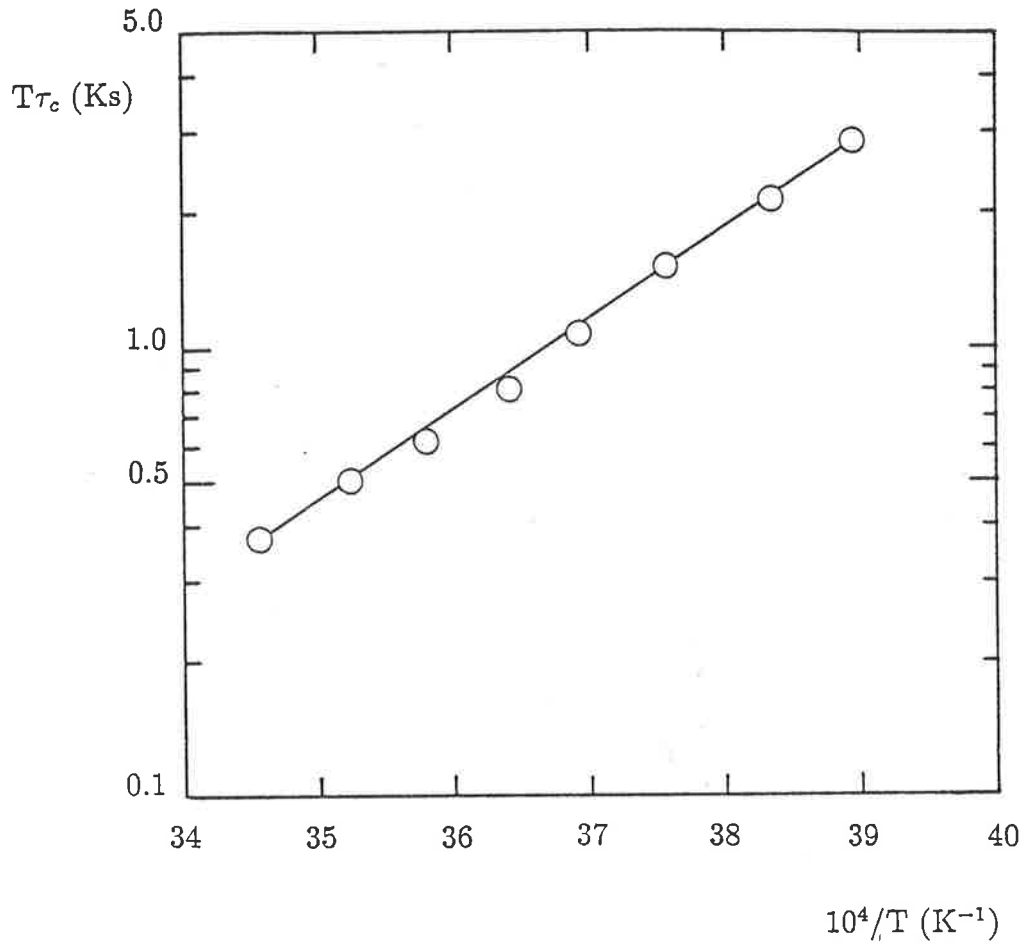

Figure 2.5:
Semilogarithmic plot of $T\tau_c$ against $\frac{10^4}{T}$ for tmu exchange on $[Dy(tmu)_6]^{3+}$ in CD_3CN solution. The solid line represents a linear regression line for the fit of the data set to the Eyring equation (Equation 6.31).

complete lineshape analysis are consequently greater. Hence, only one solution was studied in detail. Spectra of a solution of the complex alone in CD_3CN of similar concentration were recorded over the temperature range of coalescence to determine estimates of the linewidth and shift and of their variation with temperature for the complex in solution with tmu. These parameters for the free tmu could be determined from the spectra of the solution of both free and coordinated tmu at low temperature in the slow exchange limit and extrapolated into the coalescence region.

At low temperature, the 300.13 MHz ^1H nmr signal due to coordinated tmu appeared as a shoulder on the upfield side of that of the free ligand as can be seen in Figure 2.6. The sharp upfield resonance is due to the proton impurity of CD_3CN. The areas of the peaks due to tmu (estimated from lineshaping) are consistent with $[Ho(tmu)_6]^{3+}$ being the predominant holmium species in solution. Complete lineshape analysis of the coalescence of the free and coordinated tmu resonances of a CD_3CN (15.59 M) solution of $[Ho(tmu)_6](ClO_4)_3$ (0.1170 M) and tmu (0.6951 M) yielded the parameters $\Delta H^{\ddagger} = 40.9 \pm 0.9$ kJ mol^{-1}, $\Delta S^{\ddagger} = -55.9 \pm 3.1$ J K mol^{-1} and k(298.2 K) = 510 ± 20 s^{-1}. Some of the experimental spectra and best fit calculated lineshapes are shown in Figure 2.6 with the relevant temperatures and τ_c values. The spectra are also consistent with rotation about the C–N bond in tmu being fast on the nmr timescale. A semilogarithmic plot of $T\tau_c$ against $\frac{10^4}{T}$ for the solution is shown along with the linear regression line for the fit of the data to the Eyring equation (Equation 6.31) in Figure 2.7. Again, the exchange mechanism could not be determined from the variation of k_{ex} with [tmu].

2.6 Ligand Exchange on Hexakis(1,1,3,3-tetramethylurea)erbium(III)

Solutions of the complex $[Er(tmu)_6](ClO_4)_3$ and tmu in d^3-acetonitrile exhibited an ^1H resonance attributable to the coordinated ligand downfield from that of the free ligand under slow exchange conditions (Figure 2.8). Comparisons of the integrated areas of the two resonances for the three solutions whose compositions are given in Table 2.5 indicated that $[Er(tmu)_6]^{3+}$ was the predominant erbium(III)

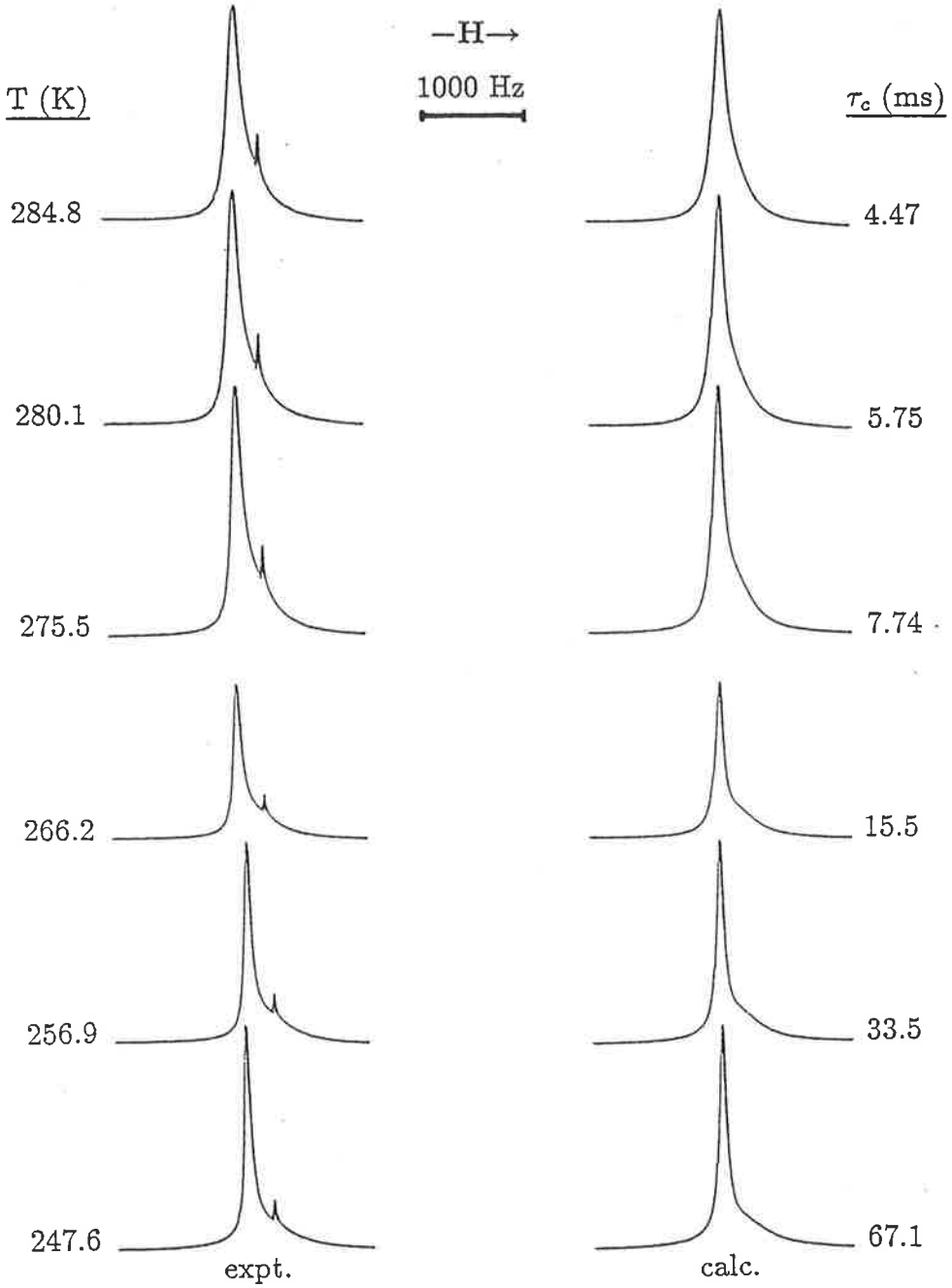

Figure 2.6:
300.13 MHz ^{1}H nmr spectra characterising ligand exchange for a CD_3CN solution (15.59 M) of $[Ho(tmu)_6](ClO_4)_3$ (0.1170 M) and tmu (0.6951 M). The experimental spectra and the corresponding temperatures appear to the left and the best fit calculated lineshapes and corresponding τ_c values appear to the right of the figure. The resonance due to coordinated tmu is the upfield shoulder on the side of the free tmu resonance and the narrow signal appearing upfield arises from the CD_3CN proton impurity.

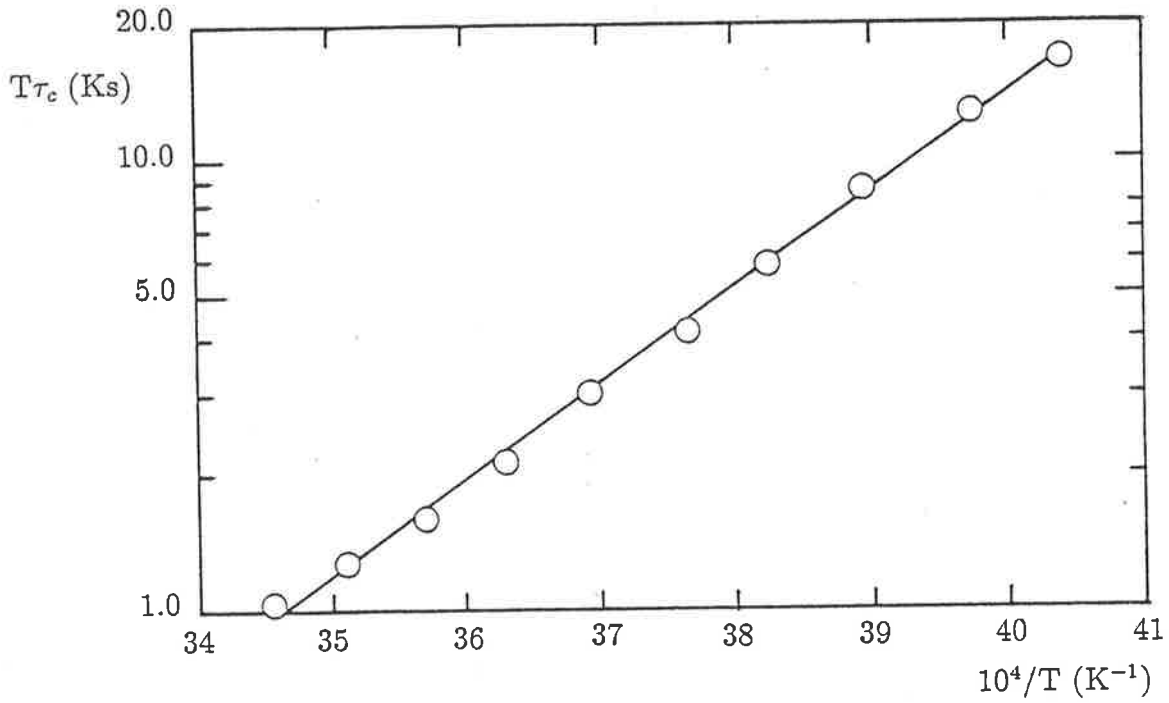

Figure 2.7:
Semilogarithmic plot of $T\tau_c$ against $\frac{10^4}{T}$ for tmu exchange on $[Ho(tmu)_6]^{3+}$ in CD_3CN solution. The solid line represents a linear regression line for the fit of the data set to the Eyring equation (Equation 6.31).

Table 2.5: Solution Compositions for Ligand Exchange of 1,1,3,3-Tetramethylurea on $[Er(tmu)_6]^{3+}$ in CD_3CN

Solution	$[[Er(tmu)_6](ClO_4)_3]$ mol dm^{-3}	$[tmu]_{free}$ mol dm^{-3}	$[CD_3CN]$ mol dm^{-3}	CN[1]
i	0.1012	0.6681	16.22	6.0 ± 0.1
ii	0.04841	0.3553	17.15	6.0 ± 0.1
iii	0.02539	0.1977	17.36	5.9 ± 0.1

[1] Coordination number (see text).

Table 2.6: Kinetic Parameters for Intermolecular Exchange of 1,1,3,3-Tetramethylurea on $[Er(tmu)_6]^{3+}$ in CD_3CN

Solution	$\Delta H^{\ddagger 1}$ $kJmol^{-1}$	$\Delta S^{\ddagger 1}$ $JK^{-1}mol^{-1}$	$k(298.2\ K)^1$ s^{-1}
i	33.8 ± 0.4	−86.6 ± 1.2	220.5 ± 1.2
ii	35.4 ± 0.5	−81.4 ± 1.5	216.5 ± 1.5
iii	37.4 ± 0.4	−75.4 ± 1.5	203.5 ± 1.4
i – iii	35.5 ± 0.5	−81.3 ± 1.7	213.6 ± 1.7

[1]Quoted errors represent one standard deviation.

species in solution. Singlet resonances for both coordinated and free tmu were observed down to 235 K consistent with rotation about the C–N bonds in tmu being in the fast exchange limit of the nmr timescale.

Complete lineshape analysis of the coalescence of the free and coordinated tmu resonances yielded the mean site lifetime of a single coordinated ligand, τ_c. Typical experimental spectra and best fit calculated lineshapes for solution (i) are depicted in Figure 2.8 with the corresponding τ_c values at that temperature. A semilogarithmic plot of $T\tau_c$ against $\frac{10^4}{T}$ for all the solutions studied is shown in Figure 2.9 and the derived kinetic parameters are given in Table 2.6.

It can be seen from the kinetic data obtained from the five solutions studied that k_{ex} (where $k_{ex} = \frac{1}{\tau_c}$) shows only a small variation over the four-fold variation in [tmu]. The 8.4% variation in k_{ex} with the 3.4-fold variation in [tmu] may, to some extent, reflect minor changes in the immediate environment of $[Er(tmu)_6]^{3+}$

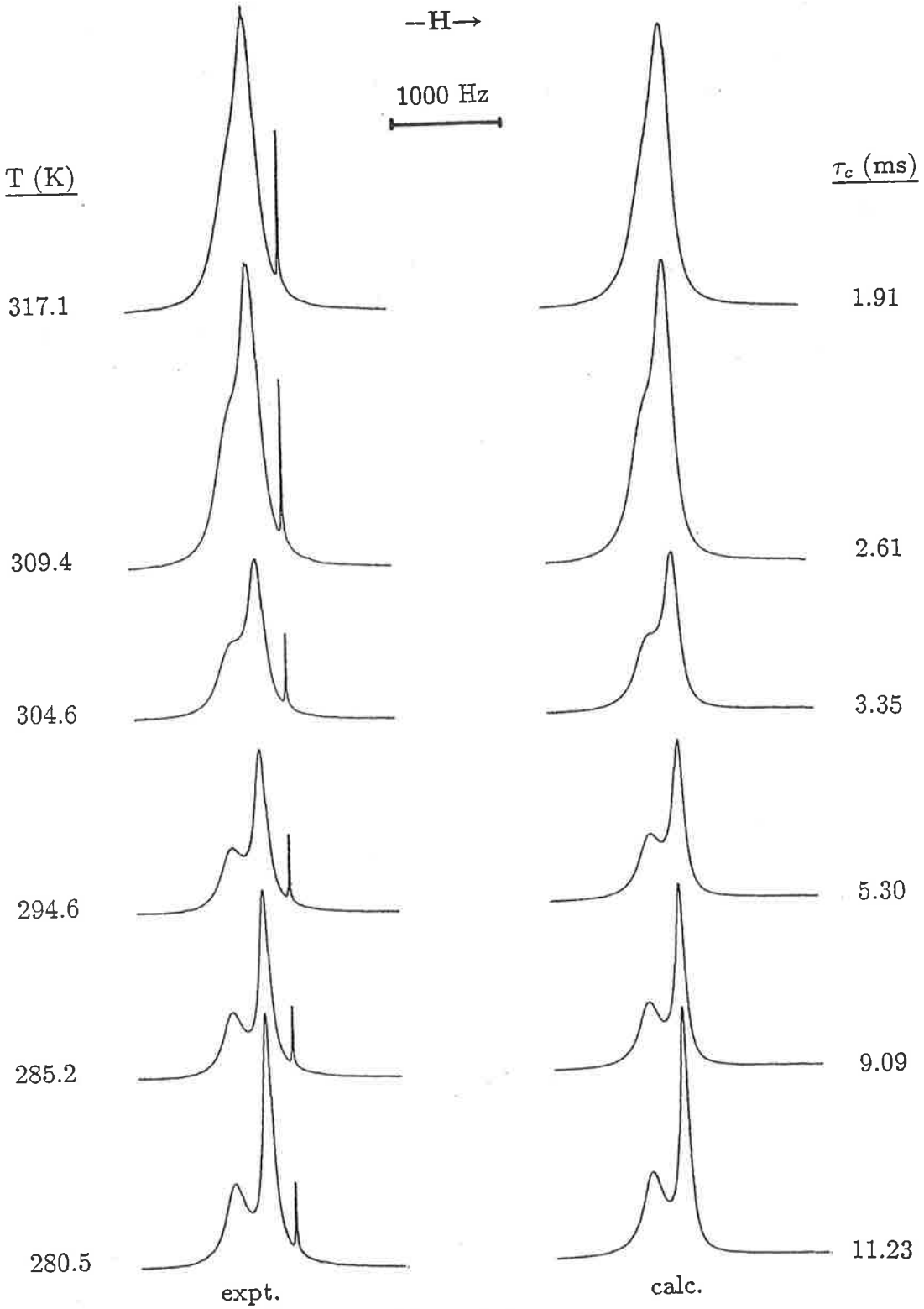

Figure 2.8:
300.13 MHz ^{1}H nmr spectra characterising ligand exchange for a solution in which [$[Er(tmu)_6](ClO_4)_3$], [tmu] and [CD_3CN] were respectively 0.1012 M, 0.6681 M and 16.22 M. The experimental spectra and the corresponding temperatures appear to the left and the best fit calculated lineshapes and corresponding τ_c values appear to the right of the figure. The resonance due to coordinated tmu is downfield.

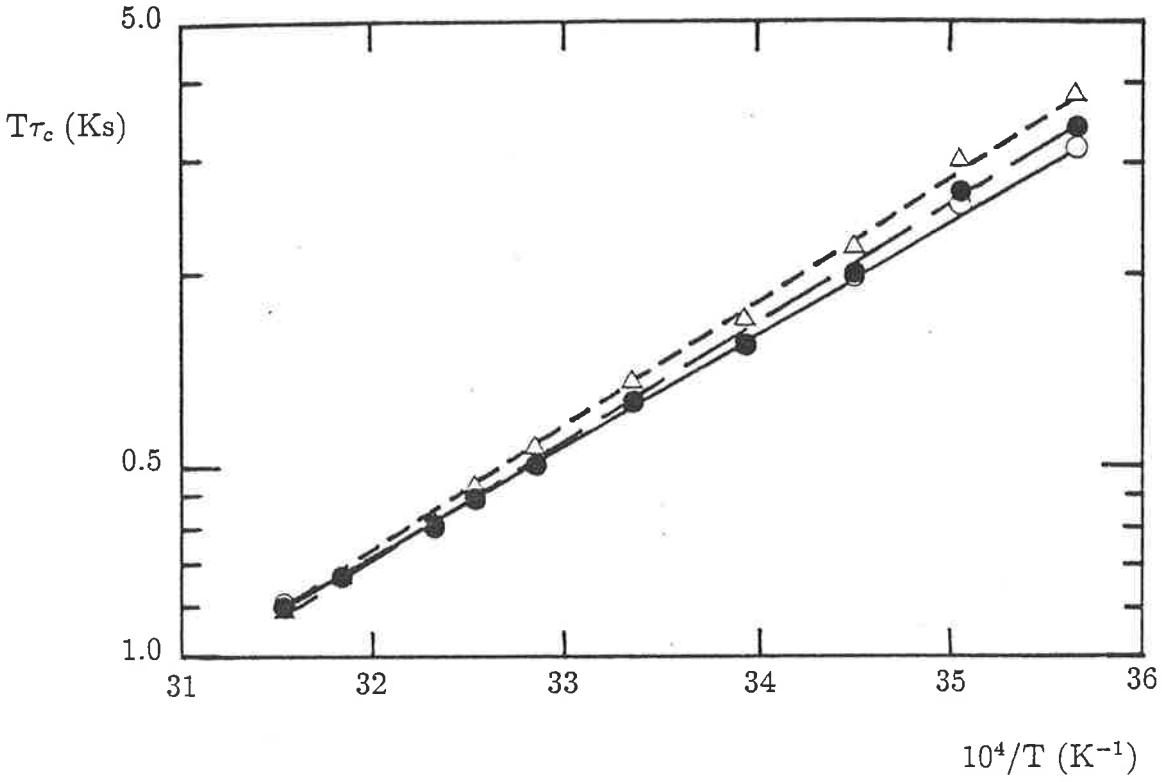

Figure 2.9:
Semilogarithmic plots of $T\tau_c$ against $\frac{10^4}{T}$ for tmu exchange on $[Er(tmu)_6]^{3+}$ in CD_3CN solution. Experimental data points and the linear regression lines for the fit of each data set to the Eyring equation (Equation 6.31) for solutions (i) to (iii) are represented respectively as (i)——○——, (ii) ——●——and (iii) — △ — .

as the concentration is altered. This is consistent with the operation of a **D** exchange mechanism in which the rate determining step is the formation of the five coordinate reactive intermediate $[Er(tmu)_5]^{3+}$. The results are also consistent with the operation of an $\mathbf{I}_d$ mechanism as described in Section 1.2. The implications of this will be discussed in Section 2.10.

2.7 Ligand Exchange on Hexakis(1,1,3,3-tetramethylurea)thulium(III)

The complex $[Tm(tmu)_6](ClO_4)_3$ was moderately hygroscopic, hydrating visibly after some hours of exposure to the atmosphere. Solutions of $[Tm(tmu)_6](ClO_4)_3$ and tmu in d^3-acetonitrile exhibited ^1H nmr singlet resonances due to the coordinated and free ligand down to 235 K consistent with rotation about the C–N bonds in tmu being in the fast exchange limit of the nmr timescale. The coordinated tmu signal appeared downfield from that of the free ligand under slow exchange conditions (Figure 2.10). Comparisons of the integrated areas of the two resonances for the four solutions studied indicated that $[Tm(tmu)_6]^{3+}$ was the predominant thulium(III) species in solution. The solution compositions are presented in Table 2.7.

The mean site lifetime of a single coordinated ligand, τ_c was determined by complete lineshape analysis of the coalescence of the free and coordinated tmu resonances. Typical experimental spectra and best fit calculated lineshapes for a solution in which the concentrations of $[Tm(tmu)_6](ClO_4)_3$, tmu and CD_3CN were 0.09220 M, 0.5167 M and 16.21 M respectively are shown in Figure 2.10. The relevant temperatures and corresponding τ_c values at that temperature are also given. The derived kinetic parameters are given in Table 2.8 and a semilogarithmic plot of $T\tau_c$ against $\frac{10^4}{T}$ is shown in Figure 2.11.

From the kinetic results obtained from the four solutions studied, it can be seen that k_{ex} does not show a systematic variation with the four-fold variation in [tmu] (the observed first order rate constant, k_{ex} is related to the lifetime of a coordinated tmu ligand by Equation 1.4). This is consistent with the operation of a **D** exchange mechanism in which the rate determining step is the loss of a ligand

Table 2.7: Solution Compositions for Ligand Exchange of 1,1,3,3-Tetramethylurea on $[Tm(tmu)_6]^{3+}$ in CD_3CN

Solution	$[[Tm(tmu)_6](ClO_4)_3]$ mol dm^{-3}	$[tmu]_{free}$ mol dm^{-3}	$[CD_3CN]$ mol dm^{-3}	CN[1]
i	0.1188	0.8675	15.47	5.9 ± 0.1
ii	0.09220	0.5167	16.21	6.0 ± 0.2
iii	0.06367	0.3568	17.00	6.0 ± 0.1
iv	0.03006	0.1753	17.84	6.0 ± 0.1

[1] Coordination number (see text).

Table 2.8: Kinetic Parameters for Intermolecular Exchange of 1,1,3,3-Tetramethylurea on $[Tm(tmu)_6]^{3+}$ in CD_3CN

Solution	$\Delta H^{\ddagger}$[1] $kJmol^{-1}$	$\Delta S^{\ddagger}$[1] $JK^{-1}mol^{-1}$	k(298.2 K)[1] s^{-1}
i	31.6 ± 0.3	−97.8 ± 1.1	141 ± 1
ii	28.6 ± 0.2	−107 ± 1	153 ± 1
iii	28.1 ± 0.4	−109 ± 1	147 ± 1
iv	29.4 ± 0.5	−105 ± 2	141 ± 2
i – iv	29.3 ± 0.3	−105 ± 1	145 ± 1

[1]Quoted errors represent one standard deviation.

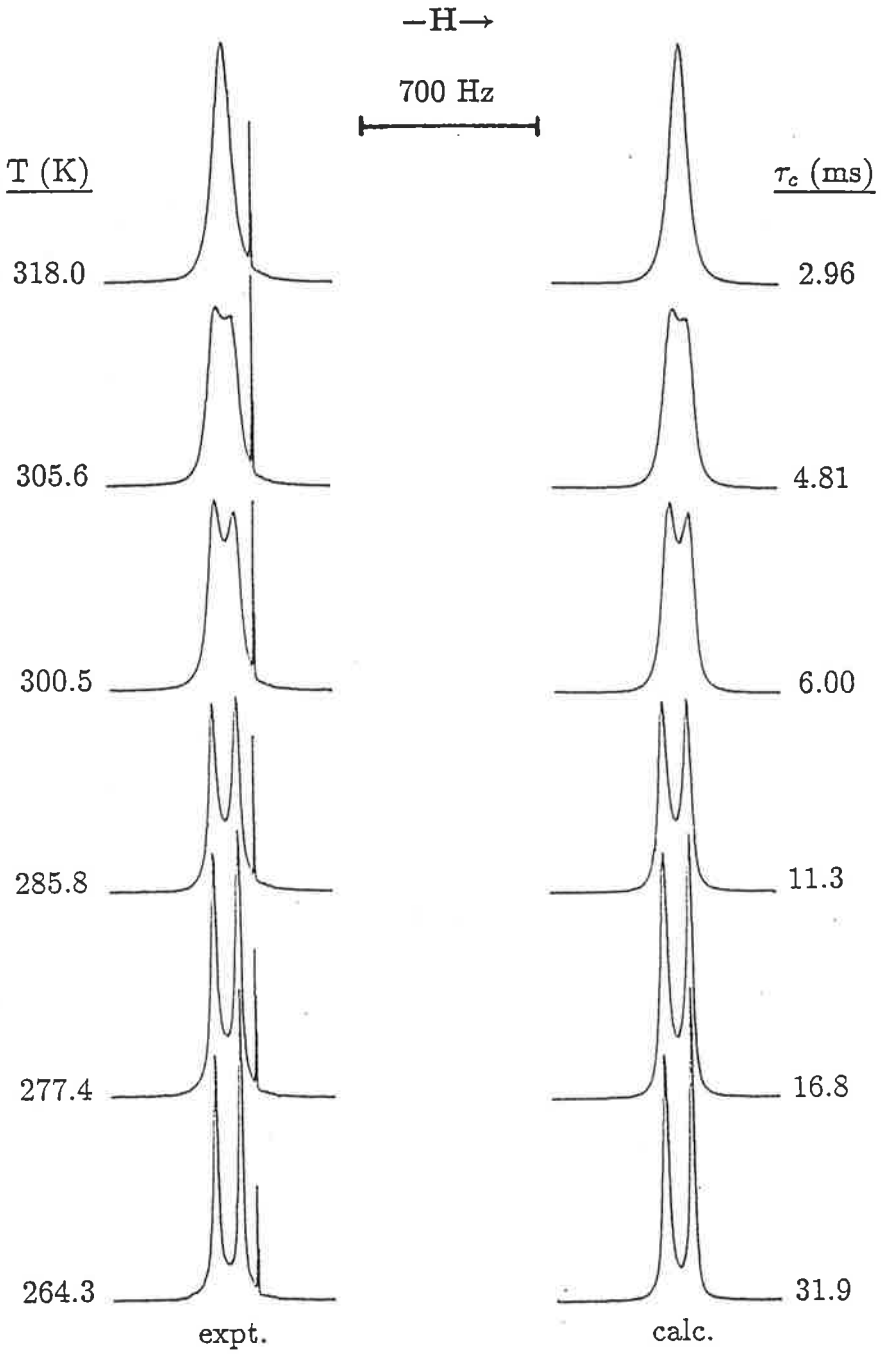

Figure 2.10:
90 MHz ^{1}H nmr spectra characterising ligand exchange for a CD_3CN solution (16.21 M) of $[Tm(tmu)_6](ClO_4)_3$ (0.09220 M) and tmu (0.5167 M). The experimental spectra and the corresponding temperatures appear to the left and the best fit calculated lineshapes and corresponding τ_c values appear to the right of the figure. The resonance due to coordinated tmu is downfield and the narrow multiplet appearing at high field arises from the CD_3CN proton impurity.

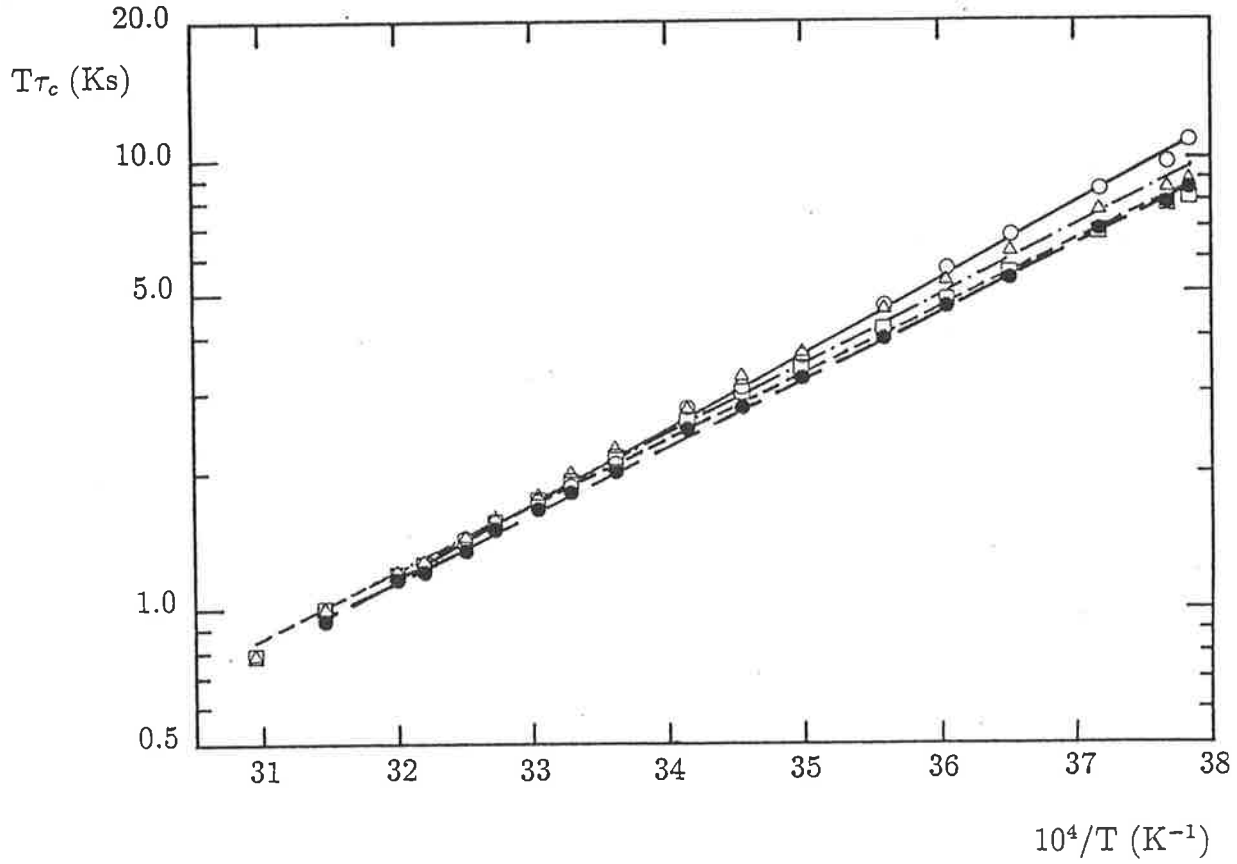

Figure 2.11:
Semilogarithmic plots of $T\tau_c$ against $\frac{10^4}{T}$ for tmu exchange on $[Tm(tmu)_6]^{3+}$ in CD_3CN solution. Experimental data points and the linear regression lines for the fit of each data set to the Eyring equation (Equation 6.31) for solutions (i) to (iv) are represented respectively as (i) —○—, (ii) —●—, (iii)– –□– – and (iv) –·△–·–.
The lines for solutions (iii) and (iv) are coincident at high temperatures.

to form a five coordinate reactive intermediate $[Tm(tmu)_5]^{3+}$. For similar reasons to those discussed in Section 1.2, although the results are also consistent with an I_d mechanism, this is not considered a likely possibility.

A study of the ligand exchange processes on this complex has also been attempted in CD_3NO_2 [50] but proved intractable. The population of free tmu was found to increase significantly on increasing the temperature from the slow exchange region. This is presumably due to the complex losing ligands to form a complex of lower coordination number. Vicentini and Nunes [24 (d)] employed a similar effect for the preparation of $Ln(tmu)_2(ReO_4)_3$ from $Ln(tmu)_5(ReO_4)_2$, (Ln = La – Nd, Sm) which involved dissolving $Ln(tmu)_5(ReO_4)_2$ in nitromethane and upon dilution with a large excess of solvent, the complex $Ln(tmu)_2(ReO_4)_3$ precipitated from solution. The perrhenate ions replace the tmu ligands by coordinating through one or two oxygen atoms. An analogous effect, although to a lesser degree, may be responsible for the observed behaviour of the perchlorate salts in nitromethane. No evidence of precipitation was found in the case of the perchlorate complexes in acetonitrile solution at the concentrations studied.

2.8 Ligand Exchange on Hexakis(1,1,3,3-tetramethylurea)ytterbium(III)

A complex of stoichiometry $[Yb(tmu)_6](ClO_4)_3$ was obtained by the method described in Chapter 5 and showed similar hygroscopic properties to the thulium complex. Solutions of the complex and tmu in d^3-acetonitrile exhibited an ^1H resonance attributable to the coordinated ligand downfield from that of the free ligand under slow exchange conditions (Figure 2.12). Comparisons of the integrated areas of the two resonances for the five solutions whose compositions are given in Table 2.9 indicated that $[Yb(tmu)_6]^{3+}$ was the predominant ytterbium(III) species in solution. Singlet resonances for both coordinated and free tmu were observed down to 235 K consistent with rotation about the C–N bonds in tmu being in the fast exchange limit of the nmr timescale.

Complete lineshape analysis of the coalescence of the free and coordinated tmu resonances yielded the mean site lifetime of a single coordinated ligand, τ_c. Typical

Table 2.9: Solution Compositions for Ligand Exchange of 1,1,3,3-Tetramethylurea on $[Yb(tmu)_6]^{3+}$ in CD_3CN

Solution	$[[Yb(tmu)_6](ClO_4)_3]$ mol dm^{-3}	$[tmu]_{free}$ mol dm^{-3}	$[CD_3CN]$ mol dm^{-3}	CN[1]
i	0.1216	0.6866	15.38	6.0 ± 0.1
ii	0.09352	0.5514	15.89	6.0 ± 0.2
iii	0.06145	0.3766	16.71	5.9 ± 0.1
iv	0.02385	0.1541	18.44	5.9 ± 0.1
v	0.01500	0.0919	18.18	5.9 ± 0.1

[1] Coordination number (see text).

Table 2.10: Kinetic Parameters for Intermolecular Exchange of 1,1,3,3-Tetramethylurea on $[Yb(tmu)_6]^{3+}$ in CD_3CN

Solution	$\Delta H^{\ddagger}$[1] $kJmol^{-1}$	$\Delta S^{\ddagger}$[1] $JK^{-1}mol^{-1}$	k(298.2 K)[1] s^{-1}
i	36.2 ± 0.8	−89.8 ± 2.6	58.5 ± 0.6
ii	36.1 ± 0.4	−89.2 ± 1.4	64.6 ± 0.4
iii	37.4 ± 0.4	−85.0 ± 1.3	63.8 ± 0.3
iv	40.5 ± 0.5	−73.6 ± 1.7	70.0 ± 0.5
v	40.5 ± 0.5	−73.8 ± 1.5	70.7 ± 0.5
i – v	38.3 ± 0.9	−81.8 ± 3.1	65.5 ± 0.9

[1] Quoted errors represent one standard deviation.

experimental spectra and best fit calculated lineshapes for solution (ii) are depicted in Figure 2.12 with the corresponding τ_c values at that temperature. A semilogarithmic plot of $T\tau_c$ against $\frac{10^4}{T}$ for all the solutions studied is shown in Figure 2.13 and the derived kinetic parameters are given in Table 2.10.

It can be seen from the kinetic data obtained from the five solutions studied that k_{ex} shows only a small variation over the 7.5-fold variation in [tmu] and actually decreases slightly with increasing [tmu] and is therefore probably not of kinetic significance. This is consistent with the operation of a **D** exchange mechanism in which the rate determining step is the formation of the five coordinate reactive intermediate $[Yb(tmu)_5]^{3+}$. The results are also consistent with an $\mathbf{I}_d$ mechanism

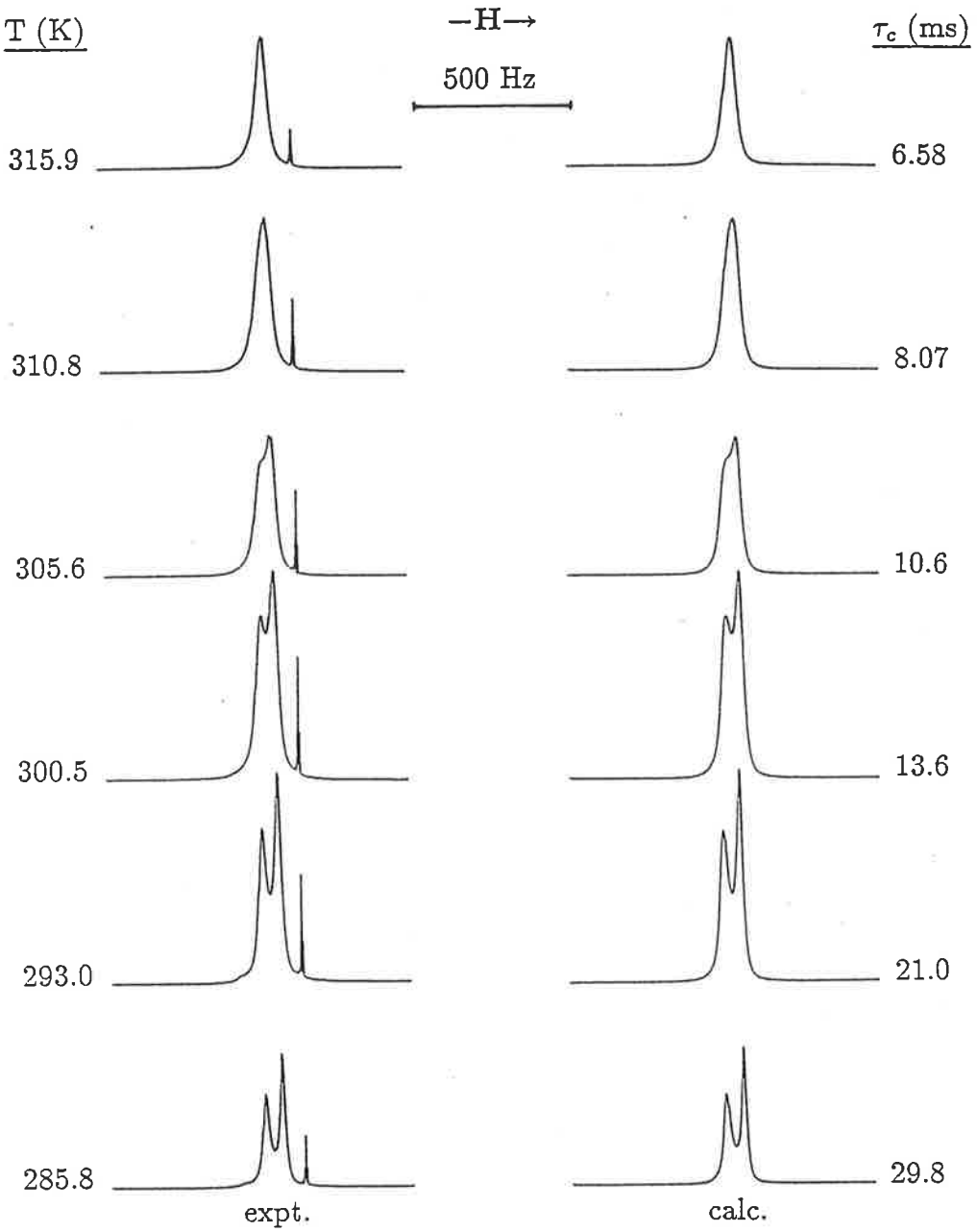

Figure 2.12:
90 MHz ^{1}H nmr spectra characterising ligand exchange for a solution in which $[[Yb(tmu)_6](ClO_4)_3]$, [tmu] and $[CD_3CN]$ were respectively 0.09352 M, 0.5514 M and 15.89 M. The experimental spectra and the corresponding temperatures appear to the left and the best fit calculated lineshapes and corresponding τ_c values appear to the right of the figure. The resonance due to coordinated tmu is downfield.

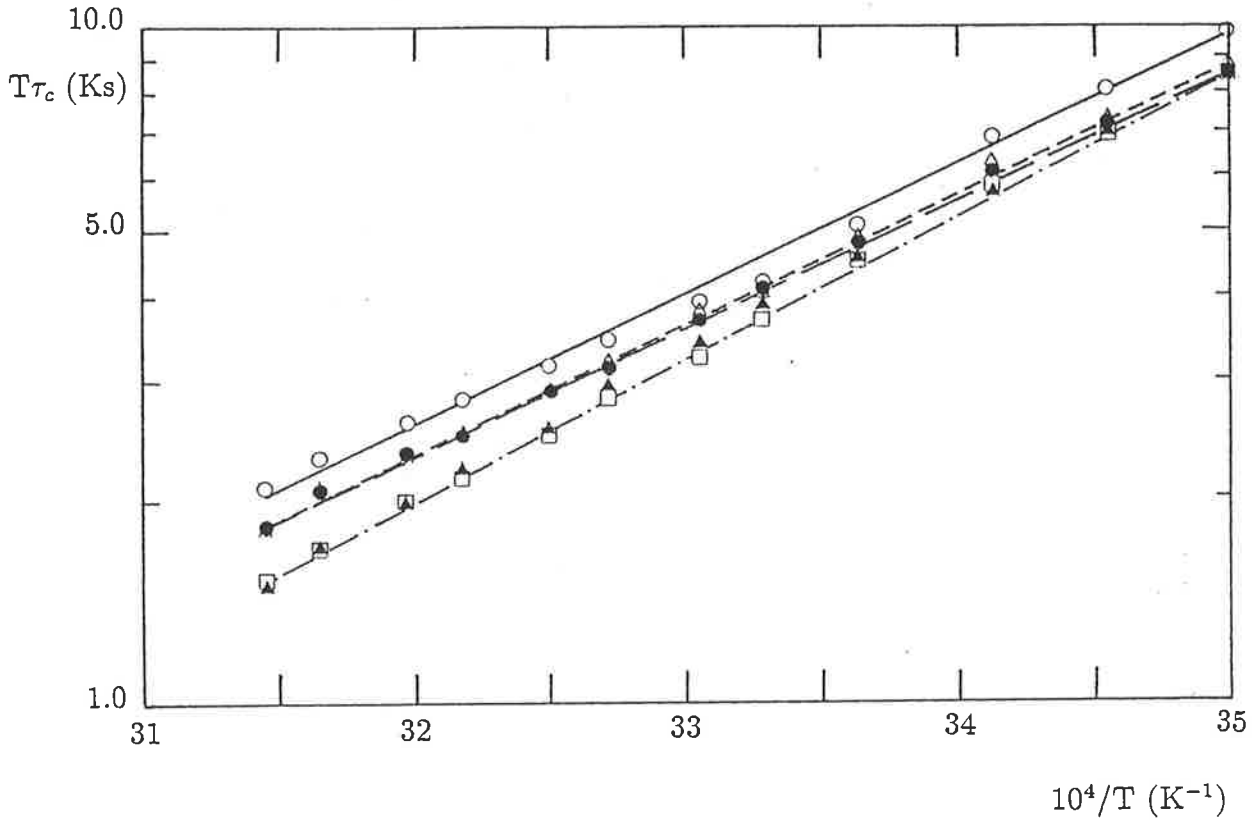

Figure 2.13:
Semilogarithmic plots of $T\tau_c$ against $\frac{10^4}{T}$ for tmu exchange on $[Yb(tmu)_6]^{3+}$ in CD_3CN solution. Experimental data points and the linear regression lines for the fit of each data set to the Eyring equation (Equation 6.31) for solutions (i) to (v) are represented respectively as (i) —○—, (ii) —●—, (iii)- –△– -, (iv) —·▲—· and (v) —·□—·. The lines for solutions (iv) and (v) are coincident.

but, as explained in Section 1.2, this is considered unlikely.

A study of the kinetics of ligand exchange on this complex has also been attempted in CD_3NO_2 [50] but again proved intractable for similar reasons to those discussed for the thulium case (Section 2.1.2).

2.9 Intramolecular Ligand Exchange on Hexakis-(1,1,3,3-tetramethylurea)lanthanide(III) Ions

Solutions of $[Pr(tmu)_6](ClO_4)_3$ and $[Tm(tmu)_6](ClO_4)_3$ in CD_2Cl_2 were studied using 300.13 MHz ^1H nmr to determine if the internal rotation about the C–N bonds could be slowed sufficiently to allow complete lineshape analysis to obtain the kinetic parameters. This solvent was chosen because the internal rotation could not be observed in CD_3CN down to the freezing point of the solutions (*ca.* 235 K) and CD_2Cl_2 has a lower freezing point (*ca.* 180 K). The metal ions were chosen to represent the lighter and heavier lanthanides respectively. However, when these solutions were run, several peaks were observed which could not be attributed solely to the slowing of the C–N bond rotation (e.g. see Figure 2.14 which shows the praseodymium case). The many peaks observed appears to indicate the presence of more than one species of unknown coordination number. The most likely explanation is that some ligands have dissociated from the complex leaving some of a species of lower coordination number (as described for the d^3-nitromethane solutions of $[Tm(tmu)_6](ClO_4)_3$ and $[Yb(tmu)_6](ClO_4)_3$). The exchange between the complexes and free ligands and the slowing of the internal rotation in the complexed ligands probably gives the complex coalescence pattern observed.

2.10 Mechanistic and Kinetic Effects of the Lanthanide Contraction

The kinetic parameters characterising the exchange of tmu on $[Ln(tmu)_6]^{3+}$ are summarised in Table 2.11. The rates of tmu exchange are about a factor of 10^4 less than those for dmf exchange on $[Ln(dmf)_8]^{3+}$ (Table 2.3) [9] and a factor of *ca.* 10^5 less than those for H_2O exchange on $[Ln(H_2O)_9]^{3+}$ (Table 2.2) [31,8]. All of

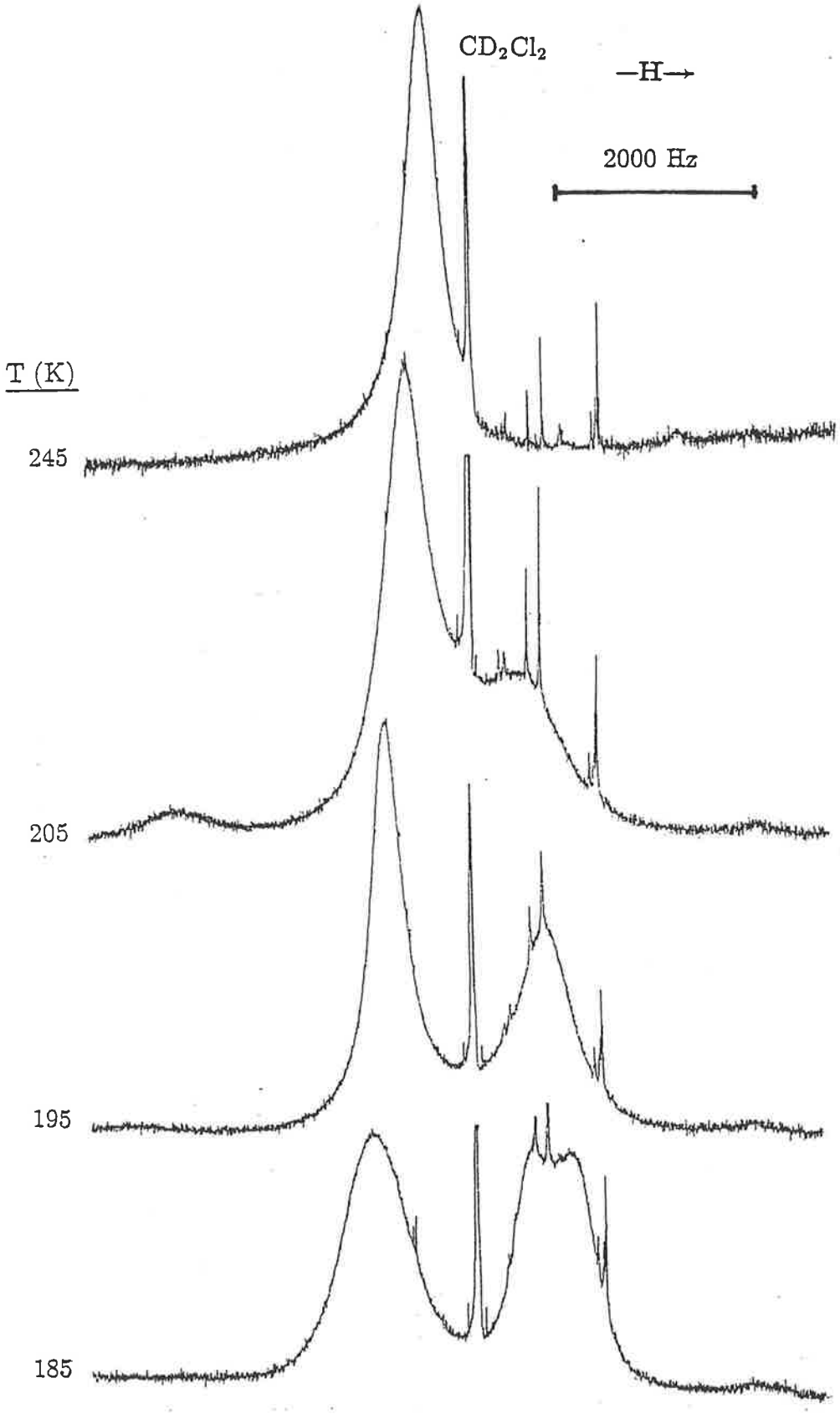

Figure 2.14:
300.13 MHz ^1H nmr spectra of a solution in which [$[Pr(tmu)_6](ClO_4)_3$] and [CD_2Cl_2] were respectively 0.02909 M and 14.6884 M. The corresponding temperatures appear to the left.

Table 2.11: Kinetic Parameters Characterising Exchange of tmu on $[Ln(tmu)_6]^{3+}$

Ln^{3+}	$r(M^{3+})$[1] pm	$k(298\ K)$[2] s^{-1}	$\Delta H^{\ddagger}$ [1] kJ mol^{-1}	$\Delta S^{\ddagger}$ [1] J $K\ mol^{-1}$
Y[3]	90.0	253	27.1 ± 0.5	−108 ± 2
Tb	92.3	1377 ± 21	38.2 ± 0.5	−56.7 ± 1.8
Dy	91.2	1285 ± 33	38.6 ± 0.7	−56.0 ± 2.4
Ho	90.1	510 ± 20	40.9 ± 0.9	−55.9 ± 3.1
Er	89.0	213.6 ± 1.7	35.5 ± 0.5	−81.3 ± 1.7
Tm	88.0	145.2 ± 1.1	29.3 ± 0.3	−105.4 ± 1.1
Yb	86.8	65.5 ± 0.9	38.3 ± 1.0	−81.8 ± 3.1
Lu[4]	86.1	41.9 ± 2.7	41.7 ± 0.6	−74 ± 2
Sc[5]	74.5	0.90	68.6 ± 1.3	−15.7 ± 3.8

[1] Effective ionic radius [11].
[2] Quoted errors represent one standard deviation.
[3] Reference [30].
[4] Reference [28].
[5] Reference [29].

these ligands are oxygen donor ligands and tmu and dmf are of comparable electron donating ability having Gutmann donor numbers of 29.6 and 26.6 respectively [52]. Thus, the greater lability of $[Ln(dmf)_8]^{3+}$ and $[Ln(H_2O)_9]^{3+}$ must be mainly a consequence of the greater coordination number and resultant greater effective ionic radii of these complexes. This gives longer and weaker Ln–O bonds compared to those in $[Ln(tmu)_6]^{3+}$, decreasing the energy required to break the bond (decreasing $\Delta H^{\ddagger}$) and increasing the lability of exchange. Further evidence of these longer Ln–O bonds comes from the observed solid state Er–O bond lengths in the tricapped trigonal prismatic $[Er(H_2O)_9]^{3+}$. The capping and prismatic Er–OH_2 bond lengths are 2.52 and 2.37 Å respectively [53] compared with bond lengths of 2.185 – 2.198 Å in the octahedral $[Er(tmu)_6]^{3+}$ [27]. The tricapped trigonal prismatic geometry, due to the longer lanthanide to capping ligand bonds, may also enhance the lability. In the solid state, the Ln to capping water bonds in $[Ln(H_2O)_9]^{3+}$ (Ln = Y, La, Pr, Sm, Gd, Ho, Er, Yb and Lu) [34], are 1.01 – 1.09 times longer than the Ln to prismatic water bonds.

The rates of exchange of tmu on $[Ln(tmu)_6]^{3+}$ decrease monotonically with de-

creasing effective ionic radius from terbium to lutetium. A similar trend is observed in k(200 K) for dmf exchange on $[Ln(dmf)_8]^{3+}$ for Ln = Tb – Yb and k(298 K) for H_2O exchange on $[Ln(H_2O)_9]^{3+}$ for Ln = Gd – Yb (Tables 2.3 and 2.2 and Figure 2.15). The activation parameters, $\Delta H^{\ddagger}$ and $\Delta S^{\ddagger}$, for these systems are plotted against $10^4/r$ in Figure 2.16. The change in effective ionic radius on changing the coordination number causes the different plots to appear in different regions of the graph. The $\Delta H^{\ddagger}$ values for each system are shown as open symbols and $\Delta S^{\ddagger}$ values are shown as filled symbols.

The trends in the values for the H_2O and dmf systems have been discussed in Section 2.1.2. The rates of exchange of tmu on $[Ln(tmu)_6]^{3+}$ are significantly lower than those for dmf exchange on $[Ln(dmf)_8]^{3+}$ and H_2O exchange on $[Ln(H_2O)_9]^{3+}$ which appears to be a consequence of the generally higher $\Delta H^{\ddagger}$ values (due to the lower coordination number and consequently shorter, and stronger, Ln–O bonds) and more negative $\Delta S^{\ddagger}$ values. Some of the differences in values between these three systems may be attributable to different experimental conditions. For example, the parameters for the dmf systems were obtained in neat dmf and the mechanisms determined using CD_3NO_2 as diluent while the tmu systems were studied using CD_3CN diluent which could have a marked effect on the activation parameters and even the mechanism. This is the case for several ligand exchange studies on Sc^{3+} in Table 2.4 (For example, tmp exchange on $[Sc(tmp)_6]^{3+}$ proceeds via an **A** mechanism in CD_3NO_2 while proceeding via a **D** mechanism in CD_3CN [43]).

In the simplest analysis, it is expected that $\Delta S^{\ddagger}$ will be positive for a dissociatively activated exchange process due to the increased degree of freedom available to the transition state as a consequence of the lengthening of one chemical bond as a ligand leaves the first coordination sphere. Conversely, for an associatively activated exchange process, $\Delta S^{\ddagger}$ would be expected to be negative due to the decreased degree of freedom available to the transition state as an incoming ligand enters the first coordination sphere. For the tmu system, all the $\Delta S^{\ddagger}$ values are negative even though **D** mechanisms are assigned for the exchange processes for Tm^{3+}, Yb^{3+} and Lu^{3+}. Similarly, all the values of $\Delta S^{\ddagger}$ for water and those for dmf exchange on Tb – Er are also negative. An inspection of Table 2.4 reveals that the

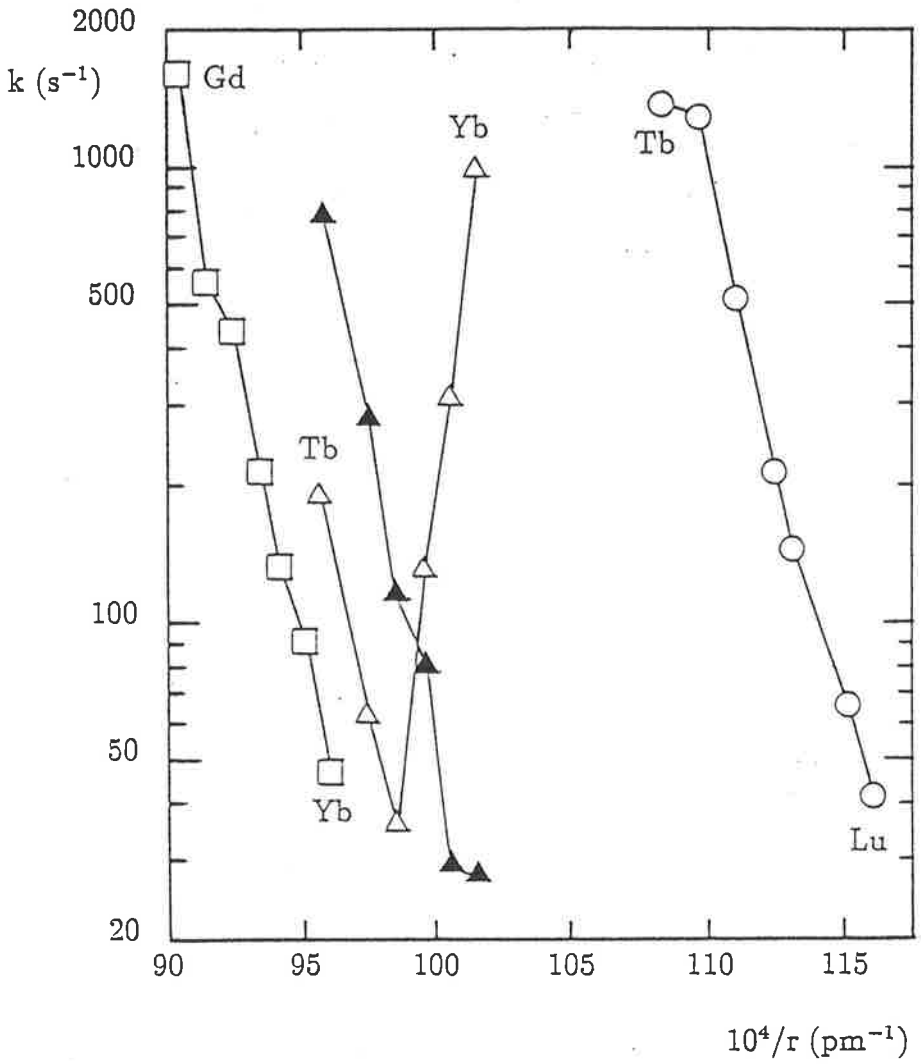

Figure 2.15:
Semilogarithmic plots of 10^{-6}k(298 K) for H_2O exchange on $[Ln(H_2O)_9]^{3+}$ (○) [8], 10^{-5}k(298 K) and 10^{-3}k(200 K) for dmf exchange on $[Ln(dmf)_8]^{3+}$ (△ and ▲ respectively) [9] and k(298 K) for tmu exchange on $[Ln(tmu)_6]^{3+}$ (□) against 10^4/r.

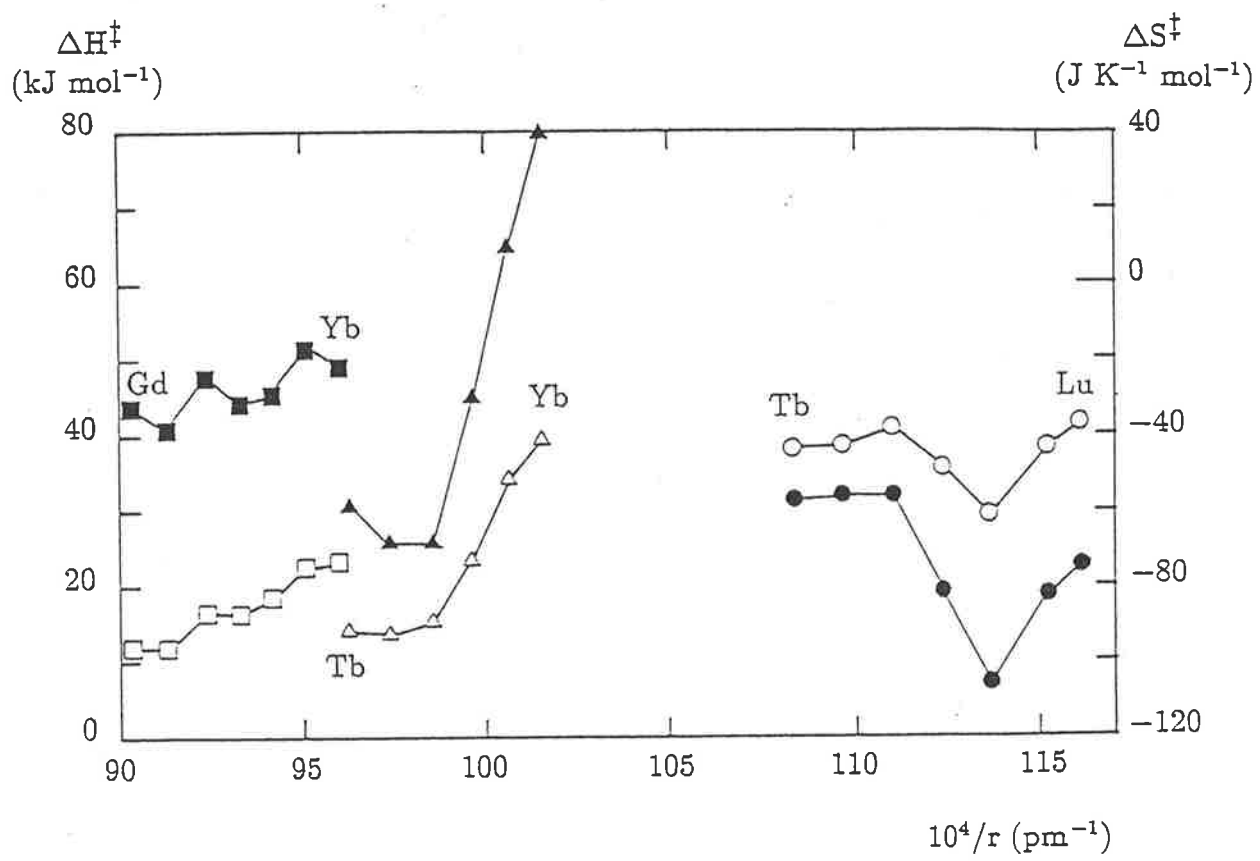

Figure 2.16:
Plots of $\Delta H^{\ddagger}$ and $\Delta S^{\ddagger}$ against $10^4/r$ for $[Ln(H_2O)_9]^{3+}$ (square symbols) [8], $[Ln(dmf)_8]^{3+}$ (triangles) [9] and $[Ln(tmu)_6]^{3+}$ (circles). The $\Delta H^{\ddagger}$ values are represented by open symbols and the $\Delta S^{\ddagger}$ values by filled symbols. The scales for $\Delta H^{\ddagger}$ and $\Delta S^{\ddagger}$ appear on the left and right of the figure respectively.

$\Delta S^{\ddagger}$ values are generally negative for exchange on Sc^{3+} and Y^{3+} regardless of the assigned mechanism. The only cases where $\Delta S^{\ddagger}$ is positive occur when CD_3NO_2 is used as the diluent. Thus it appears that there is a significant contribution to $\Delta S^{\ddagger}$ from interactions outside the first coordination sphere. These interactions appear particularly feasible for the trivalent lanthanide ions in view of their propensity for high coordination numbers.

As described in Section 2.1.2, the tricapped trigonal prismatic structure has been established for $[Ln(H_2O)_9]^{3+}$ [34], and the water molecules may rapidly interchange via a capped square antiprism intermediate in solution. If the tricapped trigonal prism is taken as the reference geometry for $[Ln(tmu)_6]^{3+}$, as one Ln–tmu bond lengthens to form the dissociative transition state, and the outgoing tmu assumes some of the character of a capping ligand, the remaining five tmu ligands may rearrange (with concomitant changes in bond lengths and angles) towards a trigonal prismatic geometry. Simultaneously, an incoming tmu molecule comes into position from the capping position to take the vacant place in the sixth prismatic position. This geometric rearrangement is particularly possible for lanthanide ions as there is no loss of ligand field stabilisation energy on changing the geometry from octahedral to trigonal prismatic. Due to the steric bulk of the tmu molecules, the ligands in the capping positions are likely to be more distant, relative to those in the prismatic positions, than those in $[Ln(H_2O)_9]^{3+}$ and hence the interactions between capping acetonitrile molecules and the metal ion are expected to be much weaker. Nevertheless, this mechanism would produce considerable ordering into the second coordination sphere and a substantial negative entropy contribution to the transition state leading to a negative $\Delta S^{\ddagger}$ even though the tmu exchange process is dissociative. This contribution appears to be greater in d^3-acetonitrile solution than in d^3-nitromethane, leading to the negative $\Delta S^{\ddagger}$ values observed in Tables 2.4 and 2.11. This is possibly a result of the greater donor number of acetonitrile (14.1) than nitromethane (2.7) [52]. The dielectric constants for these solvents are similar (38.0 and 35.9 respectively) so that this is probably not a significant factor.

This proposed mechanism is highly idealised, but it does suggest that in the ligand exchange processes of the six-coordinate trivalent lanthanides, the second

coordination sphere may need to be considered to a much greater extent than in studies of lighter six-coordinate metal ions. For example, for the smaller Sc^{3+} ion with monodentate ligands there appears to be no reported case of a coordination number greater than six and it seems likely that the involvement of the second coordination sphere in the $[Sc(tmu)_6]^{3+}$ exchange process would not be as significant as for $[Ln(tmu)_6]^{3+}$. Similarly, the involvement of the second coordination sphere is not expected to be as significant for $[Ln(dmf)_8]^{3+}$ as for $[Ln(tmu)_6]^{3+}$ as the surface charge density is lower due the greater effective ionic radius making the electrostatic interaction with the second coordination sphere to be weaker. However, the dmf complexes could interact with the second coordination sphere via the capped square antiprism geometry mentioned earlier and this may be responsible for the the observed interchange mechanism in the lighter lanthanides [9].

For $[Ln(tmu)_6]^{3+}$, a plot of $\Delta H^{\ddagger}$ and $\Delta S^{\ddagger}$ against $10^4/r$ (Figure 2.16) reveals that as r decreases, $\Delta H^{\ddagger}$ is practically constant from Tb – Ho, decreases from Ho – Tm and then increases from Tm – Lu. Similarly, $\Delta S^{\ddagger}$ is almost constant from Tb – Ho, becomes more negative from Ho – Tm and less negative from Tm – Lu. This may be indicative of a mechanistic crossover on proceeding along the series from terbium to ytterbium similar to that observed for exchange on the dmf complexes of the lanthanides [9]. In the case of these dmf complexes, an interchange mechanism prevails for Tb – Er and a **D** mechanism for Tm and Yb. For the tmu complex of erbium, $[Er(tmu)_6]^{3+}$, the plot of $T\tau_c$ against $\frac{10^4}{T}$ (Figure 2.9), illustrates the slight dependence of the rate on [tmu]. This may be a consequence of the operation of an $\mathbf{I}_d$ mechanism. If this is the case, it appears that the mechanisms of ligand exchange on $[Ln(tmu)_6]^{3+}$ could reflect those of $[Ln(dmf)_8]^{3+}$ with an $\mathbf{I}_d$ mechanism predominating for Tb – Er and a **D** mechanism prevailing for Tm – Lu. The trend in the values of k(298 K) for these complexes (Table 2.11 and Figure 2.15) is consistent with this explanation as the values of k_i for an $\mathbf{I}_d$ mechanism are expected to be approximately those for k_1 for a **D** mechanism as M–L bond breaking is the rate determining step in both, as discussed in Section 1.2. For the tmu complexes of the elements across the series from La to Lu, there may be a progression from an **A** mechanism to $\mathbf{I}_a$, $\mathbf{I}_d$ and finally **D** similar to that believed to occur for the dmf

complexes discussed in Section 2.1.2.

If, on the other hand, there is no change in mechanism across the lanthanide series, the observed changes in $\Delta H^{\ddagger}$ and $\Delta S^{\ddagger}$ (Table 2.11 and Figure 2.16) may be rationalised in the following way. As r decreases, the surface charge density increases and the ionic field increases. This has two effects. Firstly, the Ln–O bond strength increases, increasing $\Delta H^{\ddagger}$, which also increases $\Delta S^{\ddagger}$ because as the bond strength increases (increasing $\Delta H^{\ddagger}$) the freedom of movement of ligands in the ground state decreases (increasing $\Delta S^{\ddagger}$). Secondly, the electrostatic interaction with the second coordination sphere increases, decreasing the difference in energy between the ligands in the first and second coordination spheres and hence decreasing $\Delta H^{\ddagger}$ and $\Delta S^{\ddagger}$. Superimposed on these effects are steric and geometric factors. As the radius decreases, the steric crowding around the ion might be expected to favour the five-coordinate intermediate (just as in $[Ln(dmf)_8]^{3+}$ a nine-coordinate intermediate is favoured for the lighter lanthanides) and hence decrease $\Delta H^{\ddagger}$ and $\Delta S^{\ddagger}$. How the decreasing radius might affect the relative stabilities of various geometries is not known but it may be assumed that there is some effect on the activation parameters.

Thus it appears that contributions to $\Delta H^{\ddagger}$ and $\Delta S^{\ddagger}$ come from several effects whose contributions vary as the ionic radius changes. This may be the reason for the observed values for these parameters for $[Ln(tmu)_6]^{3+}$. For $[Ln(dmf)_8]^{3+}$ and $[Ln(H_2O)_9]^{3+}$, because of their larger coordination number and consequently larger ionic radii, the effects are likely to be quite different. In particular, the effects from outside the first coordination sphere would be expected to have much less effect. For these systems, the dominant effect appears to be the increase in surface charge density increasing $\Delta H^{\ddagger}$ and $\Delta S^{\ddagger}$ as the radius decreases. These effects are besides those which arise from the different ligands complexation abilities and steric interactions which are responsible for the different coordination numbers observed in the different complexes.

2.11 Other Lanthanide(III) Complex Exchange Studies

2.11.1 1,1,3-Trimethylurea Complex of Ytterbium(III)

Several attempts to prepare a complex of ytterbium perchlorate with 1,1,3-trimethylurea resulted in complexes of stoichiometry $Yb(trmu)_x(ClO_4)_3$ with x = 6.3, 4.5 and 4.3 as measured by metal analysis (Section 5.3). The infrared spectra did not show conclusively the presence or absence of coordinated perchlorate due to ligand absorbances in the regions of the perchlorate absorbances [23]. A solution of the complex of the latter stoichiometry (0.05829 M) and 1,1,3-trimethylurea (0.3909 M) in CD_3CN (17.23 M) was observed using 300.13 MHz nmr to determine the coordination number in solution and, if possible, study the ligand exchange. Unfortunately, the spectra were very complex with resonances that were not readily assignable and probably indicate the presence of various species of differing coordination numbers. These lanthanide-trmu complex studies were therefore discontinued.

2.11.2 Trifluoromethanesulphonate Complexes

At the beginning of this work, it appeared, for several reasons, that the ideal complexes to prepare were trifluoromethanesulphonate salts. The anion was known to not coordinate for several lanthanide complexes of hmpa [54], H_2O [34,55] and several cyclic ureas [55] both in the solid state and in solution (however, trifluoromethanesulphonate is known to coordinate in many other compounds such as $[Co(NH_3)_5(CF_3SO_3)](CF_3SO_3)_2$ [56]). Trifluoromethanesulphonic acid is readily available and the complexes can be prepared with relative safety compared to perchlorate complexes (explosions of compounds of the latter anion are well documented [57,58, and references therein]).

Several lanthanide trifluoromethanesulphonate complexes of tmu were prepared as described in Chapter 5. The compounds displayed reasonable six-coordinate stoichiometry in the solid compounds (Table 5.1). Five d^3-acetonitrile solutions of $Tm(tmu)_6(CF_3SO_3)_3$ and tmu were prepared with complex concentrations ranging from 0.03424 M to 0.1216 M. Ninety megahertz nmr spectra were recorded of the

solutions over the temperature range 235 – 335 K and lineshaping was attempted in the normal way. In each case, the population of coordinated tmu was found to decrease by about 50% over this temperature range while the free tmu population increased by the same amount. This is consistent with a decrease in the number of tmu ligands coordinated to the metal ion which is probably a consequence of the coordination of the trifluoromethanesulphonate anion. This was subsequently confirmed by the studies using perchlorate anion where no population variation was observed. Hence, the trifluoromethanesulphonate complex studies were discontinued and the lanthanide studies restricted to complexes with perchlorate as the anion.

Chapter 3

Intra- and Inter-molecular Ligand Exchange on Dioxouranium(VI) Complexes

3.1 Introduction

3.1.1 Dioxouranium(VI) Complexes

The dioxouranium(VI) ion, UO_2^{2+}, is linear, or approximately so [59], with the oxo ligands trans to each other. This structure has been confirmed by many crystal structures (e.g. [60,61,62,63,64,65] and [66,67, and references therein]) showing octahedral and pentagonal bipyramidal geometry respectively when four or five other ligand donor atoms are coordinated. The oxo ligands are kinetically inert [68,69] and restrict the coordination of other ligands to an equitorial plane. Thus the UO_2^{2+} cation provides an opportunity to study inter- and intra-molecular exchange processes in a well-defined sterically hindered environment.

The simplest dioxouranium(VI) complexes are those containing only a single type of monodentate oxygen donor ligand. Some of these complexes that have been reported either in the solid state or in solution are presented in Table 3.1. Several of these complexes are closely related in that the oxygen donor atom is part of a carbonyl group. These are complexes of formamides, acetamides and ureas.

Table 3.1: Some Reported Dioxouranium(VI) Complexes of Monodentate Oxygen Donor Ligands

Complex	Reference	Complex	Reference
$[UO_2(hmpa)_4](ClO_4)_2$	[60,70,71,72]	$[UO_2(H_2O)_4](ClO_4)_2$	[73]
$[UO_2(tmu)_4](ClO_4)_2$	[10]	$[UO_2(urea)_5](NO_3)_2$	[74]
$[UO_2(dea)_5](ClO_4)_2$	[75]	$[UO_2(dma)_5](ClO_4)_2$	[76]
$[UO_2(dmf)_5](ClO_4)_2$	[77]	$[UO_2(dmmp)_5](ClO_4)_2$	[78]
$[UO_2(dmso)_5](ClO_4)_2$	[79]	$[UO_2(fpr)_5](ClO_4)_2$	[80]
$[UO_2(nma)_5](ClO_4)_2$	[81]	$[UO_2(tep)_5](ClO_4)_2$	[82]
$[UO_2(tmp)_5](ClO_4)_2$	[82]	$[UO_2(OPMe_2Ph)_5](ClO_4)_2$	[83]

3.1.2 Previous Intramolecular Ligand Exchange Studies on Dioxouranium(VI) Complexes

It has been found that coordination of formamides and acetamides through oxygen can substantially decrease the rate of rotation about the carbon–nitrogen bond in these ligands [84,85]. For a urea this effect has been observed for 1,1,3,3-tetramethylurea (tmu) on coordination to dioxouranium(VI) [10] which is of particular interest as tmu and several other ureas have a particularly low barrier to rotation about the carbonyl–nitrogen bond in comparison with formamides and acetamides. This is a consequence of the delocalisation of the lone pair on each urea nitrogen electronically stabilising the excited state of the other and steric destabilisation of the ground state of the other by the bulky substituents [86,87]. This slowing of the C–N bond rotation of tmu on coordination was also observed in complexes of the lanthanides in this work (Section 2.1.2) but under conditions which prevented the determination of quantitative kinetic data. Hence, the complexes of dioxouranium(VI) with several substituted ureas were investigated to compare with these systems and to determine if the decrease in the rate of rotation on coordination is general for these ligands.

Intramolecular rearrangements of bidentate ligands in dioxouranium(VI) complexes have been reported [88,89,90,91,92] but, in general, these processes involve dissociation of at least one end of the ligand as the rate-determining step and so are not analogous to the intramolecular rotation in formamides, acetamides and ureas and so will not be discussed in detail.

3.1.3 Previous Intermolecular Ligand Exchange Studies on Dioxouranium(VI) Complexes

The intermolecular exchange for several seven-coordinate dioxouranium(VI) complexes, $[UO_2(L)_5]^{2+}$, where L is a neutral monodentate oxygen-donor ligand (including tmu [10], dea [75], dma [76], dmmp [78], dmso [79], nma [81], tep [82], tmp [82] dmf [77], and $OPMe_2Ph$ [83]) is found to take place through a **D** type [4] mechanism in which the intermediate is of the type $[UO_2(L)_4]^{2+}$. The rate law for this type of exchange process is:

$$\text{exchange rate} \quad = \quad 5k_{ex}[[UO_2(L)_5]^{2+}]$$

and is independent of the concentration of free ligand. These results will be discussed in more detail in Section 3.6.

On the other hand, the exchange of fpr (N-formylpyrrolidine) on $[UO_2(fpr)_5]^{2+}$ is characterised [80] by a two-term rate law:

$$\text{exchange rate} \quad = \quad 5(k_1 + k_2[fpr])[[UO_2(fpr)_5]^{2+}].$$

In this case, a proportion of the exchange occurs through a **D** mechanism, and a proportion through either a dissociative interchange ($\mathbf{I}_d$) or, more probably, an associative (**A**) mechanism. The operation of the latter mechanism has been rationalised in terms of the conformational restriction of the pyrrolidine ring favouring the high degree of ordering required by the **A** transition state, $[UO(fpr)_6]^{2+}$ [75]. The exchange of hmpa on $[UO_2(hmpa)_4]^{2+}$ is also consistent with a two term rate law [71]:

$$\text{exchange rate} \quad = \quad 4(k_1 + k_2[hmpa])[[UO_2(hmpa)_4]^{2+}].$$

For this complex, a combination of the stabilisation of a species of low coordination number by the size and high donicity (DN = 38.8) of hmpa and the ability of the dioxouranium(VI) ion to accommodate more ligands in the equatorial plane probably leads to transition states for the **D** mechanism ($[UO_2(hmpa)_3]^{2+}$) and the **A** mechanism ($[UO_2(hmpa)_5]^{2+}$) of similar energy providing parallel paths for ligand exchange.

Thus, intermolecular exchange on the dioxouranium(VI) ion is capable of proceeding through a variety of mechanisms depending on the number and type of ligands coordinated. The intermolecular exchange of tmu in lanthanide complexes was found to be amenable to study (Chapter 2) and hence the exchange of substituted ureas on dioxouranium(VI) complexes were investigated, where possible, to compare with these results.

3.2 Intramolecular Ligand Exchange on Pentakis(1,1-dimethylurea)dioxouranium(VI)

The method described in Chapter 5 was used to prepare the dioxouranium(VI) complex of 1,1-dimethylurea (1,1-dmu), $[UO_2(1,1\text{-dmu})_5](ClO_4)_2$. In CD_3CN solution at 233.7 K, $[UO_2(1,1\text{-dmu})_5]^{2+}$ exhibits ^1H nmr doublets for the $-NH_2$ ($\delta = 6.14$ and 5.79 ppm) and $-NMe_2$ ($\delta = 3.21$ and 3.11 ppm) groups of 1,1-dmu consistent with rotation about both carbonyl–nitrogen bonds occurring slowly on the nmr timescale as shown in Figures 3.2 and 3.4. As the temperature was increased, these doublets coalesced to singlets over the temperature ranges 233.7 – 260.8 K for $-NH_2$ and 246.9 – 275.9 K for $-NMe_2$ consistent with the rate of rotation about the carbonyl–nitrogen bonds increasing. Complete lineshape analysis of these coalescing doublets was performed as outlined in Section 6.2 and the kinetic parameters for rotation about these bonds are presented in Table 3.4 in Section 3.5. In the case of the $-NH_2$ resonances, the observed first order rate constants, k_{ex}, characterise rotation about the C–NH_2 bond. In this case, $k_{ex} = \frac{1}{\tau}$, where τ is the lifetime of one of the hydrogens in one of the two possible sites a or b in Figure 3.1. The expression $\frac{\tau_a}{\chi_a} = \frac{\tau_b}{\chi_b}$, where τ_a and τ_b are the lifetimes of a hydrogen atom in sites a and b respectively and χ_a and χ_b are the corresponding mole fractions in each site, now becomes trivial as rotation about the bond necessarily exchanges the hydrogens in sites a and b so $\tau_a = \tau_b$ and $\chi_a = \chi_b$. The rate of rotation about the bond is $\frac{k_{ex}}{2}$ as two such exchanges must occur for a complete rotation about the bond. A similar situation prevails for a hydrogen atom on one of the methyl groups as rotation about the C–NMe_2 bond occurs. A plot of $T\tau$ against $\frac{10^4}{T}$ for intramolecular

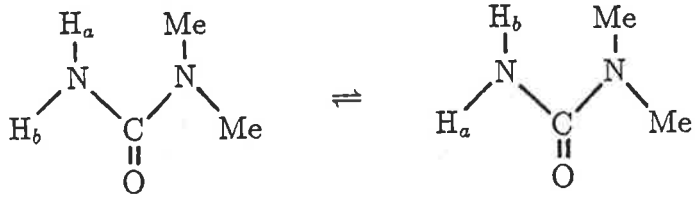

Figure 3.1: Rotation About C–NH_2 Bond Causing Intramolecular Exchange of the Hydrogen Atoms in Sites a (H_a) and b (H_b).

exchange of the –NH_2 protons is presented in Figure 3.3 and a similar plot for the –NMe_2 protons in Figure 3.5.

For the coalescence of the –NH_2 doublet, the freezing points of the solutions (*ca.* 231 K) precluded the extrapolation of the non-exchange modified linewidths (W_A and W_B) and chemical shifts (δ) from a substantial slow exchange temperature range. Hence, these parameters were obtained by the following method. At the lowest temperature examined (233.7 K) the –NH_2 doublet components still showed a small amount of chemical exchange induced broadening but the δ values were not affected significantly at this slow exchange rate. Above 261 K, exchange is in the fast exchange limit, such that the temperature variation of the singlet resonance linewidth is the environmental average of the coalesced doublet components. By assuming this temperature variation to apply to the non-exchange modified –NH_2 doublet, the component linewidths were obtained to a reasonable approximation. Chemical shift values without significant exchange modification for the –NH_2 doublet components were only observed below 235 K and accordingly, anchored on these data, δ was allowed to vary systematically in the coalescence temperature

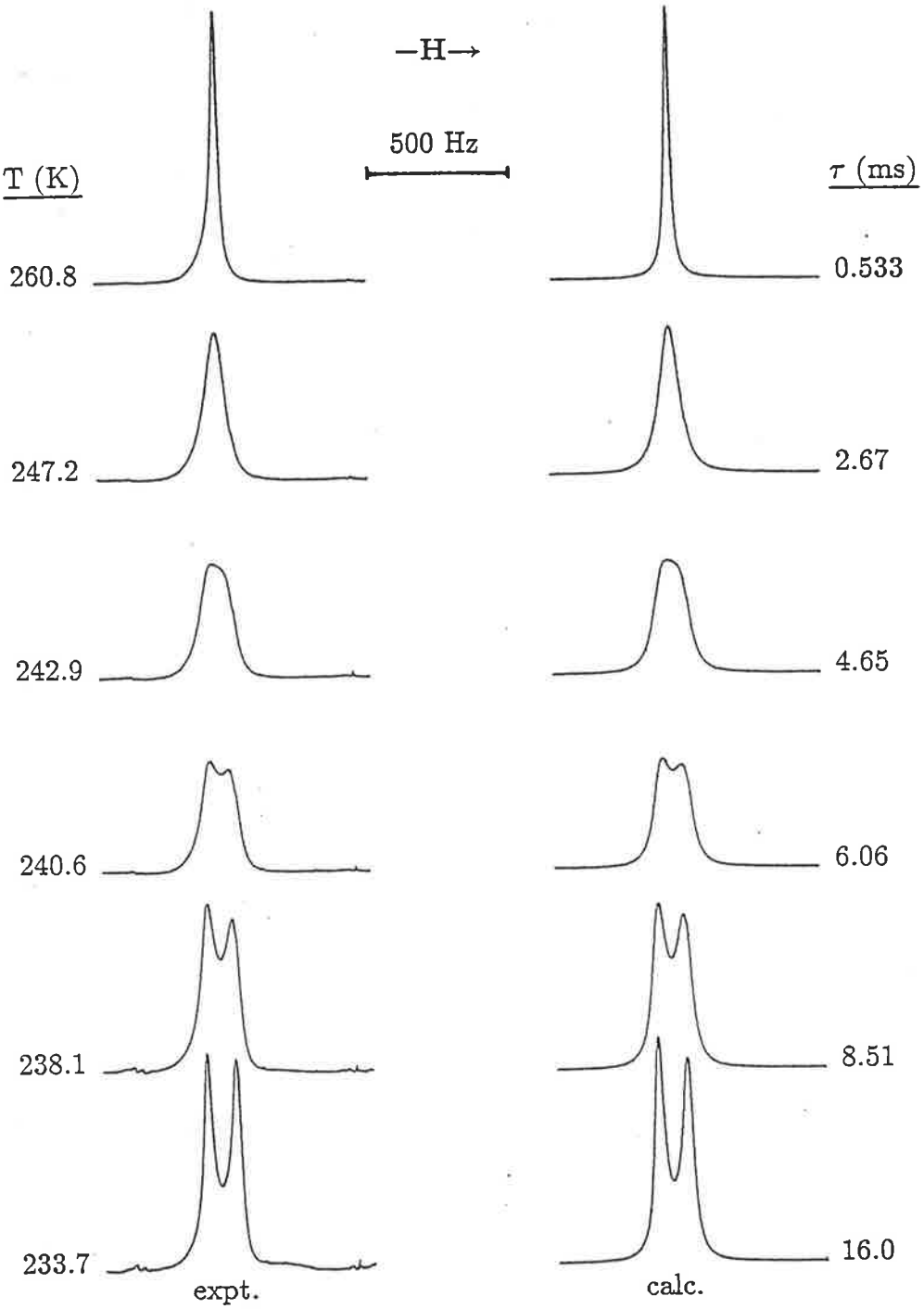

Figure 3.2:
Intramolecular exchange modified 300.13 MHz ^{1}H nmr spectra of a solution of $[UO_2(1,1\text{-dmu})_5](ClO_4)_2$ (0.05676 M) in CD_3CN (18.48 M) showing the NH_2 resonances. Experimental spectra and corresponding temperatures are shown at the left, and best fit calculated lineshapes and derived τ values are shown to the right.

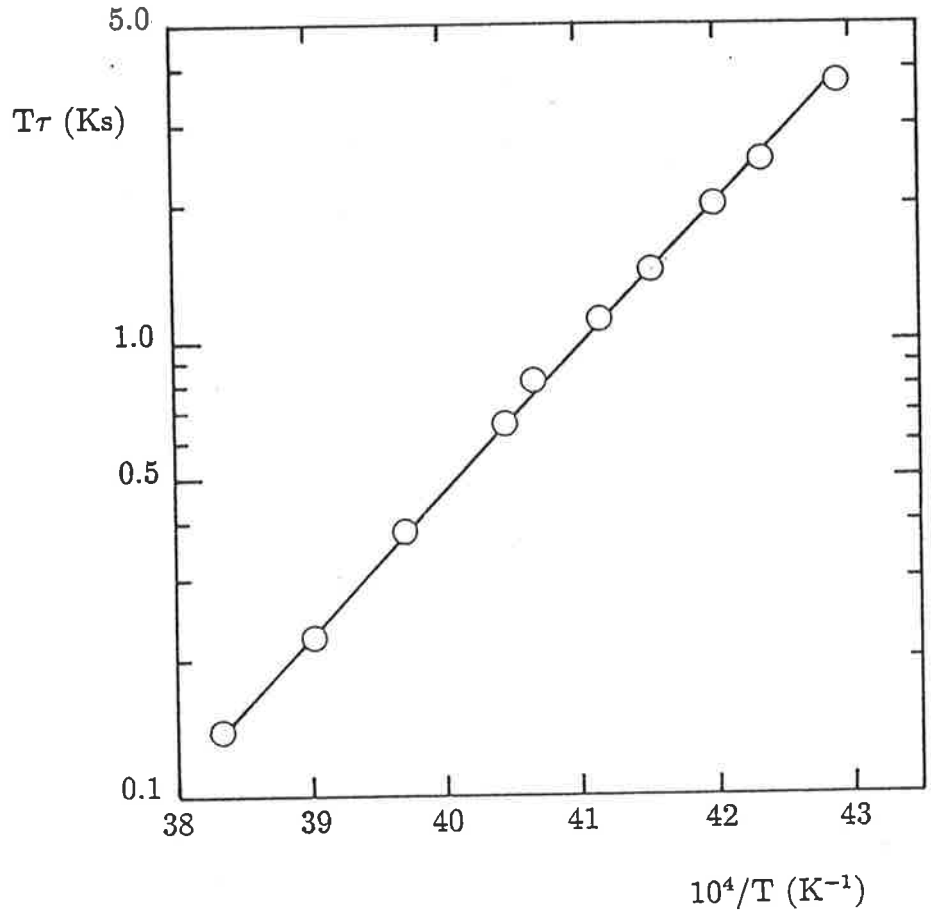

Figure 3.3:
The variation of $T\tau$ with $\frac{10^4}{T}$ for intramolecular exchange of the $-NH_2$ protons of 1,1-dmu coordinated to $[UO_2(1,1\text{-dmu})_5](ClO_4)_2$ (0.05676 M) in CD_3CN (18.48 M). The line represents the linear regression line for the fit of the data to the Eyring equation (Equation 6.31).

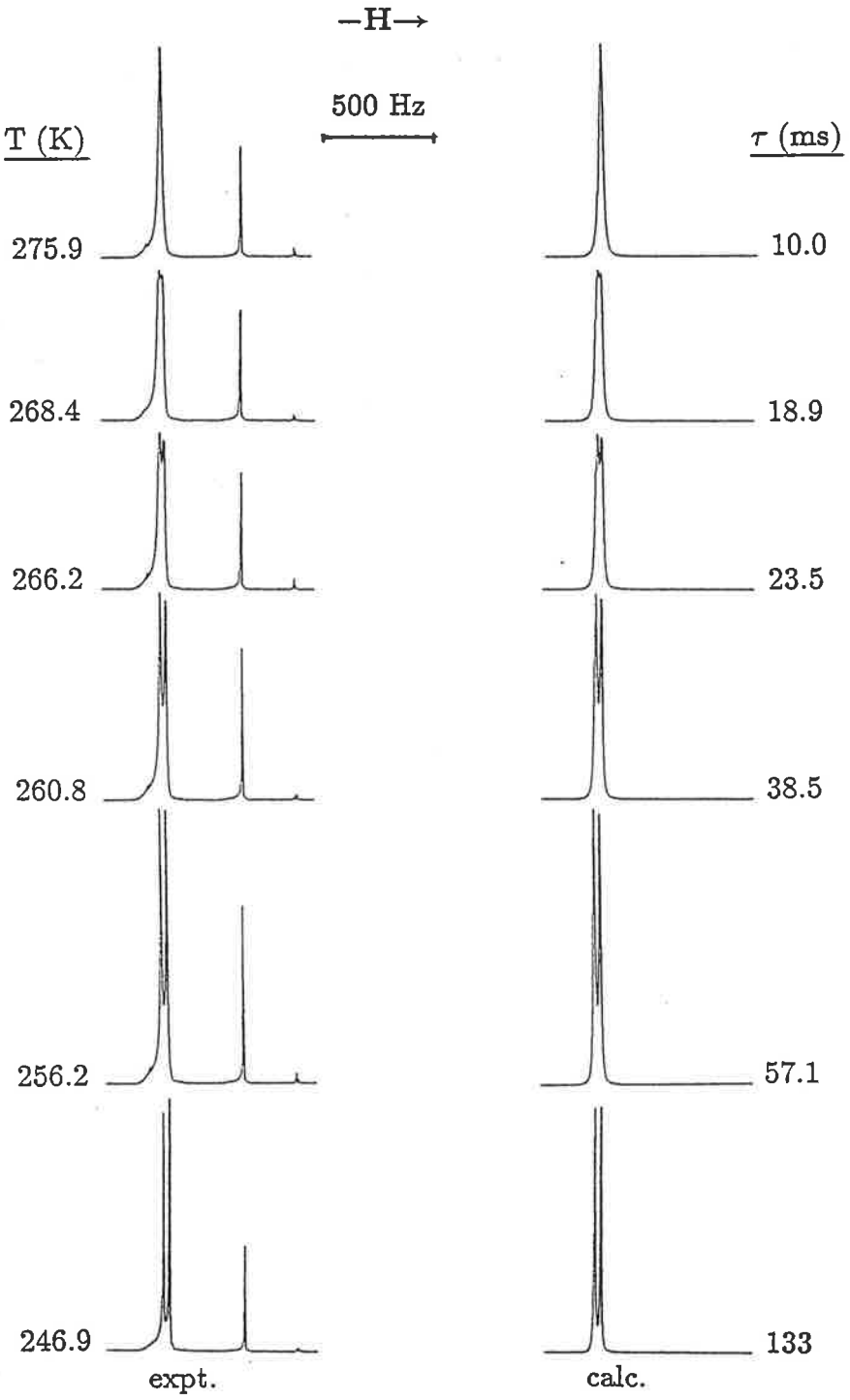

Figure 3.4:
Intramolecular exchange modified 300.13 MHz ^{1}H nmr spectra of a solution of $[UO_2(1,1\text{-dmu})_5](ClO_4)_2$ (0.05676 M) in CD_3CN (18.48 M) showing the $-NMe_2$ resonances. Experimental spectra and corresponding temperatures are shown at the left, and best fit calculated lineshapes and derived τ values are shown to the right.

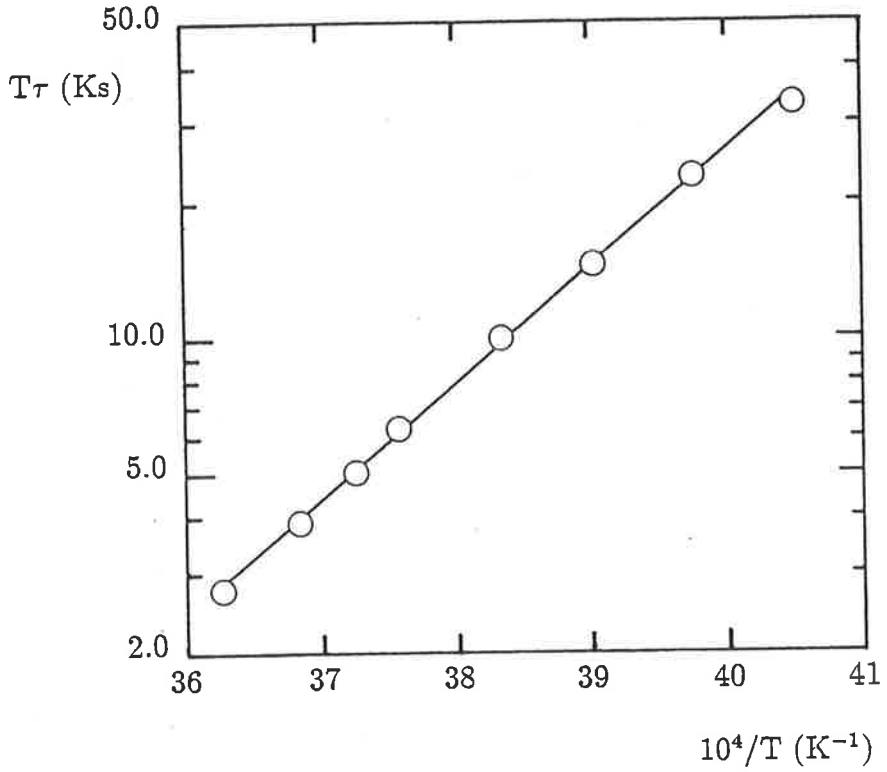

Figure 3.5:
The variation of $T\tau$ with $\frac{10^4}{T}$ for intramolecular exchange of the $-NMe_2$ protons of 1,1-dmu coordinated to $[UO_2(1,1\text{-dmu})_5](ClO_4)_2$ (0.05676 M) in CD_3CN (18.48 M). The line represents the linear regression line for the fit of the data to the Eyring equation (Equation 6.31).

range during the lineshape analyses to optimise the fits of the calculated lineshapes and the experimental spectra.

The coalescence of the $-NMe_2$ doublet occurred over a smaller temperature range (246.9 – 275.9 K) as a result of the smaller difference in δ between the doublet components. The slow exchange limit occurred at a higher temperature (*ca.* 242 K) and hence the temperature variations of the non-exchange modified $-NMe_2$ linewidths and chemical shift values were observed over a larger temperature range, which in conjunction with the approach used for the $-NH_2$ doublet provided good estimates of the variation of these parameters in the $-NMe_2$ coalescence temperature range.

The errors quoted in Table 3.4 represent one standard deviation for the linear regression fit of the rate data to the Eyring equation (Equation 6.31) and do not include the possible systematic errors arising from the estimation of the non-exchange modified linewidth and chemical shift values used in the lineshape analyses. When these possible error sources are considered, it is probable that for $[UO_2(1,1\text{-dmu})_5](ClO_4)_2$ the error in k(265 K) is three times that in Table 3.4 with commensurately increased errors in $\Delta H^{\ddagger}$ and $\Delta S^{\ddagger}$. Nevertheless, these errors do not significantly affect the discussion in Section 3.5.

3.3 Intramolecular Ligand Exchange on Pentakis(1,3-dimethylurea)dioxouranium(VI)

The 1,3-dimethylurea (1,3-dmu) complex $[UO_2(1,3\text{-dmu})_5](ClO_4)_2$ was prepared as described in Chapter 5. The three possible isomers of 1,3-dmu (A,B and C in Figure 3.6) present four chemical sites for the –NHMe and –NHMe protons. However, in CD_3CN solution at 300 K the spectrum of uncomplexed 1,3-dmu consists of a broadened –NHMe quartet (δ = 5.33 ppm) and a sharp –NHMe doublet (δ = 2.63 ppm, J(H–H) = 4.9 Hz) which, apart from systematic variations in δ, persisted down to 233 K, consistent with either a single isomer predominating or two or more isomers being in the fast exchange limit of the nmr timescale (it has been speculated [93] that uncomplexed 1,3-dmu exists predominantly as one isomer). In contrast, the spectrum of the complex $[UO_2(1,3\text{-dmu})_5]^{2+}$ at 233.7 K exhibits a

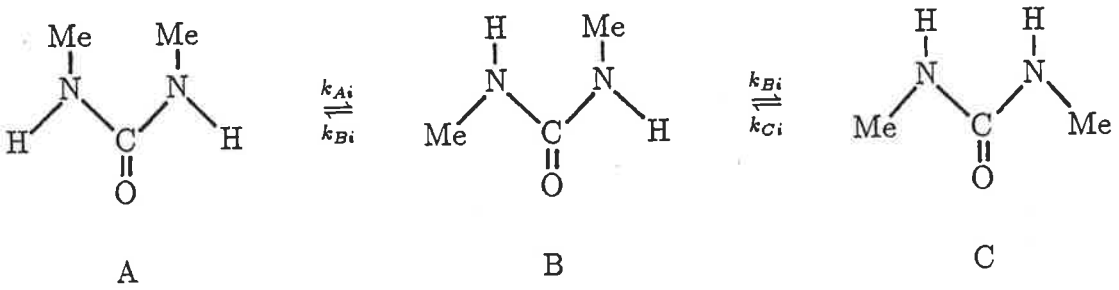

Figure 3.6: Isomers of 1,3-dimethylurea

–NHMe triplet (δ = 6.32, 6.18 and 5.88 ppm) and a –NHMe quartet (δ = 3.00, 2.80, 2.78 and 2.74 ppm) shown in Figure 3.7 consistent with rotation about the carbon–nitrogen bonds of the three isomers of 1,3-dmu (Figure 3.6) being slow on the nmr timescale. No spin-spin splitting was resolved in either case.

On addition of 1,3-dmu to a CD_3CN solution of $[UO_2(1,3\text{-dmu})_5](ClO_4)_2$ new resonances appear at δ = 5.50 and 2.63 ppm at 233.7 K, assigned to the –NHMe and –NHMe protons of the free ligand respectively, indicating that the intermolecular exchange of 1,3-dmu between the free and coordinated states is also slow. These resonances were used to assign the resonances of $[UO_2(1,3\text{-dmu})_5]^{2+}$ by assuming that the magnetic environments of H and Me most distant from the uranium ion in the coordinated 1,3-dmu ligands most closely resemble those of free 1,3-dmu. On this basis, the $[UO_2(1,3\text{-dmu})_5]^{2+}$ –NHMe resonances at δ = 6.32, 6.18 and 5.88 ppm are assigned to isomers A, B and C respectively (Figures 3.7 and 3.8) and the –NHMe resonances at δ = 2.74, 2.78, 2.80 and 3.00 ppm are assigned to isomers A, B, B and C respectively. Although the hydrogens of –NHMe of coordinated isomer B are chemically non-equivalent, they are magnetically equivalent, and the small chemical shift difference exhibited by the chemically non-equivalent methyl hydro-

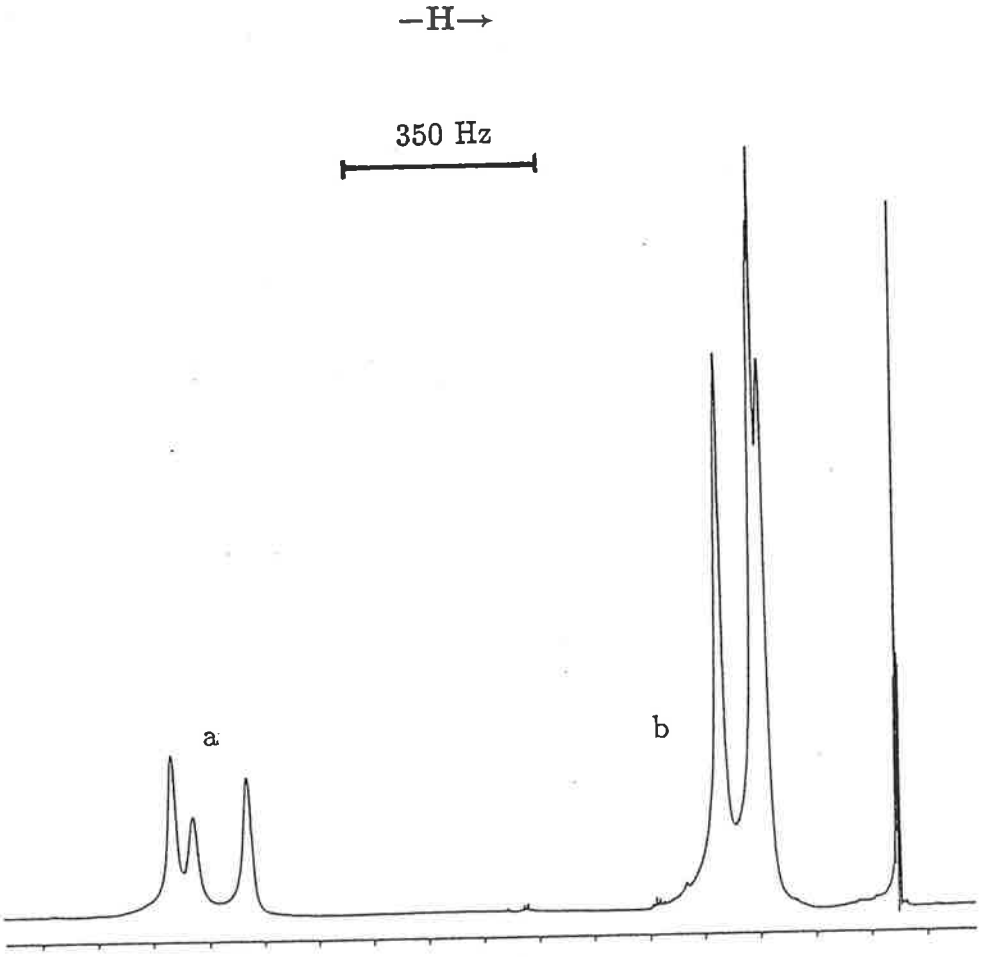

Figure 3.7:
300.13 MHz ^{1}H nmr spectrum at 233.7 K of a solution of $[UO_2(1,3\text{-dmu})_5](ClO_4)_2$ (0.07550 M) in CD_3CN (18.06 M) showing the –NHMe triplet (a) and –NHMe quartet (b). The multiplet at high field is due to the proton impurity of CD_3CN.

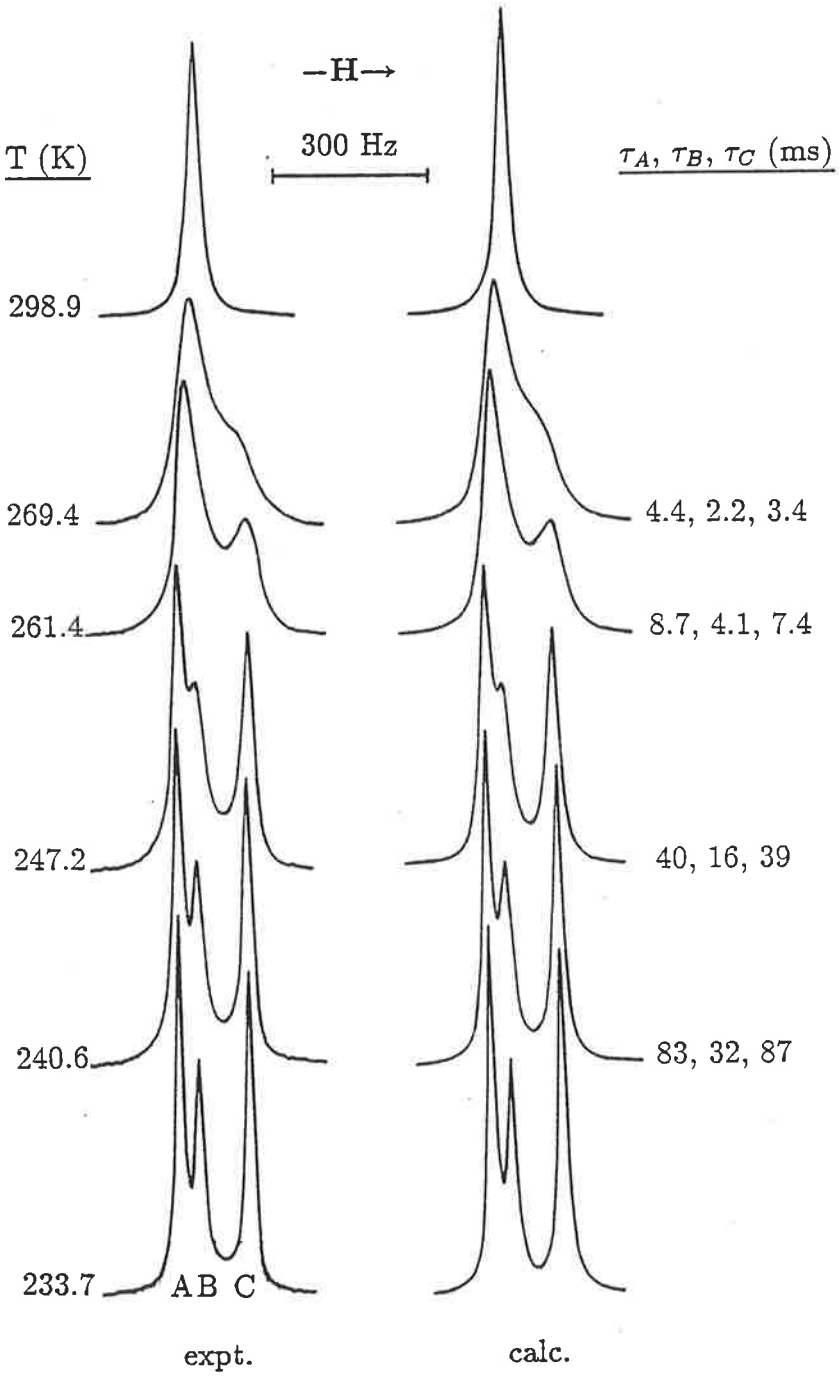

Figure 3.8:
Exchange modified 300.13 MHz ^{1}H nmr spectra of a solution of $[UO_2(1,3\text{-dmu})_5](ClO_4)_2$ (0.07550 M) in CD_3CN (18.06 M) showing the –NHMe resonances. Experimental spectra and temperatures are shown at the left, and best fit calculated lineshapes and derived τ values are shown to the right.

gens indicates that the difference between their magnetic environments is small. A similar magnetic equivalence of the methyl groups in $[UO_2(dmf)_5]^{2+}$ has been reported [77] and is probably (at least in part) a consequence of the anisotropic magnetic field of the dioxouranium(VI) ion [59,94,95]. This effect is discussed in more detail for the dmf ligand in Reference [77].

The five 1,3-dmu ligands coordinated in $[UO_2(1,3\text{-dmu})_5]^{2+}$ present a substantial number of possible combinations of isomers to produce a range of isomeric $[UO_2(1,3\text{-dmu})_5]^{2+}$ complexes. Thus the –NHMe and –NHMe resonances (Figure 3.7) are the summation of those of the isomeric complexes which evidently exhibit little or no chemical shift differences. As the temperature is raised from 233.7 K both the –NHMe (Figure 3.8) and the –NHMe resonances coalesce to a singlet, consistent with the rate of isomerisation of the coordinated 1,3-dmu ligands becoming rapid on the nmr timescale. The coalescence of the –NHMe resonances was chosen for complete lineshape analysis although, in principle, both sets of resonances should be amenable to analysis. This was due to the greater chemical shift differences in this set of resonances and the consequently greater coalescence temperature range which should give more accurate results.

The non-exchange modified linewidths and chemical shift values in the coalescence temperature range were estimated in a similar manner to the 1,1-dmu analogue described in Section 3.2 as a consequence of the slow exchange limit only being reached at the lowest temperature studied, 233.7 K. The coordinated 1,3-dmu isomer populations were determined directly from integrated resonance areas in the temperature range 233.7 – 242.9 K and, anchored on these values, were allowed to vary systematically in the coalescence temperature range to optimise the fit of the calculated lineshapes to the experimental spectra. This population variation did not exceed 20% for any isomer over the range 233.7 – 289.9 K and the variation of linewidth and chemical shift was less than 10% . The lineshape analysis was carried out using an equation which encompasses the four chemically non-equivalent –NHMe sites in the three 1,3-dmu isomers (Figure 3.6) as described in Section 6.2. A selection of experimental spectra and best-fit calculated lineshapes are shown in Figure 3.8 together with the lifetimes of the coordinated 1,3-dmu isomers τ_A, τ_B

and τ_C, and the appropriate temperatures.

As rotation about either of the equivalent carbon–nitrogen bonds in isomer A causes isomerisation to isomer B, $\tau_A = 1/k_{Ai} = 1/(2k_A)$ where k_{Ai} and k_A are the rate constants for isomerisation and rotation about one carbon–nitrogen bond respectively. Similarly, $\tau_C = 1/k_{Ci} = 1/(2k_C)$. Rotation about either of the non-equivalent carbon–nitrogen bonds of isomer B (k_B and k'_B) causes isomerisation to isomer A or C and as a consequence k_B and k'_B cannot be separately determined. Therefore, they were set equal in the lineshape analysis, described in Section 6.2. As a consequence of this and the nature of the four site lineshape analysis $\tau_B = 1/k_{Bi} = 1/k_B = 1/k'_B$. The τ values derived at ten temperatures in the range 240.6 – 272.1 K (where there is significant modification to the –NHMe lineshapes due to chemical exchange) are plotted in Figure 3.9. The associated rate constants calculated at 265 K (in the midst of the coalescence temperature range where the most accurate rate data are obtained) and the values of the exchange parameters, $\Delta H^{\ddagger}$ and $\Delta S^{\ddagger}$ are given in Table 3.4 in Section 3.5. For similar reasons to those for $[UO_2(1,1\text{-dmu})_5]^{2+}$, and also due to the assumption that $k_B = k'_B$ discussed above, it is possible that the error in k(265 K) could be up to 5 times that quoted, with commensurately increased errors in $\Delta H^{\ddagger}$ and $\Delta S^{\ddagger}$. However, these errors should not affect the discussion in Section 3.5.

3.4 Intra- and Inter-molecular Ligand Exchange on Pentakis(1,1,3-trimethylurea)dioxouranium(VI)

The complex $[UO_2(trmu)_5](ClO_4)_2$, where trmu = 1,1,3-trimethylurea, was prepared as described in Chapter 5. No resonances attributable to free trmu were observed in the spectra of the solutions of the complex alone in CD_3CN solution. As in the case of the 1,3-dmu complex, a range of populations of the two possible trmu isomers is expected to be coordinated in $[UO_2(trmu)_5]^{2+}$, but as separate resonances corresponding to differently populated $[UO_2(trmu)_5]^{2+}$ are not observed, it is concluded that the influence of these population differences on the chemical shift

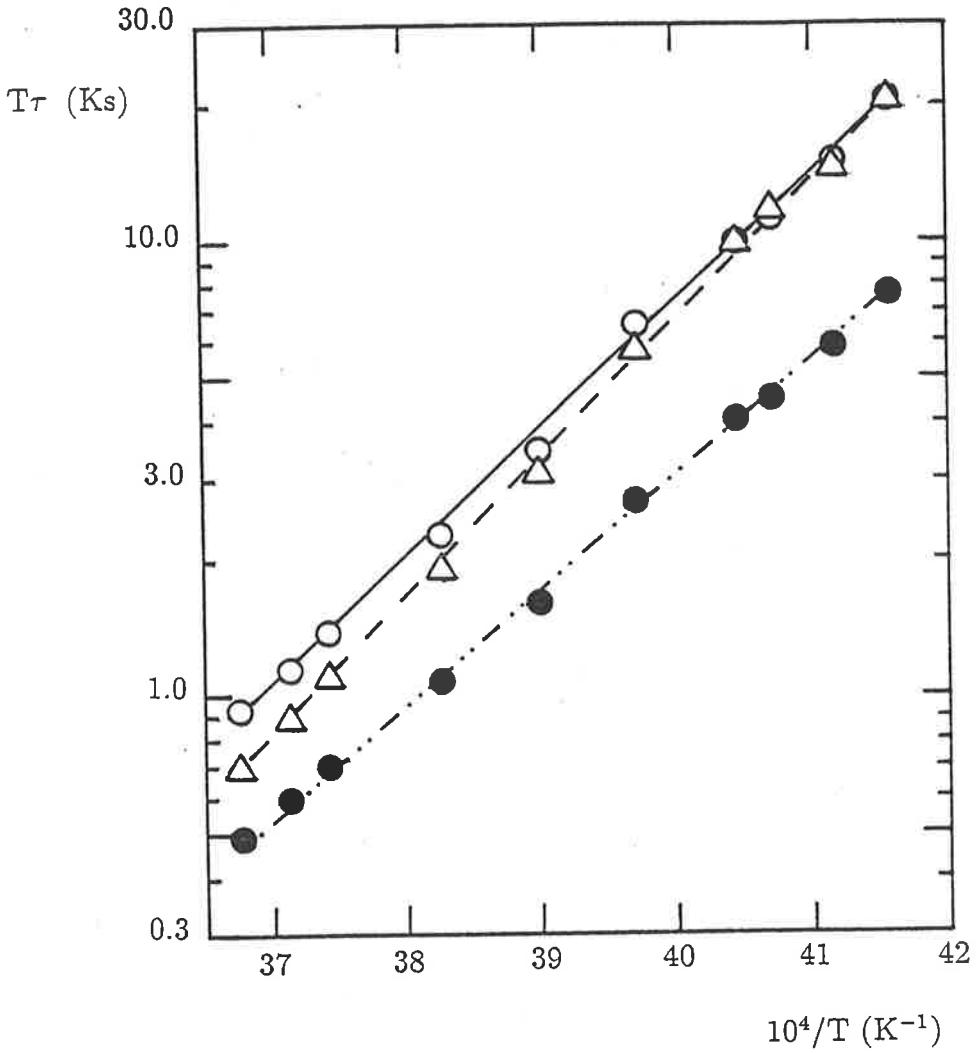

Figure 3.9:
The variation of $T\tau_A$ (○), $T\tau_B$ (●) and $T\tau_C$ (△) with $\frac{10^4}{T}$ for a solution of $[UO_2(1,3\text{-dmu})_5](ClO_4)_2$ (0.07550 M) in CD_3CN (18.06 M). The lines drawn through each data set represent the linear regression line for the fit of the data to the Eyring equation (Equation 6.31).

is negligible.

The spectra of a CD_3CN solution of $[UO_2(trmu)_5](ClO_4)_2$ and trmu recorded over a range of temperatures are shown in Figure 3.10. Integration of the resonances arising from free and coordinated trmu over the temperature range 250 – 265 K produced ratios consistent with $[UO_2(trmu)_5]^{2+}$ being the dominant complex species in solution. As the temperature is increased, the rate of rotation about the $-NMe_2$ bond in coordinated trmu increases, causing the $-NMe_2$ resonances to coalesce (labelled (c) in Figure 3.10 and also shown in Figure 3.11). The singlet $-NMe_2$ resonance of free trmu (Figure 3.10) indicates that rotation about this carbon–nitrogen bond in free trmu is in the fast exchange limit of the nmr timescale at the lowest temperature studied (238.3 K). The ^1H resonance of –NHMe is a singlet (except at very low temperature where it is a quartet due to spin-spin splitting) and the –NHMe resonance is a doublet in both coordinated and free trmu. These also indicate that, in both cases, rotation about the carbon–nitrogen bond is in the fast exchange limit of the nmr timescale. The spin-spin splitting observed for the free and coordinated trmu –NHMe doublets correspond to J(H–H) = 4.4 and 4.9 Hz respectively and, as a consequence of intermolecular trmu exchange and overlap of resonances, the latter coupling is only resolved in solutions of $[UO_2(trmu)_5](ClO_4)_2$ with no added trmu. Similarly, the quartet resonance of –NHMe is only resolved at low temperature as a consequence of exchange processes.

As the temperature is increased, the pairs of –NHMe, –NHMe and $-NMe_2$ resonances arising from free and coordinated trmu coalesce as intermolecular trmu exchange becomes increasingly rapid (Figures 3.10 and 3.13). The occurrence of the coalescences due to intramolecular and intermolecular exchange in different temperature ranges (Figure 3.10) allows the determination of the kinetic parameters characterising the C–NMe_2 bond rotation in coordinated trmu from the $-NMe_2$ doublet coalescence, and also the trmu ligand exchange on $[UO_2(trmu)_5]^{2+}$ from coalescence of the –NHMe resonances of coordinated and free trmu using complete lineshape analyses (described in Section 6.2).

A selection of experimental spectra and best-fit calculated lineshapes of the

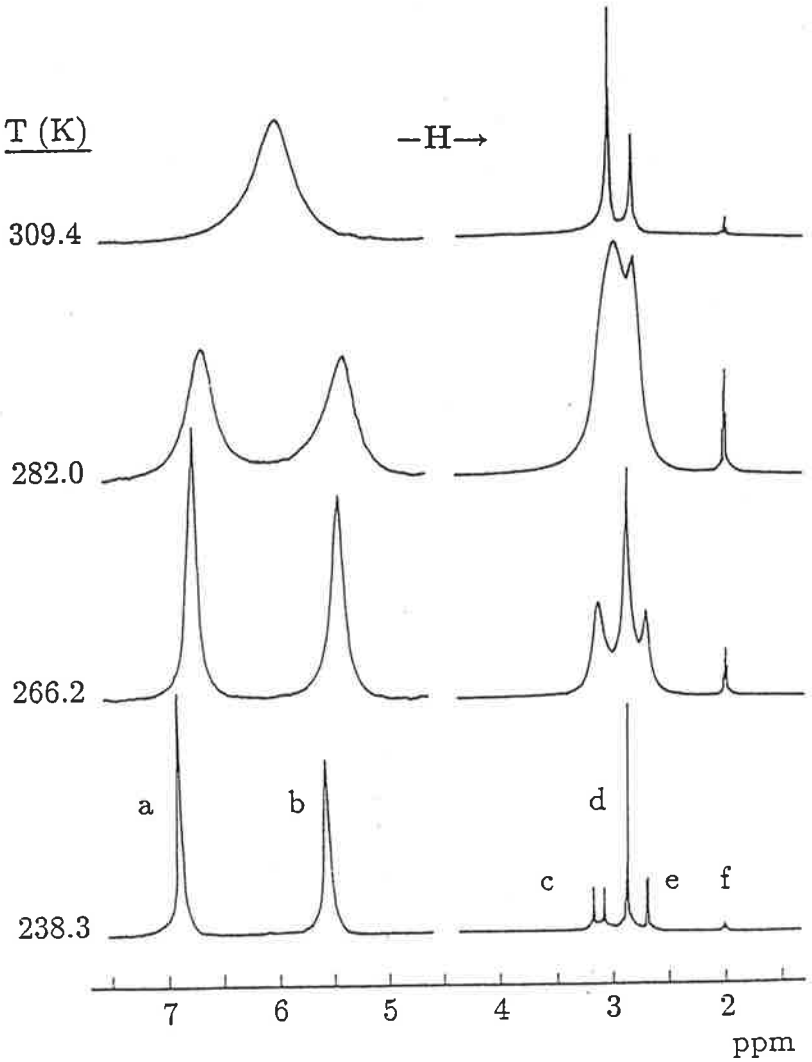

Figure 3.10:
Exchange modified 300.13 MHz ^{1}H nmr spectra of a solution of $[UO_2(trmu)_5](ClO_4)_2$ (0.08639 M) and trmu (0.4532 M) in CD_3CN (16.83 M). The resonances (with their chemical shifts from t.m.s. shown in brackets) arise from:
$[UO_2(trmu)_5]^{2+}$: (a) –N**H**Me (6.71, quartet with J(H–H) = 4.9 Hz), (c) $-NMe_2$ (3.09 and 3.00) and (d) –NH**Me** (2.81).
free trmu: (b) –N**H**Me (5.41), (d) $-NMe_2$ (2.81) and (e) –NH**Me** (2.63, doublet with J(H–H) = 4.4 Hz).
(f) is the proton impurity in CD_3CN (1.95).
The left hand side of the spectrum is plotted on a greater vertical scale than the right hand side.

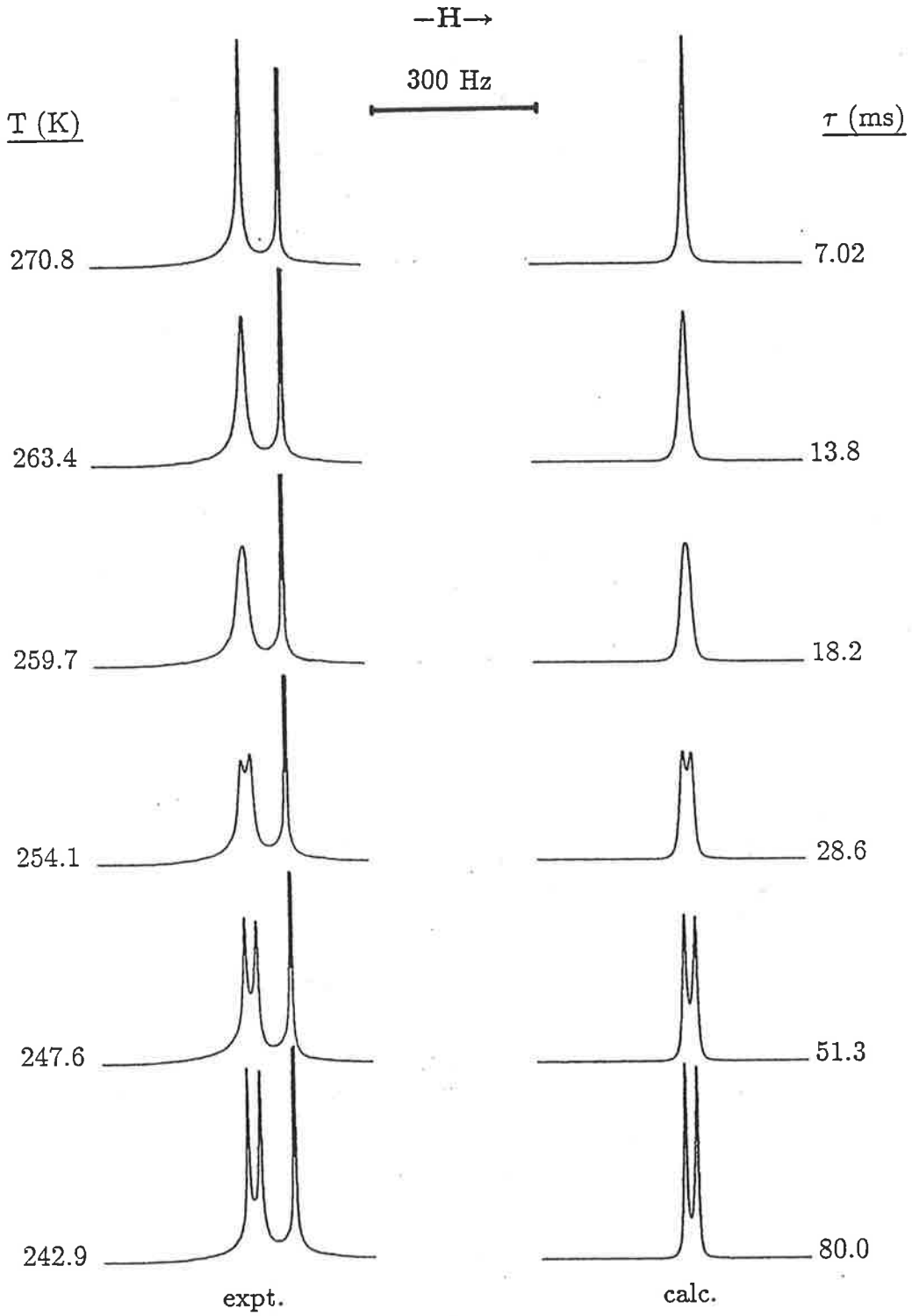

Figure 3.11:
Intramolecular exchange modified 300.13 MHz ^{1}H nmr spectra of a solution of $[UO_2(trmu)_5](ClO_4)_2$ (0.05854 M) in CD_3CN (18.56 M) showing the $-NMe_2$ resonances. Experimental spectra and temperatures are shown to the left and best fit calculated lineshapes and derived τ values are shown to the right.

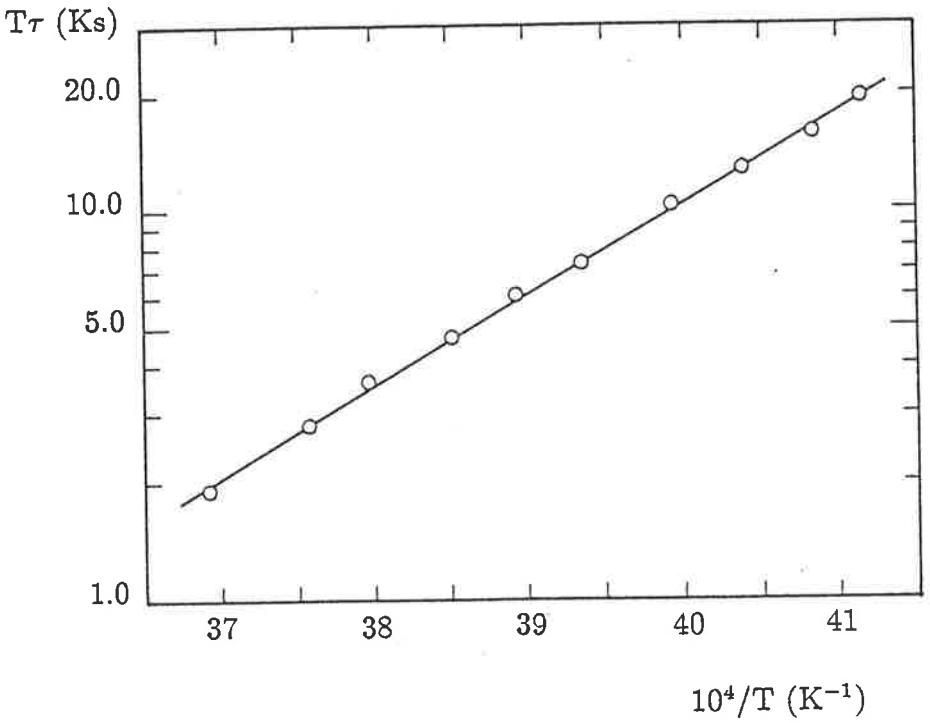

Figure 3.12:
The variation of $T\tau$ with $\frac{10^4}{T}$ for intramolecular exchange of the $-NMe_2$ protons of trmu coordinated to $[UO_2(trmu)_5](ClO_4)_2$ (0.05854 M) in CD_3CN (18.56 M). The line represents the linear regression line for the fit of the data to the Eyring equation (Equation 6.31).

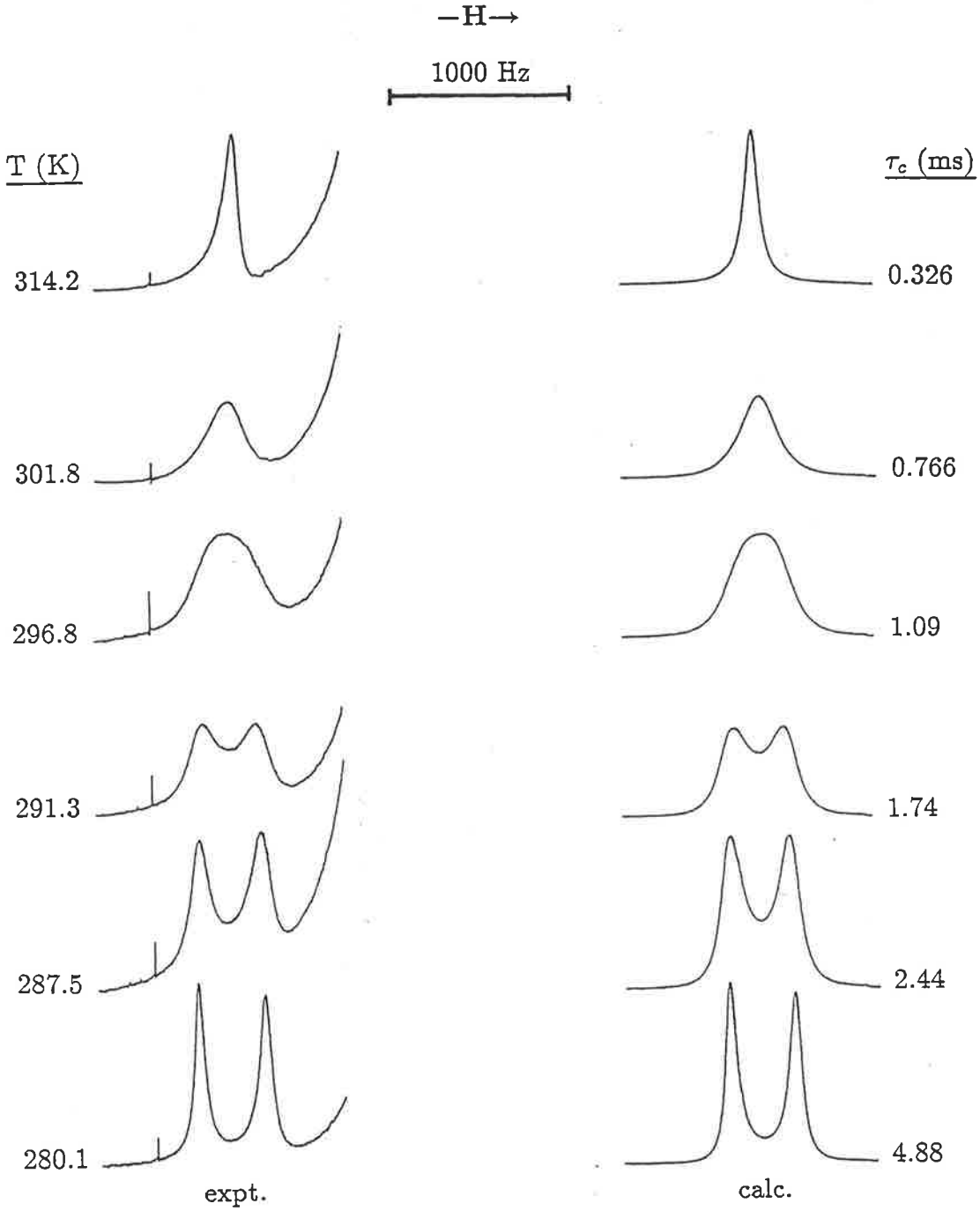

Figure 3.13:
Intermolecular exchange modified 300.13 MHz ^{1}H nmr spectra of a solution of $[UO_2(trmu)_5](ClO_4)_2$ (0.08639 M) and trmu (0.4532 M) in CD_3CN (16.82 M) showing the –NHMe resonances used to obtain the intermolecular exchange parameters. Experimental spectra and temperatures are shown to the left and best fit calculated lineshapes and derived τ_c values are shown to the right. The signal due to coordinated trmu is upfield from that due to free trmu. The experimental spectra curve up at high field due to the proximity of the methyl resonances.

Table 3.2: Solution Compositions for Intermolecular Exchange of Trimethylurea on $[UO_2(trmu)_5]^{2+}$ in CD_3CN

Solution	$[[UO_2(trmu)_5](ClO_4)_2]$ mol dm^{-3}	$[trmu]_{free}$ mol dm^{-3}	$[CD_3CN]$ mol dm^{-3}	CN[1]
i	0.1345	0.6955	15.88	5.0 ± 0.1
ii	0.08639	0.4532	16.82	5.1 ± 0.1
iii	0.03006	0.1697	17.54	5.0 ± 0.1
iv	0.01063	0.0582	18.13	5.0 ± 0.1

[1] Coordination number (see text).

NMe_2 resonances of trmu in $[UO_2(trmu)_5]^{2+}$ over the range 242.9 – 270.8 K used to obtain the kinetic parameters characterising rotation about this carbon–nitrogen bond are presented in Figure 3.11. Also given are the lifetimes of a methyl group in each environment and the appropriate temperature. The kinetic parameters are presented with the results from several other systems in Table 3.4 in Section 3.5.

The mean lifetime of a single coordinated trmu ligand, τ_c ($= \tau_f \chi_c / \chi_f = 1/k_{ex}$ where τ_f is the mean lifetime of free trmu, χ_c and χ_f are the mole fractions of coordinated and free trmu, and k_{ex} is the observed first order rate constant), characterising intermolecular ligand exchange on $[UO_2(trmu)_5]^{2+}$ was determined from complete lineshape analysis of the coalescing –NHMe resonances of free and coordinated trmu at *ca.* 3 K intervals over the range 280.1 – 309.4 K. A selection of the experimental spectra and best-fit lineshapes are presented in Figure 3.13. The variation of $T\tau_c$ with $10^4/T$ for the four solutions studied is shown in Figure 3.14. The compositions of the four solutions studied and the kinetic parameters characterising intermolecular exchange in each of them are presented in Tables 3.2 and 3.3 respectively. The coordination number given in Table 3.2 is the number of trmu ligands in the first coordination sphere of the dioxouranium(VI) ion determined from a comparison of the integrated coordinated and free ligand resonance areas.

The kinetic parameters for the intermolecular exchange of trmu (Table 3.3) show little dependence on concentration, consistent with the overall exchange rate law

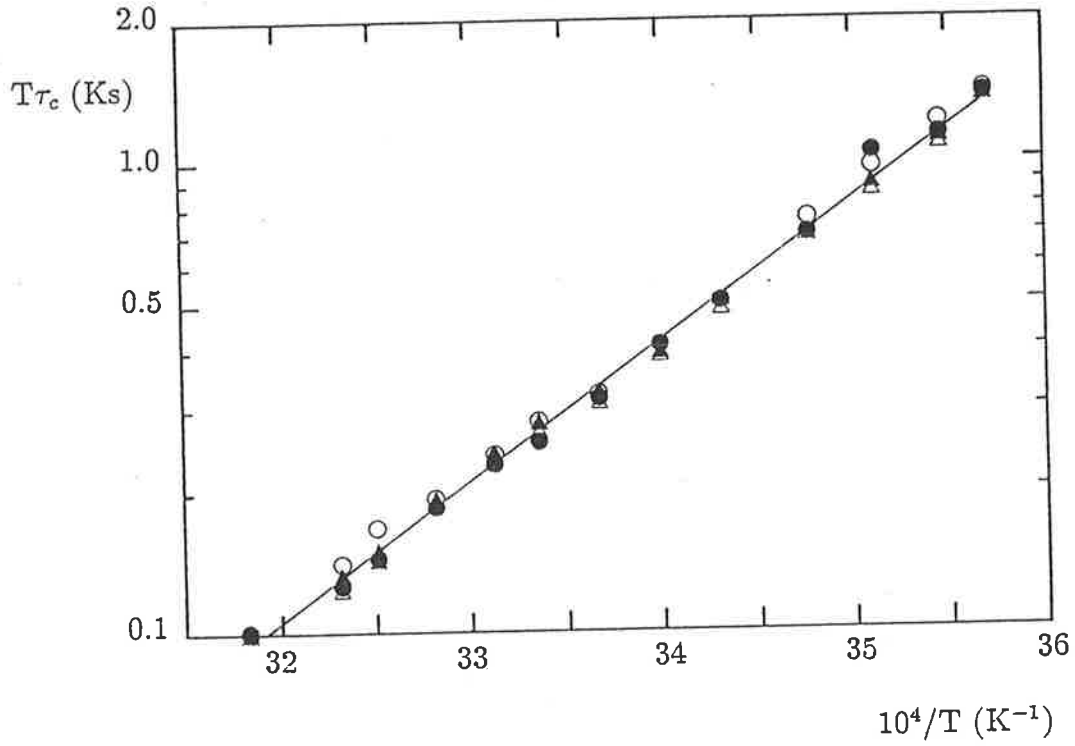

Figure 3.14:
The variation of $T\tau_c$ with $\frac{10^4}{T}$ for intermolecular exchange of trmu on $[UO_2(trmu)_5]^{2+}$. The data for solutions i – iv in Tables 3.2 and 3.3 are shown as open circles, closed circles, open triangles and closed triangles respectively. The line represents the best-fit linear regression line of the combined data to the Eyring equation (Equation 6.31).

Table 3.3: Kinetic Parameters for Intermolecular Exchange of Trimethylurea on $[UO_2(trmu)_5]^{2+}$ in CD_3CN

Solution	$\Delta H^{\ddagger 1}$ $kJmol^{-1}$	$\Delta S^{\ddagger 1}$ $JK^{-1}mol^{-1}$	k(298.2 K)[1] s^{-1}
i	56.1 ± 1.0	0.3 ± 3.3	939 ± 13
ii	57.6 ± 1.2	5.5 ± 3.9	981 ± 15
iii	56.1 ± 0.9	0.8 ± 3.0	1020 ± 12
iv	56.7 ± 0.8	2.6 ± 2.7	993 ± 10
i – iv	56.6 ± 0.6	2.2 ± 1.9	983 ± 8

[1]Quoted errors represent one standard deviation.

over the concentration range studied being:

$$\text{exchange rate } = 5k_{ex}[[UO_2(trmu)_5]^{2+}].$$

This is consistent with trmu exchange on $[UO_2(trmu)_5]^{2+}$ proceeding through a **D** mechanism. Ground state species, $[UO_2(ligand)_4]^{2+}$, with a coordination number of six, have been observed both in the solid state and in solution (see Table 3.1) lending plausibility to the postulation of the six coordinated reactive intermediate species, $[UO_2(trmu)_4]^{2+}$, required by a **D** mechanism.

This rate law is also consistent with the operation of an **I** mechanism under conditions such that all $[UO_2(trmu)_5]^{2+}$ exists in an encounter complex with an entering trmu ligand residing in the second coordination sphere and trmu exchange proceeding through interchange of a trmu ligand in the first coordination sphere with one in the second. For this condition to apply for the most dilute solution studied (solution iv in Table 3.2) the formation constant for the encounter complex would be ≥ 200 dm^3mol^{-1}. This seems unlikely as it has been reported [96] that the stability constant characterising the encounter complex formed between $[UO_2(dmf)_5]^{2+}$ and dmf in CD_2Cl_2 $K_{ass}(223.2\ K) = 1.59 \pm 0.11$ kg mol^{-1}. The more highly charged $[Tb(dmf)_8]^{3+}$ forms an analogous encounter complex in dmf/CH_3NO_2 with a formation constant $K_{ass}(239.2\ K) = 0.42 \pm 0.01$ kg mol^{-1} [9]. In CD_2Cl_2 which has a dielectric constant of 8.93, the formation constant obtained for the encounter complex between uncharged $[UO_2(acac)_2dmso]$ and dmso was $K_{ass}(283.2\ K) = 4.6 \pm 2$

dm^3mol^{-1} while in $(CD_3)_2CO$, which has a dielectric constant of 20.7, no encounter complex was found [97]. The encounter complex formed between $[UO_2(nipa)_2EtOH]$ (where nipa is nonamethylimidodiphosphoramide) and ethanol in CD_2Cl_2/CD_3NO_2 solution is characterised by $K_{ass}(263.2\ K) = 16.2\ dm^3mol^{-1}$ although this high K_{ass} value may be explained by a specific hydrogen bonding interaction between ethanol in the first and second coordination spheres [90]. Hence, it is unlikely that an encounter complex exists in significant amounts in the $[UO_2(trmu)_5]^{2+}$ solutions in Tables 3.2 and 3.3, and that the predominant exchange process is of the **D** type.

3.5 The Effect of Substitution of Ureas on the Rate of Internal Rotation

The rates of rotation about the carbonyl–nitrogen bonds in the ligands (L) of $[UO_2(L)_5]^{2+}$ for L = tmu [10], 1,1-dmu (Section 3.2) and trmu (Section 3.4) are substantially decreased by comparison to those observed for uncomplexed tmu [93], 1,1-dmu [93,98] and trmu (Tables 3.4 and 3.5). It is reasonable to assume that a similar situation prevails for 1,3-dmu although no rate data is available for this urea in the free state. The observation of the three isomers of 1,3-dmu coordinated to dioxouranium(VI) suggests that uncomplexed 1,3-dmu could exist as all three isomers undergoing rapid isomerisation, however, it is probable that the isomeric ratio changes on coordination as is observed for the two isomers of nma on coordination to scandium(III) [45] and the E and Z isomers of Boc α-amino acid esters on coordination to europium(III) [99].

The predominant cause of the decrease in the rates of rotation about the carbonyl carbon–nitrogen bonds of ureas in their dioxouranium(VI) complexes, compared to the free ligand, is probably the increase in the order of these bonds which occurs on coordination of these ureas through the carbonyl oxygen. Although the bond lengths in the crystal do not appear to change appreciably on coordination [65,100,101,102], the infra-red absorption frequencies (ν) are affected (Chapter 5 and References [103,26]) with $\nu_{C=O}$ decreased and ν_{C-N} increased indicating that there is some electronic redistribution decreasing the C=O bond order and increasing the C–N bond order. From a comparison of the limited data available for the ureas in the

Table 3.4: Kinetic Parameters for Rotation about Carbon–Nitrogen Bonds in Coordinated Ureas (L) in $[UO_2(L)_5]^{2+}$ and in Ureas in the Free State

Species	Solvent	Bond	k(265 K)[1] s^{-1}	$\Delta H^{\ddagger}$ [1] $kJmol^{-1}$	$\Delta S^{\ddagger}$ [1] $JK^{-1}mol^{-1}$
1,1-dmu[2]	$(CD_3)_2CO$	C–NMe_2	4465	36.8 ± 0.4	−35.2 ± 1.6
1,3-dmu[4]	CD_3CN	C–NHMe	large		
trmu[5]	CD_3CN	C–NHMe	large		
trmu[5]	CD_3CN	C–NMe_2	large		
$[UO_2(1,1\text{-dmu})_5]^{2+}$ [3]	CD_3CN	C–NMe_2	39.1 ± 0.4	49.1 ± 0.7	−28.3 ± 2.7
$[UO_2(1,1\text{-dmu})_5]^{2+}$ [3]	CD_3CN	C–NH_2	2960 ± 60	61.1 ± 0.5	53.1 ± 2.2
$[UO_2(1,3\text{-dmu})_5]^{2+}$ [4]	CD_3CN	C–NHMe	77.8 ± 2.6 (A)	53.2 ± 0.7	−1.7 ± 3.0
$[UO_2(1,3\text{-dmu})_5]^{2+}$ [4]	CD_3CN	C–NHMe	317 ± 5 (B)	47.6 ± 0.7	−16.3 ± 2.6
$[UO_2(1,3\text{-dmu})_5]^{2+}$ [4]	CD_3CN	C–NHMe	96.0 ± 3.0 (C)	58.8 ± 0.7	3.8 ± 2.4
$[UO_2(trmu)_5]^{2+}$ [5]	CD_3CN	C–NMe_2	86.2 ± 1.2	44.7 ± 0.6	−38.3 ± 2.4
$[UO_2(trmu)_5]^{2+}$ [5]	CD_3CN	C–NHMe	large?		
$[UO_2(tmu)_5]^{2+}$ [6]	CD_2Cl_2	C–NMe_2	20400	29.0 ± 0.5	−52 ± 3

[1]Quoted errors represent one standard deviation.
[2]Reference [98]
[3]Section 3.2
[4]Section 3.3
[5]Section 3.4
[6]Reference [10]

Table 3.5: Rate Constants Calculated at 211 K for Rotation about Carbon–Nitrogen Bonds in Coordinated Ureas (L) in $[UO_2(L)_5]^{2+}$ and in Ureas in the Free State

Species	Solvent	Bond	k(211 K) s^{-1}
1,1-dmu[1]	$(CD_3)_2CO$	C–NMe_2	49.5
1,1-dmu[2]	$(CD_3)_2CO$	C–NMe_2	42.3
1,1-dmu[2]	$(CD_3)_2CO$	C–NH_2	330
tmu[2]	$(CD_3)_2CO$/ $CHFCl_2$	C–NMe_2	187.6 (135 K)
$[UO_2(1,1\text{-dmu})_5]^{2+}$ [5]	CD_3CN	C–NMe_2	0.10
$[UO_2(1,1\text{-dmu})_5]^{2+}$ [5]	CD_3CN	C–NH_2	1.95
$[UO_2(1,3\text{-dmu})_5]^{2+}$ [3]	CD_3CN	C–NHMe	0.24 (A)
$[UO_2(1,3\text{-dmu})_5]^{2+}$ [3]	CD_3CN	C–NHMe	1.02 (B)
$[UO_2(1,3\text{-dmu})_5]^{2+}$ [3]	CD_3CN	C–NHMe	0.02 (C)
$[UO_2(trmu)_5]^{2+}$ [4]	CD_3CN	C–NMe_2	0.377
$[UO_2(tmu)_5]^{2+}$ [6]	CD_2Cl_2	C–NMe_2	560

[1]Reference [98]
[2]Reference [93]
[3]Section 3.3
[4]Section 3.4
[5]Section 3.2
[6]Reference [10]

free state with those obtained from their dioxouranium(VI) complexes (Tables 3.4 and 3.5) it appears that coordination contracts the range of C–NMe_2 rotation rates. This may be a consequence of the increased carbon–nitrogen bond order resulting from coordination dominating the steric and electron donating characteristics of the substituents on the urea nitrogens.

There is a trend in the data for the complexes of the ureas which shows that the rate of rotation increases, $\Delta H^{\ddagger}$ decreases and $\Delta S^{\ddagger}$ becomes more negative for rotation about the C–NMe_2 bond in the sequence: $H_2NC(O)NMe_2$, $MeHNC(O)NMe_2$, $Me_2NC(O)NMe_2$. In the crystal structures of complexes of urea ($OC(NH_2)_2$) with dioxouranium(VI) [65] and manganese [101], complexes of 1,3-dmu with erbium [104] and manganese [105] and complexes of tmu with thorium [100], erbium [27] and uranium [106], the ligands do not appear to be quite planar. This is presumably due to steric crowding of the bulky groups on the ligands and also, in the cases of urea and 1,3-dmu, hydrogen bonding. This distorted structure is assumed to be the most favourable in solution for the ligands in this study.

In the complexes of 1,3-dmu, the isomers B and C (Figure 3.6) predominate. In $[Mn(1,3\text{-dmu})_3Br_2]$ [105], all the ligands are present as isomer C (it is interesting to note that one of the ligands in this complex is coordinated via an unusual C–O–M angle of 180°, probably as a result of electron delocalisation, while the other two ligands are coordinated with a C–O–M angle of 129.5°) while in $[Er(1,3\text{-dmu})_6H_2O](ClO_4)_3$ [104], both B and C isomers are observed. The predominance of these isomers can be explained by the outward orientation of their N–H groups, which promotes intermolecular hydrogen bonding (this hydrogen bonding is present in the solid state but is not expected to be as significant in solution. Hence, the relative proportions of each isomer may be different in solution).

The transition state for rotation about the carbonyl carbon–nitrogen bonds in ureas is envisaged to have the $-NR_2$ entity perpendicular to the carbonyl plane. As the two urea C–N bonds are cross-conjugated, steric interactions causing $-NR_2$ to twist out of the carbonyl plane will destabilise the ground state and stabilise the transition state if the second $-NR_2$ simultaneously becomes more closely coplaner with the carbonyl group with a consequent increase in the order of the carbon–

nitrogen bond between them [87]. Thus the observed trends in k and $\Delta H^{\ddagger}$ for rotation about the C–NMe_2 bonds in coordinated 1,1-dmu, trmu and tmu may be explained as a consequence of the kinetic effects of the steric crowding within the ureas superimposing on the effects of coordination. As the steric crowding increases from 1,1-dmu to tmu, the destabilisation of the ground state and stabilisation of the transition state increases, decreasing $\Delta H^{\ddagger}$, and so the rate of rotation increases in this sequence.

The $\Delta S^{\ddagger}$ values for rotation about the C–N bonds in 1,1-dmu, trmu and tmu are all negative, probably as a consequence of the decreased rotational freedom of the methyl groups in the transition state as they are "squeezed" past obstructing groups on the same or adjacent ligands [107]. There may also be contributions from the electronic redistribution in the transition state due to the cross-conjugation. This also explains why the $\Delta S^{\ddagger}$ values for rotation about one C–N bond become more negative as the other nitrogen of the urea molecule becomes more substituted in the sequence from coordinated 1,1-dmu to tmu. As the degree of substitution increases, the rotational restriction in the transition state increases, making $\Delta S^{\ddagger}$ more negative. The $\Delta S^{\ddagger}$ value for rotation about the C–NH_2 bond in $[UO_2(1,1\text{-dmu})_5]^{2+}$ is positive because there is no change in the rotational freedom about the N–H bond on going from the ground to the transition state so that the only contributions arise from other, less well-defined, effects (such as changes in vibrational freedom and electronic redistribution). The rotation about the C–NHMe bond in the 1,3-dmu complex appears to fall between these two extremes with small positive or negative values of $\Delta S^{\ddagger}$, depending on the isomer.

3.6 The Effect of Substitution of Ureas on the Rate of Intermolecular Ligand Exchange and the Isokinetic Relationship

It is apparent from Table 3.6 that no obvious correlation exists between the structure of the ligand and the kinetic parameters characterising its exchange. As the size of the ligand is increased from nma to dea, $\Delta H^{\ddagger}$ and $\Delta S^{\ddagger}$ do not vary systematically

Table 3.6: Kinetic Parameters for Intermolecular Exchange of Some Monodentate Oxygen Donor Ligands (L) on $[UO_2(L)_5]^{2+}$

L	Solvent	k(298.2 K) [1] s^{-1}	$\Delta H^{\ddagger}$ [1] $kJmol^{-1}$	$\Delta S^{\ddagger}$ [1] $JK^{-1}mol^{-1}$	Ref.
dmf	CD_2Cl_2	17800	30.9 ± 1.2	−59.9 ± 5.6	[77]
nma	CD_2Cl_2	2545	67 ± 1	45 ± 6	[81]
nma	CD_3CN	2761	55.2 ± 0.5	6.1 ± 1.8	[81]
dma	CD_2Cl_2	778	37.2 ± 0.8	−64.9 ± 3.3	[76]
dea	CD_2Cl_2	1940	68.3 ± 1.2	47.1 ± 4.6	[75]
dea	CD_2CN	2034	76.5 ± 1.1	75.0 ± 4.0	[75]
trmu	CD_3CN	983	56.6 ± 0.6	2.2 ± 1.9	this work
tmu	CD_2Cl_2	1527	79 ± 11	81 ± 42	[10]
tmu	CD_3CN	1581	81 ± 1	88 ± 3	[10]
dmso	$(CD_3)_2CO$	3176	40.9 ± 0.5	−40.7 ± 1.8	[79]
dmmp	CH_2Cl_2	970	55.7 ± 1.0	−1.0 ± 4.0	[78]
tmp	CD_2Cl_2	447	22.6 ± 1.7	−118.4 ± 9.6	[82]
tep	CD_2Cl_2	503	40.6 ± 1.7	−57.7 ± 7.1	[82]
$OPMe_2Ph$	CD_2Cl_2	9626	82.5 ± 2.9	108 ± 11	[83]

[1] Quoted errors represent one standard deviation.

and $\Delta S^{\ddagger}$ is positive for nma and dea but negative for dma. In the case of the ureas, the similar ligands, trmu and tmu, have very different kinetic parameters which suggests that the ligand is not the only determinant of the magnitudes of $\Delta H^{\ddagger}$ and $\Delta S^{\ddagger}$. These differences may be a consequence of compensating changes in the bond distances between the uranium ion and the remaining equatorial ligands and axial oxo ligands as one ligand exchanges. It has been observed [62,108] that there is an inverse relationship between the uranium to axial oxygen distances and the uranium to equatorial ligand bond distances for a given number of equatorial ligands. Thus the variation in bond order and length as the equatorial occupancy changes can be compensated for by variation in the uranium–axial oxo bond order. As the order of each of the axial bonds is ≥ 2, small changes in distances in the transition state could substantially influence the bond distance changes in the equatorial plane and hence the activation parameters.

There may also be contributions to $\Delta H^{\ddagger}$ and $\Delta S^{\ddagger}$ from interactions outside the

first coordination sphere [109,110] rendering these parameters unreliable in mechanistic comparisons of effects occurring in the first coordination sphere. This is confirmed by the changes in activation parameters that occur on changing the solvent from CD_3CN to CD_2Cl_2. There is a significant change when the ligand is nma or dea but only a minor change when it is tmu indicating that contributions of varying magnitude, depending on the solvent and ligand, arise from interactions outside the first coordination sphere.

Nevertheless, when the activation data from the $[UO_2(L)_5]^{2+}$ systems which show a k_{ex} independence of free ligand concentration are combined, they conform well to the isokinetic relationship [82,81,111,112]:

$$\Delta H^{\ddagger} = \Delta G^{\ddagger} + T\Delta S^{\ddagger} \tag{3.1}$$

plotted in Figure 3.15. A linear regression of this wide range of $\Delta H^{\ddagger}$ and $\Delta S^{\ddagger}$ through Equation 3.1 yields an isokinetic temperature T_{iso} = 298 ± 11 K and $\Delta G^{\ddagger}_{iso}$ = 54.3 ± 0.5 kJ mol^{-1} at that temperature. For **D** ligand exchange on $[Al(ligand)_6]^{3+}$ and $[Mg(ligand)_6]^{2+}$ similar isokinetic relationships exist and yield T_{iso} = 317 and 251.5 K, and $\Delta G^{\ddagger}_{iso}$ = 75.3 and 41.8 kJ mol^{-1} respectively [82,113]. As the $[UO(L)_5]^{2+}$ values are intermediate between those of the Al(III) and Mg(II) systems it is concluded that the surface charge density (which is a major determinant of $\Delta G^{\ddagger}$ and hence the lability of ligand exchange occurring through a **D** mechanism [109,114,115]) experienced by ligands in the equatorial plane of dioxouranium(VI) lies between those of Al(III) and Mg(II). It has been suggested [109] that the changes in $\Delta H^{\ddagger}$ and $\Delta S^{\ddagger}$ are correlated (as observed in Figure 3.15) because the freedom of movement of molecules (which affects $\Delta S^{\ddagger}$) is related to the strength of the bonding (which affects$\Delta H^{\ddagger}$). Thus, as bond strength (and $\Delta H^{\ddagger}$) increases, the freedom of movement of molecules in the ground state decreases increasing the entropy difference between the ground and transition states (increasing $\Delta S^{\ddagger}$).

The rate constants for exchange of ligands in $[UO_2(L)_5](ClO_4)_2$ shown in Table 3.6 are generally slightly larger than those observed for the exchange of tmu on $[Ln(tmu)_6](ClO_4)_3$ where Ln = Tb – Lu (Chapter 2). For example, for tmu exchange in $[UO_2(tmu)_5]^{2+}$ k(298.2 K) is 1581 s^{-1} while that for $[Tb(tmu)_6]^{3+}$ is 1377 s^{-1}

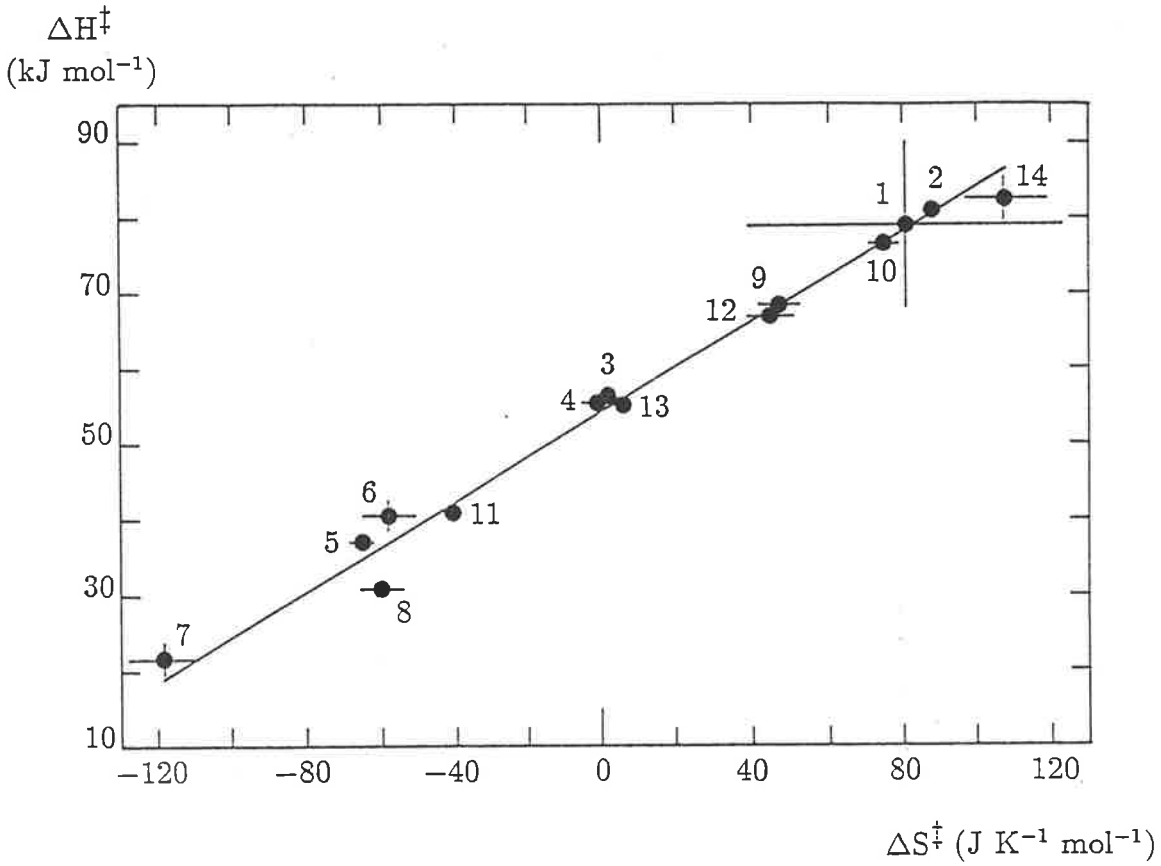

Figure 3.15:
Isokinetic plot for intermolecular exchange of monodentate ligands (L) on $[UO_2(L)_5](ClO_4)_2$. Individual ligands used are: (1) tmu in CD_2Cl_2 [10]; (2) tmu in CD_3CN [10]; (3) trmu in CD_3CN; (4) dmmp in CH_2Cl_2 [78]; (5) dma in CD_2Cl_2 [76]; (6) tep in CD_2Cl_2 [82]; (7) tmp in CD_2Cl_2 [82]; (8) dmf in CD_2Cl_2 [77]; (9) dea in CD_2Cl_2 [75]; (10) dea in CD_3CN [75]; (11) dmso in $(CD_2)_3CO$ [79]; (12) nma in CD_2Cl_2 [81]; (13) nma in CD_3CN [81] and (14) $OPMe_2Ph$ in CD_2Cl_2 [83]. The weighted linear regression line for this data is shown. The standard deviations in $\Delta H^{\ddagger}$ and $\Delta S^{\ddagger}$, where these errors are not encompassed by the symbol, are shown as bars extending beyond the symbol.

although these values arise from very different activation parameters. The steric crowding of the equatorial ligands in the dioxouranium(VI) complexes is expected to be much greater than the steric crowding of the ligands in lanthanide complexes. This should have the effect of increasing the rate of exchange (all other variables being equal). The surface charge density on UO_2^{2+} would be expected to be less than that on Ln^{3+} (at least for the heavier lanthanides) which again should increase the rate of exchange for the UO_2^{2+} complexes over the Ln^{3+} ones. This explains the generally slightly larger rates of exchange for ligands on $[UO_2(L)_5]^{2+}$ than those on $[Ln(tmu)_6]^{3+}$. For some $[UO_2(L)_5]^{2+}$ complexes, however, the rate constants are similar or smaller than those for $[Ln(tmu)_6]^{3+}$. This may be attributed to other factors such as ligand–uranium bond strength (which is related to the Gutmann donor number of the ligand [52]), the inter-relationship between the uranium–axial oxo and uranium–equatorial ligand bond lengths or effects from outside the first coordination sphere as discussed earlier.

Comparisons between $[UO_2(L)_5]^{2+}$ and $[Sc(L)_6]^{3+}$ in systems using the same ligand are difficult because, as can be seen from Tables 3.6 and 2.4, there are few studies where the same conditions have been used for both (i.e. same ligand and solvent). For tmu, the rate of exchange on $[UO_2(tmu)_5]^{2+}$ is much greater than that for either $[Sc(tmu)_6]^{3+}$ or $[Y(tmu)_6]^{3+}$ in CD_3CN. For nma and dea, there is a change of mechanism on going from $[UO_2(L)_5]^{2+}$ to $[Sc(L)_6]^{3+}$ from **D** to a two term rate law. This is probably a consequence of the greater steric crowding in the equatorial plane of the dioxouranium(VI) complex which prevents another ligand from entering into the first coordination sphere. This agrees with the observations made in Section 2.10 for the lanthanide complexes concerning the changes in rates and mechanisms of exchange that occur with increasing steric crowding.

Chapter 4

Exchange of Sodium(I) in Crown Ether Complexes

4.1 Introduction

4.1.1 Crown Ether and Related Host-Guest Complexes

The simplest cyclic polyethers (or "crown ethers") have the general formula shown in Figure 4.1. Various modifications are possible such as the addition of cyclohexane or benzene rings [116] or substitution of one or more of the oxygen atoms with nitrogen [117] or sulphur atoms [118,119]. Recently, a perfluoro crown ether has been prepared [120] by replacing the hydrogen atoms of the crown with fluorine. The crown ether nomenclature is a trivial one proposed by Pedersen [116] to be more manageable than the systematic one. Examples of the systematic and trivial nomenclatures are given in the Abbreviations at the beginning of this thesis.

In 1964 it was discovered that the macrocyclic antibiotic valinomycin selectively transports K^+ across lipophilic membranes [121]. This led to more studies of the complexation of ions by macrocyclic ligands and of their transport across membranes with similar findings of specificity (See references [122,123,124,125,126,127]). In these complexes, the macrocycle assumes a conformation such that the alkali metal ion is coordinated to the inwardly oriented oxygen donor atoms [128,129,130,131,132].

In 1967, Pedersen [116] synthesized 49 crown ethers and discovered that they were also capable of forming complexes with cations. There have now been many reports of complexes formed by crown ethers with alkali metal and other ions with var-

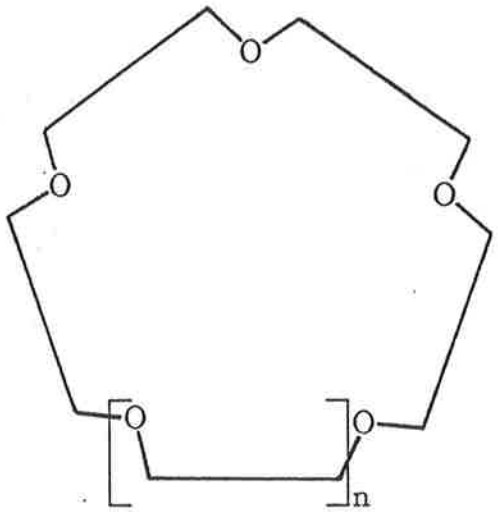

n=0 12-crown-4
n=1 15-crown-5
n=2 18-crown-6
etc.

Figure 4.1: General Crown Ether Structure

ious metal ion : ligand ratios including 3:1 [133], 2:1 [133,134,135,136,137,138], 3:2 [139,140], 4:3 [139,140,141,142], 2:3 [143], and 1:2 [135,144,145,146,147,148,149,150]. Some 1:1 complexes, whose structures have been determined by X-ray crystallography, are presented in Table 4.1. Dobler *et al.* [151] have solved the crystal structure for the mono-aqua complex [Na.18C6.H_2O].SCN . The sodium ion is coordinated to the six oxygen donor atoms of the 18-crown-6 (18C6) which almost encapsulates it. A water molecule is coordinated in a seventh coordination site. In solution, it is probable that a similar structure exists with the seventh coordination site occupied by a solvent molecule or thiocyanate anion depending on their relative coordinating abilities and steric factors. Live *et al.* [152] have deduced from nmr studies that the structure of Na.DB18C6 (where DB18C6 = dibenzo-18-crown-6) in solution is similar to that in the crystal structure [153].

Thus it is possible that crown ethers may serve as models for biological ion carriers. Their simplicity and variety of size, donor atoms, etc. makes them useful for determining the effects of various ligand, ion and solvent characteristics on

Table 4.1: Some 1:1 Crown Ether Complexes Whose Structures Have Been Determined by X-Ray Crystallography

Complex	Ref.	Complex	Ref.
LiSCN.12C4	[154]	$CaCl_2$.12C4.8H_2O	[165]
LiSCN.18C6.2H_2O	[155]	$Ca(SCN)_2$.18C6	[166]
$LiClO_4$.18C6.2H_2O	[155]	$CdCl_2$.18C6	[167]
NaSCN.15C5.$\frac{1}{2}H_2O$	[156]	$HgCl_2$.18C6	[167]
$NaBH_4$.15C5	[157]	$HgCl_2$.DB18C6	[168]
NaI.B15C5.H_2O	[153]	$La(NO_3)_3$.15C5	[169]
NaSCN.18C6.H_2O	[151]	$La(NO_3)_3$.18C6	[170]
NaSCN.DB18C6	[158]	$La(NO_3)_3$.DC18C6	[171]
NaBr.DB18C6.2H_2O	[153]	$Eu(NO_3)_3$.12C4	[172]
NaBr.DC18C6.2H_2O	[159]	$Eu(NO_3)_3$.15C5	[173]
KSCN.18C6	[160]	$Eu(NO_3)_3$.DA18C6	[174]
KNO_3.(2,6-Me_2-18C6)	[161]	$Sm(ClO_4)_3$.DB18C6	[175]
KI.DB30C10	[162]	$Nd(NO_3)_3$.15C5	[169]
RbSCN.18C6	[163]	$UO_2(NO_3)_2$.12C4.2H_2O	[176]
RbSCN.DB18C6	[158]	$UO_2(NO_3)_2$.18C6.2H_2O	[177]
CsSCN.18C6	[164]		

complex stability, cation selectivity and kinetics of exchange. They have similar structures to macrocyclic antibiotics such as valinomycin and the macrotetrolides such as nonactin although the crowns are more flexible.

Cryptands are also capable of complexing with metal ions. Cryptands have a structure similar to diaza-crown ethers with an extra polyether chain forming a very rigid macrobicyclic structure with a well defined cavity (e.g. Figure 4.2). First synthesized by Lehn *et al.* [117] in 1969, there have now been many studies on the complexation behaviour of these compounds (e.g. See [178,179]). Even more similar to the crown ethers are ligands of the type shown in Figure 4.3 which replace one of the polyether chains with a lipophilic hydrocarbon chain. Illustrated in the figure is $C21C_5$ which has five carbon atoms in the chain. This decreases the selectivity of divalent cations over monovalent cations [180] making them more similar to natural ionophores. The number of donor atoms in the ligand and the number of polyether rings is also decreased, reducing the "macrobicyclic effect" [181]. The effect of the hydrocarbon chain with respect to crown ethers will be discussed in Section 4.2.5.

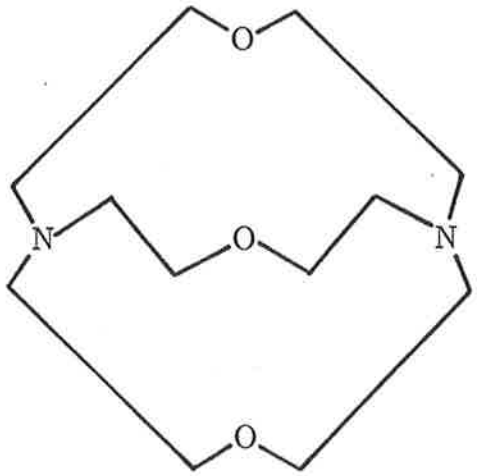

Figure 4.2: Structure of Cryptand C111

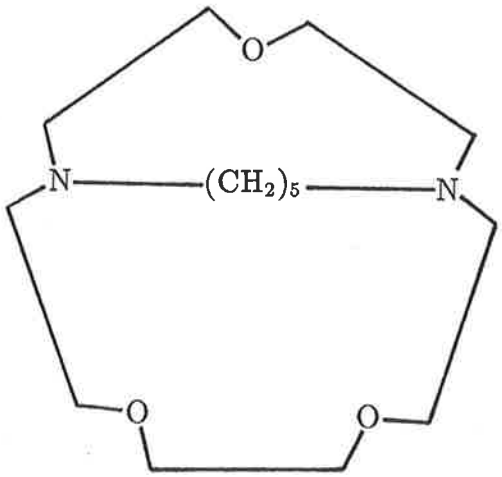

Figure 4.3: Structure of Cryptand C21C$_5$

Various other uses have been proposed for macrocyclic compounds such as valinomycin in ion-selective electrodes [182] and selective removal of Pb^{++} from environments containing Ca^{++} in the body with DC18C6 [183]. This latter area must be approached with caution, however, as 12-crown-4 has been found to cause testicular atrophy in rats [184,185]. Crown ether and cryptate complexes have even found promise as decontaminants for chemical warfare agents [186].

4.1.2 Previous Kinetic Studies of Crown Ether Complexes

A comprehensive review of thermodynamic and kinetic data for cation-macrocycle interactions covering the literature up to the end of 1983 has recently been published [178]. Hence, only the particularly relevant work from that period and the more recent work will be discussed here. The sodium ion and 18-crown-6 ether will be used here to illustrate the possible mechanisms but they are generally applicable to all alkali metals and crown ethers.

Two possible pathways for sodium ion exchange between the solvated cation Na^+ and the complexed cation $Na.18C6^+$ have been proposed [187,188,189]:

(i) the first order dissociative mechanism in which the complexed sodium ion is completely decomplexed before another sodium ion complexes with the crown ether:

$$Na^+ + 18C6 \underset{k_d}{\overset{k_c}{\rightleftharpoons}} Na.18C6^+ \tag{4.1}$$

and

(ii) the second order direct displacement process in which decomplexation and solvation of the complexed sodium ion takes place simultaneously with complexation and desolvation of a solvated ion (the asterisk is a typographical notation only to distinguish between the sodium ions):

$$^*Na^+ + Na18C6^+ \underset{k_d}{\overset{k_c}{\rightleftharpoons}} Na^+ + {}^*Na.18C6^+ \tag{4.2}$$

Strasser *et al.* [187] have found that in tetrahydrofuran (thf) solutions, the former mechanism predominates for $NaBPh_4$ with 18-crown-6 while for NaSCN the latter prevails. This is seen as a consequence of a reduction in the cation-cation repulsion by the strong ion pairing of the SCN^- anion although for NaSCN.18C6 exchange in methanol, the dissociative mechanism is predominant and for $NaBPh_4$.18C6 in propylene carbonate (pc) exchange is bimolecular [190]. For NaSCN.DB18C6, exchange in dmf is also consistent with Equation 4.1 [188]. For $KAsF_6$ with 18-crown-6 in 1,3-dioxolane solution and acetone solution, the bimolecular process dominates, but for this system in methanol a significant contribution to the rate is provided by each of the two mechanisms [191].

Other results have been consistent with the operation of the first order process for which there are at least two possible pathways, the Chock mechanism [192] and the Eigen-Winkler mechanism [193]. The Chock mechanism involves a rapid conformational rearrangement between at least two forms of the crown ether followed by the rate-determining complexation of the cation by one form of the crown, 18C6′ (Equation 4.3).

$$\begin{aligned} 18C6 &\underset{k_{-0}}{\overset{k_0}{\rightleftharpoons}} 18C6' \qquad (fast) \\ Na^+ + 18C6' &\underset{k_{-1}}{\overset{k_1}{\rightleftharpoons}} Na.18C6^{+\prime} \quad (slow) \end{aligned} \tag{4.3}$$

In the Eigen-Winkler mechanism, the initial step is the diffusion controlled formation of the encounter complex $Na^+ \ldots 18C6$. This is followed by the partial desolvation of the cation and partial rearrangement of the ligand to form an intermediate species, $Na.18C6^{+*}$, in which probably only one bond is formed between Na^+ and 18C6. The rate determining step follows which involves the sequential conformational change of the ligand and displacement of solvent bound to Na^+ to produce $Na.18C6^+$ (Equation 4.4).

$$\begin{aligned} Na^+ + 18C6 &\underset{k_{-1}}{\overset{k_1}{\rightleftharpoons}} Na^+ \ldots 18C6 \\ &\underset{k_{-2}}{\overset{k_2}{\rightleftharpoons}} Na.18C6^{+*} \\ &\underset{k_{-3}}{\overset{k_3}{\rightleftharpoons}} Na.18C6^+ \end{aligned} \tag{4.4}$$

These two mechanisms are kinetically indistinguishable from one another [194] and although the presence of the equilibrium between different conformers of 18-crown-6 (Equation 4.3) has been deduced from ultrasonic studies [194,195,196] this is insufficient evidence to prove the occurrence of exchange via the Chock mechanism. The Eigen-Winkler mechanism has recently been more generally accepted as the more valid mechanism for alkali metal crown ether complex studies and some examples where this mechanism is thought to operate follow.

Chen *et al.* [195] have deduced the occurence of the Eigen-Winkler mechanism by comparing the rate of complexation of alkali metal perchlorates by 18-crown-6 in methanol. This is a maximum for sodium over lithium and potassium and so is unlikely to be solely due to the desolvation of the cation and is probably due to the rearrangement of the ligand around the cation which corresponds to k_3 in the Eigen-Winkler mechanism (Equation 4.4). This is in contrast to the Chock mechanism where the rate-determining step is the desolvation of the cation and would not be expected to vary significantly between alkali metal cations and so the exchange rate for sodium would not be expected to be a maximum.

Maynard *et al.* [196] conclude that the Eigen-Winkler mechanism predominates for NaSCN and KSCN complexation with 18-crown-6 in dimethylformamide. Similar results have been found by Wallace *et al.* [197] by varying the rigidity of the ligand by using 18C6, DC18C6 and DB18C6 with various alkali metal perchlorates in dmf and methanol solutions. Increasing the rigidity of the ligand affects the rate of complexation and hence is attributable to the rate-determining step being the rearrangement of the crown around the metal ion.

Some of the complexation rate constants obtained in these studies are presented in Table 4.2. Ultrasound studies have generally derived the rate constant k_2 in the Eigen-Winkler scheme (Equation 4.4) while NMR studies usually obtain the overall complexation rate k_c or decomplexation rate k_d (see Equation 4.1). Some of the relevant decomplexation rate constants are discussed in conjunction with results from this work in Section 4.2.5.

Thus, despite much work in this area, the kinetics and mechanisms of exchange on crown ether complexes remain unresolved and appear to be a complex combi-

Table 4.2: Complexation Rate Constants for Na^+ Exchange on $Na.18C6^+$

Anion	Solvent	Rate constants k(298 K)	Reference
ClO_4^-	dmf	k_2 4.6 × 10^8 s^{-1}	[197]
	CH_3OH	k_2 2.8 × 10^8 s^{-1}	[197]
		k_3 1.6 × 10^6 s^{-1}	[197]
	CH_3CH_2OH	k_2 2.9 × 10^8 s^{-1}	[198]
SCN^-	dmf	k_2 4.6 × 10^8 s^{-1}	[198]
		k_2 3.7 × 10^8 s^{-1}	[196]
	CH_3OH	k_c 7.6 × 10^8 $M^{-1}s^{-1}$	[190]
BPh_4^-	pc	k_c >1.3 × 10^9 $M^{-1}s^{-1}$	[190]

nation of effects due to the metal ion, anion, crown and solvent. Accordingly, the following study was undertaken to determine the various effects on the rate and mechanism of exchange of alkali metal ions in crown ether complexes.

4.2 Exchange of Sodium(I) on the Sodium 18-Crown-6 Cation

4.2.1 Exchange in Methanol Solution

Sodium thiocyanate and 18-crown-6 were purified and dried and solutions made up as outlined in Chapter 5 . Two solutions of NaSCN and 18-crown-6 in methanol were prepared under anhydrous conditions such that the ratios of free sodium to complexed sodium were approximately 1 : 1 and 1 : 3 . Due to a great increase in the linewidth of the resonance of the complexed sodium at low temperature and because of the small shift difference between the free and complexed sodium signals, the lineshape parameters could not be obtained solely from the extrapolation from low temperature where no exchange induced modification of the lineshape is occurring. Hence, solutions containing only free sodium in methanol and a solution containing equimolar quantities of sodium and 18-crown-6 (i.e. all complexed sodium) were also prepared for the purposes of obtaining the lineshape parameters. In all cases the total concentration of sodium was approximately 0.1 M. Solution compositions are given in Table 4.3.

The exchange of sodium between the free and complexed environments was observed using ^{23}Na nmr. A typical set of exchange modified ^{23}Na nmr spectra are displayed in Figure 4.4 , showing a narrow low field and a broad high field resonance arising from the free and complexed Na^+ respectively. The concentration range used was limited by the small shift difference and the large difference in width of the resonances of the free and complexed sodium. From the stability constant given in Table 4.10 it can be calculated that virtually all 18-crown-6 is bound in $Na.18C6^+$ at the concentrations studied.

A complete lineshape analysis (as described in Section 6.2) of the spectra in the range 233.8 – 266.1 K for solution (i) and 233.8 – 261.5 K for solution (ii) yielded the exchange parameters given in Table 4.4. The values are given for a fit of each solution and for both sets of data combined. The values of k_d, the dissociation rate constant, are given at 245 K which is in the midst of the coalescence region. At this temperature, the modification to the spectra due to the chemical exchange is at a maximum and hence the most reliable values for k_d are obtained. From these k_d values and from the variation of $T\tau_c$ with temperature (shown in Figure 4.5), where τ_c is the mean lifetime of a coordinated sodium ion, it can be seen that within the concentration range studied, τ_c $(= k_d^{-1})$ is independent of concentration and that the predominant exchange process is first order with the exchange mechanism shown in Equation 4.1 rather than by an alternative second order direct displacement process of the form shown in Equation 4.2. The mean lifetimes of a single sodium ion in the coordinated and free states (τ_c and τ_f respectively) are related to each other via the mole fractions in each state (χ_c and χ_f respectively) by the equation:

$$\frac{\tau_c}{\chi_c} = \frac{\tau_f}{\chi_f} \tag{4.5}$$

4.2.2 Exchange in Pyridine Solution

Sodium thiocyanate and 18-crown-6 were purified and dried and solutions made up as outlined in Chapter 5 . Four pyridine solutions were prepared under anhydrous conditions such that the total concentration of sodium thiocyanate was approximately 0.1 M. Two solutions of NaSCN and 18-crown-6 were prepared such that

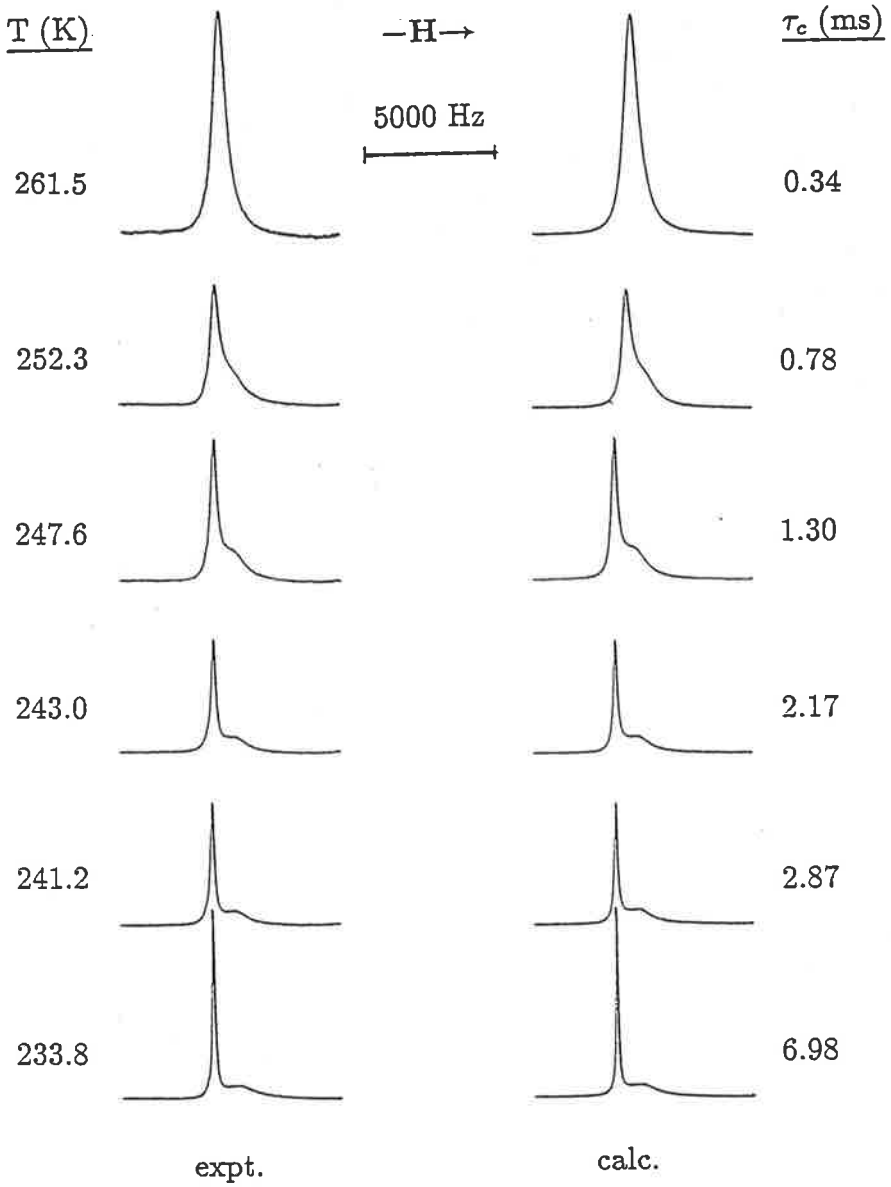

Figure 4.4:
Exchange modified 79.39 MHz ^{23}Na nmr spectra of a methanol solution of NaSCN (0.09792 M) and 18-crown-6 (0.04778 M). Experimental spectra and temperatures are shown at the left, and best fit calculated lineshapes and derived τ_c values are shown to the right.

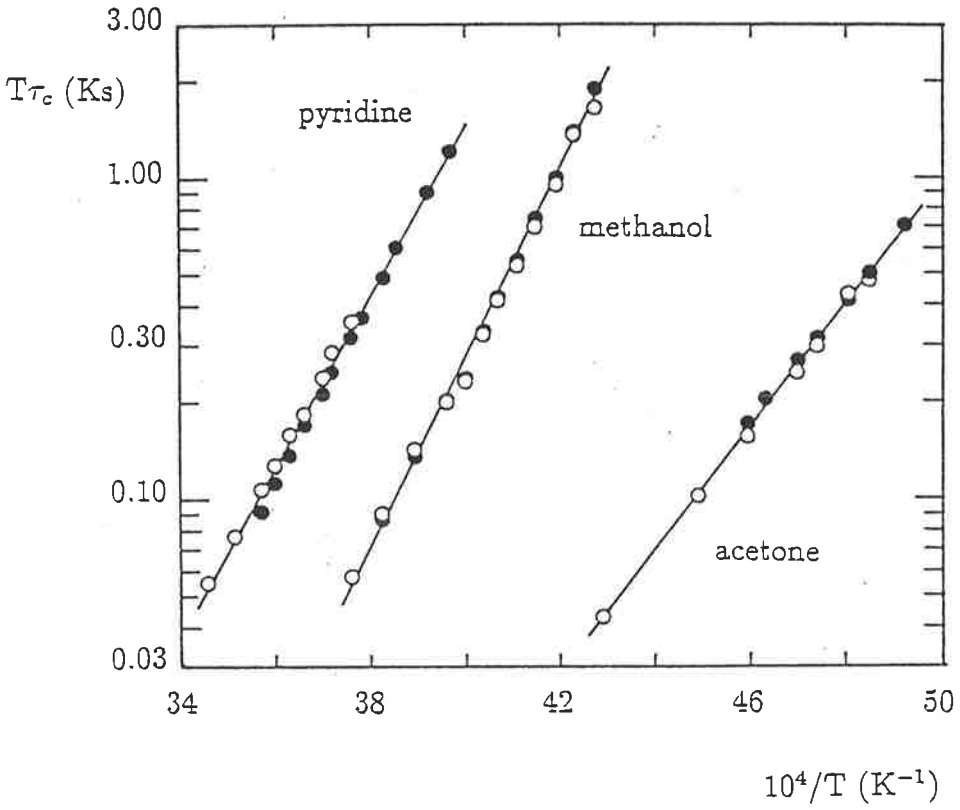

Figure 4.5:
Variation of $T\tau_c$ with $\frac{10^4}{T}$ for solutions of NaSCN and 18-crown-6. The open circles represent data derived from solutions (i) in methanol, pyridine and acetone. The closed circles represent the corresponding solutions (ii). The compositions of the solutions are given in Tables 4.3, 4.5 and 4.7 respectively. The solid lines represent the best fit of the combined data from each pair of solutions to Equation 6.31 obtained from linear regression analyses.

Table 4.3: Solution Compositions for Sodium Ion Exchange on the Sodium 18-Crown-6 Cation in Methanol.

Solution	$[NaSCN]_{total}$ mol dm^{-3}	$[18C6]_{total}$ mol dm^{-3}	$[Na^+]_{free}$ mol dm^{-3}	$[CH_3OH]$ mol dm^{-3}
i	0.09792	0.04778	0.05014	23.54
ii	0.09552	0.07368	0.02184	23.96

Table 4.4: Kinetic Parameters for Sodium Ion Exchange on the Sodium 18-Crown-6 Cation in Methanol.

Solution	$\Delta H^{\ddagger}$[1] kJ mol^{-1}	$\Delta S^{\ddagger}$[1] J $K^{-1}mol^{-1}$	k_d(245 K)[1] s^{-1}
i	52.4 ± 1.0	22.8 ± 3.7	542 ± 20
ii	55.6 ± 0.8	35.6 ± 3.2	523 ± 14
i & ii	53.6 ± 0.8	27.8 ± 2.9	532 ± 14

[1]Quoted errors represent one standard deviation.

the ratios of free sodium to complexed sodium were approximately 1 : 1 and 1 : 2 . Two solutions, one containing only free sodium and one containing equimolar amounts of NaSCN and 18-Crown-6 (i.e. all complexed sodium) were prepared for the purpose of obtaining the lineshape parameters. The range of concentrations available for study was restricted for similar reasons to those outlined in the methanol solution case. Solution compositions are given in Table 4.5 .

A typical set of ^{23}Na nmr spectra showing the exchange of sodium between the free and complexed environments are displayed in Figure 4.6, the low and high field resonances arising from free and complexed Na^+ respectively. From the stability constant given in Table 4.10 it can be calculated that virtually all 18-crown-6 is bound in $Na.18C6^+$ at the concentrations studied.

A complete lineshape analysis (Section 6.2) of the spectra in the range 266.1 – 289.2 K for solution (i) and 252.3 – 279.9 K for solution (ii) yielded the exchange parameters given in Table 4.6. The values of k_d, the dissociation rate constant, are given at 265 K at which the modification to the spectra due to the chemical exchange

Table 4.5: Solution Compositions for Sodium Ion Exchange on the Sodium 18-Crown-6 Cation in Pyridine.

Solution	$[NaSCN]_{total}$ mol dm^{-3}	$[18C6]_{total}$ mol dm^{-3}	$[Na^+]_{free}$ mol dm^{-3}	$[C_5H_5N]$ mol dm^{-3}
i	0.09920	0.04990	0.04930	12.14
ii	0.09850	0.06736	0.03114	11.79

Table 4.6: Kinetic Parameters for Sodium Ion Exchange on the Sodium 18-Crown-6 Cation in Pyridine.

Solution	$\Delta H^{\ddagger}$[1] kJ mol^{-1}	$\Delta S^{\ddagger}$[1] J $K^{-1}mol^{-1}$	k_d(265 K)[1] s^{-1}
i	52.5 ± 0.4	7.8 ± 1.4	645 ± 10
ii	53.2 ± 0.7	11.7 ± 2.5	744 ± 14
i & ii	50.5 ± 1.2	1.4 ± 4.2	716 ± 30

[1]Quoted errors represent one standard deviation.

is at a maximum and hence the most reliable values for k_d are obtained. From these k_d values and from the variation of $T\tau_c$ with temperature (shown in Figure 4.5) it can be seen that within the concentration range studied, τ_c is independent of concentration and that the predominant exchange process is first order with the exchange mechanism shown in Equation 4.1.

4.2.3 Exchange in Acetone Solution

Sodium thiocyanate and 18-crown-6 were purified and dried and two acetone solutions prepared under anhydrous conditions as outlined in Chapter 5 . The solutions were made up such that the ratios of free sodium to complexed sodium were approximately 1 : 1 and 1 : 2 . A solution containing only free sodium in acetone and a solution containing equimolar quantities of sodium and 18-crown-6 (i.e. all complexed sodium) were also prepared for the purposes of obtaining the lineshape parameters. Similar restrictions to the concentration range amenable to study applied in this case as in the cases of the other solvents. In all cases the total

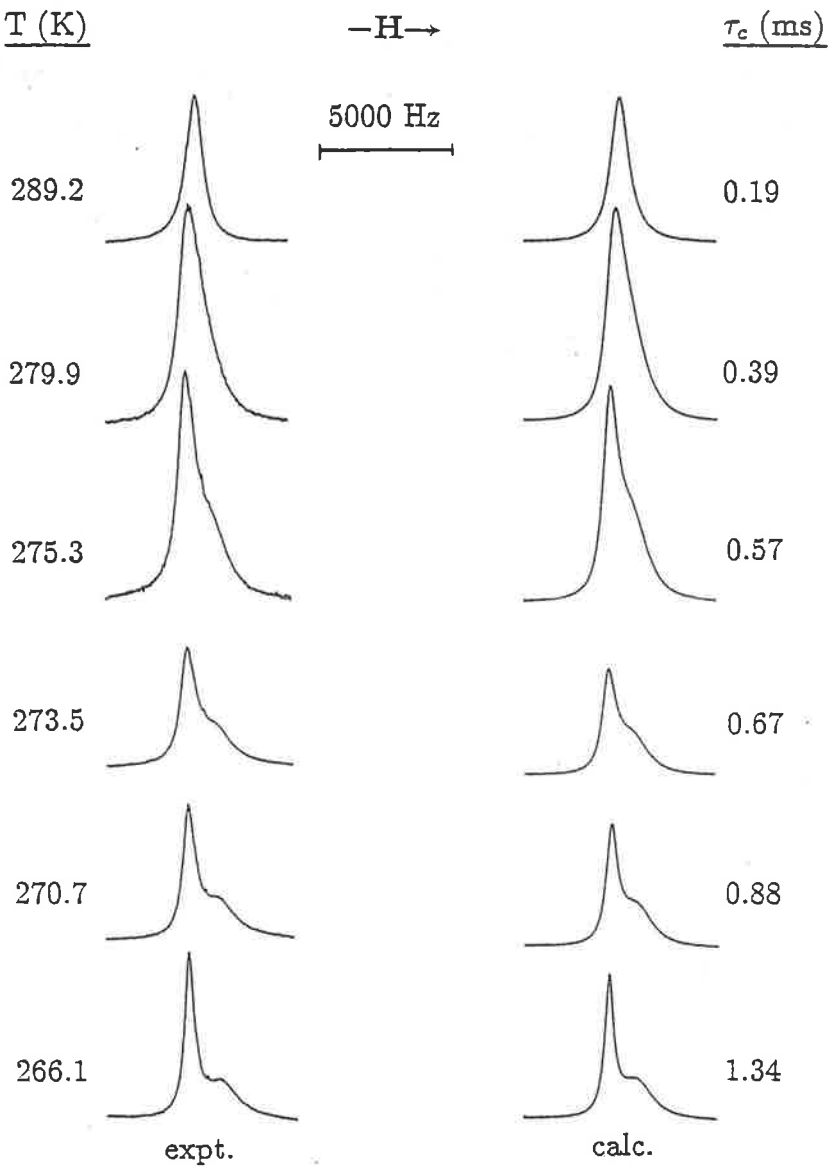

Figure 4.6:
Exchange modified 79.39 MHz ^{23}Na nmr spectra of a pyridine solution of NaSCN (0.09920 M) and 18-crown-6 (0.04990 M). Experimental spectra and temperatures are shown at the left, and best fit calculated lineshapes and derived τ_c values are shown to the right.

Table 4.7: Solution Compositions for Sodium Ion Exchange on the Sodium 18-Crown-6 Cation in Acetone.

Solution	$[NaSCN]_{total}$ mol dm^{-3}	$[18C6]_{total}$ mol dm^{-3}	$[Na^+]_{free}$ mol dm^{-3}	$[(CH_3)_2CO]$ mol dm^{-3}
i	0.09860	0.04843	0.05017	13.26
ii	0.09979	0.06787	0.03192	13.02

concentration of sodium was approximately 0.1 M. Solution compositions are given in Table 4.7 .

The exchange of sodium between the free and complexed environments was observed using ^{23}Na nmr. A typical set of ^{23}Na nmr spectra are shown in Figure 4.7, the low and high field resonances arising from free and complexed Na^+ respectively. From the stability constant given in Table 4.10 it can be calculated that virtually all 18-crown-6 is bound in $Na.18C6^+$ at the concentrations studied.

Complete lineshape analysis was performed as described in Section 6.2 for spectra in the range 206.1 – 233.0 K for solution (i) and 203.2 – 217.7 K for solution (ii) yielding the exchange parameters given in Table 4.8. The values of k_d, the dissociation rate constant, are given at 210 K where the chemical exchange modification to the spectra is at a maximum and where the most reliable values for k_d are obtained. From these k_d values and from the variation of $T\tau_c$ with temperature (shown in Figure 4.5) it can be seen that τ_c is independent of concentration within the concentration range studied, and that the predominant exchange process is first order with the exchange mechanism shown in Equation 4.1.

4.2.4 Exchange in Other Solvents

The solutions detailed above proved amenable to lineshape analysis and yielded kinetic data from which the activation parameters could be calculated. Solutions of similar concentration to those above were prepared in several other solvents to observe the effect of the solvent on the rate and mechanism of exchange. These solutions were studied using ^{23}Na nmr in a similar manner to the solutions in acetone, methanol and pyridine.

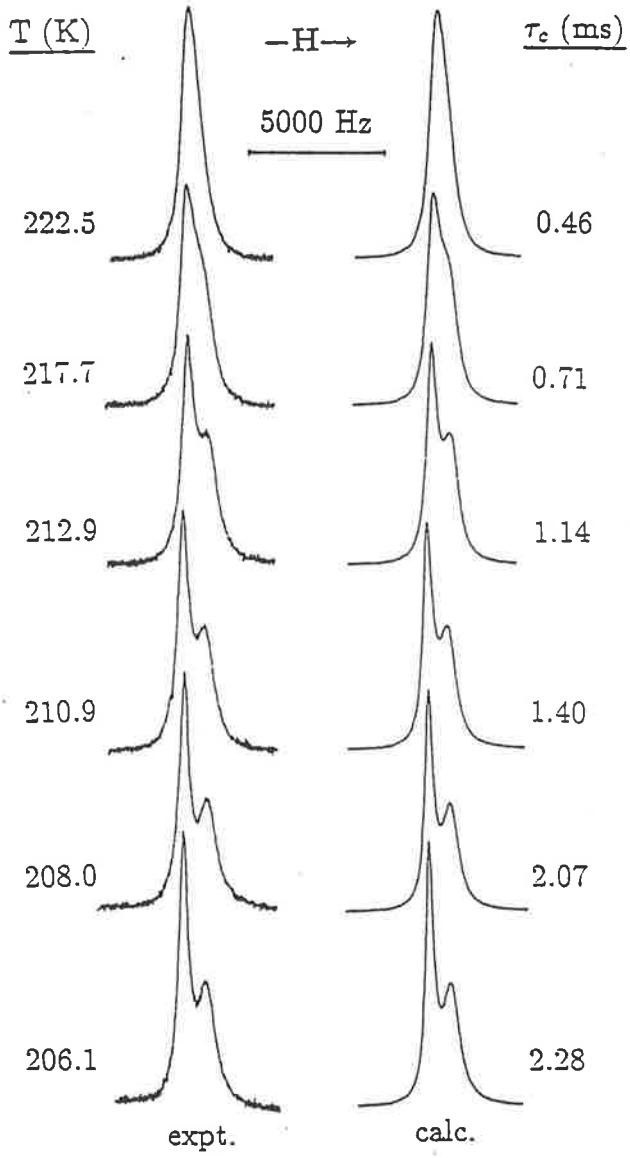

Figure 4.7:
Exchange modified 79.39 MHz ^{23}Na nmr spectra of an acetone solution of NaSCN (0.09860 M) and 18-crown-6 (0.04843 M). Experimental spectra and temperatures are shown at the left, and best fit calculated lineshapes and derived τ_c values are shown to the right.

Table 4.8: Kinetic Parameters for Sodium Ion Exchange on the Sodium 18-Crown-6 Cation in Acetone.

Solution	$\Delta H^{\ddagger 1}$ kJ mol^{-1}	$\Delta S^{\ddagger 1}$ J K^{-1}mol^{-1}	k_d(210 K)[1] s^{-1}
i	36.1 ± 0.8	−16.5 ± 3.5	640 ± 25
ii	35.8 ± 0.6	−18.3 ± 2.5	597 ± 8
i & ii	36.7 ± 0.7	−14.0 ± 3.2	615 ± 18

[1]Quoted errors represent one standard deviation.

Solutions were prepared in dimethylsulphoxide (dmso), hexamethylphosphoramide (hmpa), dimethylformamide (dmf), propylene carbonate (pc), acetonitrile and water. Only one peak is observed down to the freezing point of each solution. Due to the large shift difference between the solution containing only uncomplexed sodium and the solution with a 1 : 1 ratio of free to complexed sodium (see Table 4.9) it is inferred that they are in the fast exchange limit of the nmr timescale. It is possible in the cases of water and hexamethylphosphoramide, due to the small shift difference, that there is little or no complexation but this seems unlikely in light of the small Gutmann donor number of water and high donor number of hmpa and so is probably fortuitous. A solution was also prepared in nitromethane but the salt was found to be partially insoluble hence studies in this solvent were not pursued.

4.2.5 Discussion and Conclusions

The variation of the mean lifetime of Na.18C6$^+$, τ_c, with temperature presented in Figure 4.5 shows that within the concentration range studied τ_c does not vary within each pair of solutions for each of the three solvents which yielded kinetic data, *viz.* acetone, methanol and pyridine. This indicates that the predominant exchange process is first order as shown in Equation 4.1 rather than by an alternative second order process in which Na^+ exchanges on Na.18C6$^+$ through a direct displacement mechanism as shown in Equation 4.2.

The k_d values determined from the nmr studies reported here characterise the slowest of the sequential decomplexation steps (the rate-determining step) and is

Table 4.9: Compositions and ^{23}Na shifts of NaSCN / 18C6 Solutions in Various Solvents

Solution	Solvent	DN[1]	[NaSCN] mol dm^{-3}	[18C6] mol dm^{-3}	Shift[2] Hz
i	CH_3CN	14.1	0.1028	0.0000	−352
ii			0.1493	0.0675	−628
iii	pc	15.1	0.1008	0.0000	−581
iv			0.1115	0.0579	−872
v	H_2O	18.0	0.1009	0.0000	−2
vi			0.1524	0.0669	−170
vii	dmf	24.0	0.1033	0.0000	−293
viii			0.0999	0.0505	−638
ix	dmso	29.8	0.1023	0.0000	17
x			0.0904	0.0504	−301
xi	hmpa	38.8	0.1028	0.0000	310
xii			0.0692	0.0330	293

[1]Gutmann donor number [52]
[2]At 300 K relative to 1 M NaCl in H_2O

equated to k_{-3} in Equation 4.4. From this and the value for k_3 given in Table 4.2 it can be calculated that, in methanol, Na.18C6$^+$ is more stable than Na.18C6^{+*} by a factor of *ca.* 22.

For the systems studied, it is probable that k_d characterises the displacement of an 18-crown-6 oxygen atom from its Na^+ binding site by a solvent molecule, which is followed by more rapid displacements until decomplexation is complete. Any dependence of k_d on the nature of the solvent probably arises through a combination of the solvent's:

(i) ability to compete with 18C6 for coordination sites on Na^+

(ii) influence on the formation of ion pairs between Na.18C6$^+$ and SCN^- (as mentioned in Section 4.1.2) and

(iii) influence on the conformational energetics of 18C6. It has been shown that various solvents interact with 18C6 to different degrees [199]. It is suggested that these interactions affect the stabilities of 18C6 metal

complexes and therefore their complexation and decomplexation rates also. However, it is difficult to quantify this factor and hence this influence is not discussed in detail further.

If the electron donating ability of the solvent was the only factor determining the rapidity of decomplexation then k_d should increase in the sequence of increasing Gutmann donor number (DN) [52]: acetone < methanol < pyridine. It is seen that k_d increases in the order: pyridine < methanol < acetone (Table 4.10). This suggests that the effect of DN on k_d is obscured by other factors. Steric hindrance of the incoming solvent molecule may be one such factor whereby the unexpectedly low k_d value of pyridine (on the basis of its DN) may be rationalised. As a consequence of the incorporation of the nitrogen donor atom into its ring structure, pyridine is sterically hindered in its approach to complexed Na^+ by comparison to the smaller acetone and methanol molecules.

Alternatively, the low k_d value for pyridine may be due to a lower solvating ability than that expected from its donor number alone. This lower solvating ability has been observed by Ahmad *et al.* [200] and Greenberg *et al.* [201] and has been rationalised as a consequence of pyridine being a "soft base" and hence not solvating a "hard acid" ion such as sodium [202]. This would result in a more stable $Na.18C6^+$ complex in this solvent and a consequent decrease in k_d. A similar inconsistency in the expected order of complex stability on the basis of donor number has been found for the complex Na.DA18C6 (where DA18C6 = 1,10-diaza-18-crown-6) [203]. For all the solvents studied except for pyridine the stability of the complex decreases with increasing donicity of the solvent. In pyridine, a more stable complex is formed than that expected by its high Gutmann donor number of 33.1 and is rationalised in terms of the soft basicity of pyridine. A similar explanation is given for the strong complexation of Cs^+ with 18C6, DB18C6 and DC18C6 in pyridine [204]. A study of alkali metal ion complexation with DA18C6 and 18C6 in acetonitrile, propylene carbonate and acetone [205] has found that the values of formation constants for the DA18C6 complexes generally follow the expected pattern (i.e. a decrease with increasing donor number of the solvent) but the values for the 18C6 complexes do not. This is attributed to lack of consideration of effects due to the solvation of the

ligand.

However, in this study, even in acetone and methanol, the k_d do not show the variation expected on the basis of DN alone. In view of the ion pairing discussed in Section 4.1.2 and the probability that the extent of ion pairing between SCN^- and $Na.18C6^+$ varies with the dielectric constants and donor numbers of acetone, pyridine and methanol (borne out by the variations in mechanisms observed with various anions in different solvents detailed in Section 4.1.2), it is possible that some of the variation in k_d characterising Na^+ exchange in these solvents may reflect the effects of ion pairing on the lability of Na^+ exchange through the first order mechanism.

In the limited range of solvents studied here the variation of k_d cannot be assigned to a single solvent characteristic. Strasser *et al.* [190] have proposed a linear relationship between log k_d and DN and have taken this as evidence for DN being the dominant solvent characteristic determining Na^+ exchange on $Na.18C6^+$ in thf, methanol and water. Even assuming that the different anions involved (BPh_4^-, SCN^- and Cl^- respectively for the three solvents) do not affect the exchange and that the donor numbers of 25.7 and 33 respectively assigned to methanol [206] and water [207] are more appropriate than the 19.0 and 18.0 originally proposed by Gutmann, the log k_d determined in this study in acetone and pyridine still do not lie close to the linear relationship proposed for the three solvents studied by Strasser *et al.* . This indicates for acetone and pyridine, at least, factors other than DN significantly affect the variation of k_d.

In several sodium cryptate systems, increases in k_d have been found to correlate reasonably well with increases in DN in a range of solvents [208]. It may be that the more rigid cryptate conformation is less susceptible to solvent-ion effects and ion pairing effects than is $Na.18C6^+$ with the result that the solvent interaction with complexed metal ions in the cryptates becomes a dominant kinetic factor leading to a direct correlation between the magnitudes of DN and k_d. It may also be an effect due to the solvent influence on the conformational energetics of the ligand mentioned earlier. Even so, k_d for the decomplexation of $Na.C21C_5^+$ (where $C21C_5$ is 4,7,13-trioxa-1,10-diazabicyclo[8.5.5]eicosane, shown in Figure 4.3) in pyridine is

substantially less than k_d observed in acetone and methanol [209] (Table 4.10).

The variation in k_d for sodium exchange in C222, C221 and C211 may be explained in terms of an optimum cavity size for sodium with C221. This is also reflected in the value for log K being a maximum for this complex. The rates of formation, k_c, increase monotonically with increasing ligand size which can be explained by the greater flexibility of the larger ligands facilitating interaction with the incoming cation [208]. The values of k_d in methanol increase from the cryptates C222, C221 and C211 to $C21C_5$. This can be seen as a consequence of the decrease in the number of donor atoms on the ligand making decomplexation easier. The k_d values also increase from $C21C_5$ to 18C6 even though the number of donor atoms increases which may be attributed to the greater flexibility of 18C6 by comparison with $C21C_5$.

In Table 4.10 the activation parameters from the combined fit for each solvent studied are presented with the parameters for some other host-guest complex systems. The k_d values are given at 298.2 K for the purpose of comparison. At this temperature all three systems are in the very fast exchange limit of the nmr timescale and are hence subject to larger errors. The values for methanol obtained in Section 4.2.1 and those obtained by Strasser *et al.* [190] are also presented. Although the derived activation parameters differ significantly, the decomplexation and complexation rate constants, k_d and k_c, for the two sets of data differ by a factor of less than two. The source of the difference in activation parameters appears to be experimental as the two sets of data do not superimpose in the overlapping segments of their temperature ranges. The results from this study were obtained at 79.39 MHz whereas those of Strasser *et al.* were obtained at 47.61 MHz. The higher frequency gives a greater shift difference between the comlexed and uncomplexed sodium resonances allowing complete lineshape analysis. Thus the results from this study should be more accurate.

Table 4.10: Kinetic Parameters of Na^+ exchange on $Na.18C6^+$ and Some Other Host-Guest Complexes

Solvent	DN[1]	anion	$10^{-4}k_d$ (298.2 K) s^{-1}	$\Delta H^{\ddagger}$ kJ mol^{-1}	$\Delta S^{\ddagger}$ J $K^{-1}mol^{-1}$	logK	$10^{-9}k_c^2$ (298.2 K) $M^{-1}s^{-1}$
$Na.18C6^+$							
acetone[3]	17.0	SCN^-	43.4	36.7	−14.0	> 4[8]	> 4.1
methanol[3]	19.0	SCN^-	7.2	53.6	27.8	4.32[9]	1.5
methanol[4]	19.0	SCN^-	3.65	38.1	−30.1	4.32[9]	0.76
pyridine[3]	33.1	SCN^-	1.03	50.5	1.4	> 3[8]	> 0.1
thf[5]	20.0	BPh_4^-	53	47.3	−52.3	> 4[8]	> 0.5
water[6]	18.0	Cl^-	3400			0.8[10]	0.21
			$10^{-4}k_d$ (298.2 K) $M^{-1}s^{-1}$				
thf[5]	20.0	SCN^-	9.16	11.7	−113		
$Na.C21C_5^+$							
			$10^{-4}k_d$ (298.2 K) s^{-1}				
acetone[7]	17.0	ClO_4^-	0.0878	54.4	−6.1	3.98	0.0084
methanol[7]	19.0	ClO_4^-	0.180	44.9	−31.9	3.76	0.0104
pyridine[7]	33.1	ClO_4^-	0.0093	62.8	3.3	3.71	0.00048
$Na.C222^+$							
methanol[11]	19.0		0.000287			7.98	0.27
pyridine[12]	33.1	Br^-	0.000114	56.9	−52.7		
$Na.C221^+$							
methanol[13]	19.0	ClO_4	1.96×10^{-6}	64.6	−61	9.65	0.0874
$Na.C211^+$							
methanol[11]	19.0		0.00025			6.1[14]	0.0031

[1]Reference [52] [2]$k_c = Kk_d$ [3]Results from this chapter
[4]Reference [190] [5]Reference [187] [6]Reference [210]
[7]Reference [209] [8]Reference [211] [9]Reference [212]
[10]Reference [213] [11]Reference [214] [12]Reference [215]
[13]Reference [216] [14]Reference [217]

Table 4.11: Compositions and ^{23}Na shifts of NaSCN / 15C5 Solutions in Various Solvents

Solution	Solvent	[NaSCN] mol dm^{-3}	[15C5] mol dm^{-3}	Shift[1] Hz
i	methanol	0.1016	0.0000	−212
ii		0.1013	0.0496	−249
iii	pyridine	0.1014	0.0000	273
iv		0.0994	0.0488	76
v	acetone	0.1031	0.0000	−342
vi		0.0986	0.0489	−305
vii	CH_3CN	0.1028	0.0000	−352
viii		0.0994	0.0499	−288
ix	H_2O	0.1009	0.0000	−2
x		0.0988	0.0496	−46
xi	dmf	0.1016	0.0000	−293
xii		0.1000	0.0499	−369
xiii	dmso	0.1023	0.0000	17
xiv		0.1015	0.0496	−85
xv	hmpa	0.1028	0.0000	310
xvi		0.1010	0.0498	300
xvii	pc	0.1008	0.0000	−581
xviii		0.0993	0.0504	−469

[1]At 300 K relative to 1 M NaCl in H_2O

4.3 Other Crown Complex Studies

4.3.1 Sodium(I) 15-Crown-5 Studies

Solutions of sodium thiocyanate and 15-crown-5 were prepared as outlined in Chapter 5 in nine solvents with the compositions given in Table 4.11. 79.39 MHz ^{23}Na nmr spectra were obtained over the accessible temperature range of the solvents. All the solutions exhibited only one peak over the entire temperature range. The peak shifts and linewidths are also given in Table 4.11. A solution in nitromethane was also prepared but the complex proved insoluble in this solvent.

From the large shift differences between the solutions containing only uncomplexed sodium and the solutions with a 1 : 1 ratio of free to complexed sodium it appears that the exchange is in the fast exchange limit in these solvents. The

methanol spectrum at 192.7 K shows a slight bulge on the side of the peak indicating that exchange is slowed (Figure 4.8). The small shift in the hmpa signal on addition of 15-crown-5 may be attributed to the weak or non-complexation of the metal ion with the crown due to the large Gutmann donor number (38.8) of this solvent.

4.3.2 Lithium(I) Studies

It was established above that the sodium ion forms a sufficiently stable and long-lived complex with 18-crown-6 to be able to be observed with nmr spectroscopy. On the other hand, the sodium 15-crown-5 complex exchange was too fast to be observed. Due to the smaller ionic radius of the lithium(I) ion compared to the sodium(I) ion, the lithium complex formed with the smaller crown ether 15-crown-5 should be more favoured and hence more amenable to exchange studies than the sodium one. For this reason, several solutions were prepared of lithium thiocyanate and 15-crown-5 were prepared as described in Chapter 5. 116.64 MHz ^{7}Li nmr spectra were obtained for each over the liquid temperature range of the solvents. The solution compositions and shifts are given in Table 4.12.

Solutions in nitromethane, acetonitrile and acetone were also prepared but the salt proved to be insoluble in these solvents. This may be due to the low Gutmann donor numbers of these solvents (2.7, 14.1 and 17.0 respectively) which may not be high enough to solvate the ions to dissociate the salt.

In methanol, pyridine and propylene carbonate, the large shift difference between the solutions with added crown and those with only salt appears to indicate that the complex in these solvents is in fast exchange at ambient temperature. The small shift in the lithium signals on addition of crown ether to the H_2O, dmso, hmpa and dmf is explained by Smetana *et al.* [218]. They found that no complex is formed in H_2O and dmso and that "in general, the stability of the complex varies inversely with the Gutmann donor number of the solvent". Thus it appears that the low donor number solvents do not solvate the ions strongly enough to dissolve the salt while the high donor number solvents solvate them so strongly that the energy required to remove them to form the crown ether complex is too great to give a

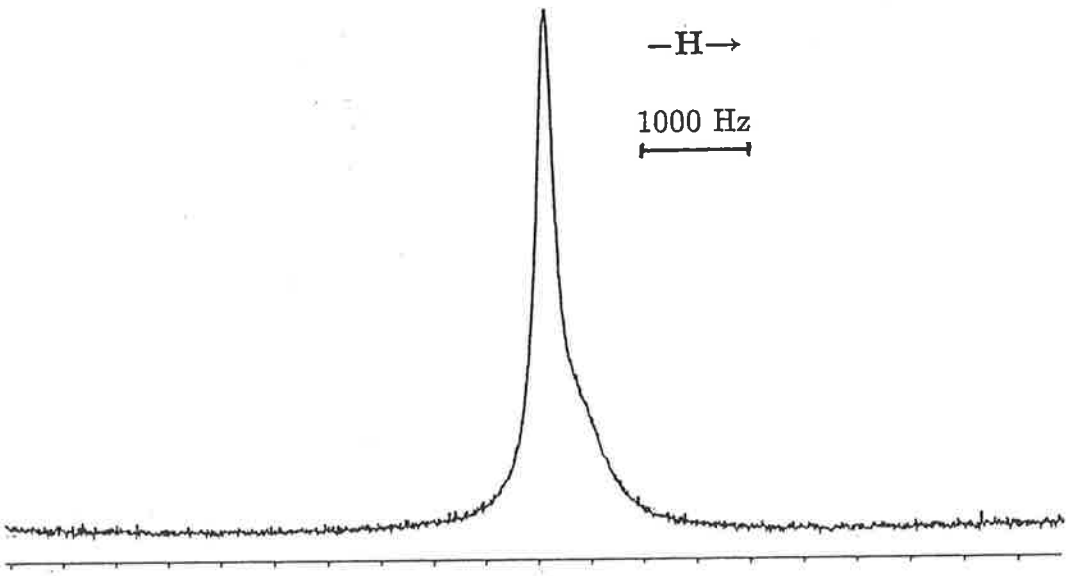

Figure 4.8:
79.39 MHz ^{23}Na nmr spectra of a methanol solution of NaSCN (0.1013 M) and 15-crown-5 (0.0496 M) at 192.7 K showing a small bulge attributable to the slowing of the exchange at low temperature.

Table 4.12: Compositions and ^{7}Li shifts of LiSCN / 15C5 Solutions in Various Solvents

Solution	Solvent	[LiSCN] mol dm^{-3}	[15C5] mol dm^{-3}	Shift[1] Hz
i	methanol	0.1023	0.0000	14
ii		0.0985	0.0504	−14
iii	pyridine	0.1000	0.0000	239
iv		0.1001	0.0488	143
ix	H_2O	0.0873	0.0000	1
x		0.0997	0.0484	5
xi	dmf	0.1047	0.0000	95
xii		0.1022	0.0518	91
xiii	dmso	0.1000	0.0000	−80
xiv		0.0981	0.0481	−82
xv	hmpa	0.1014	0.0000	−52
xvi		0.0996	0.0499	−44
xvii	pc	0.1023	0.0000	−118
xviii		0.1010	0.0494	−151

[1]At 300 K relative to 1 M LiCl in H_2O

stable complex. The complexes in fast exchange appear to strike a compromise between these two extremes.

Similar results have been found by Shamsipur *et al.* [203] in a study of alkali metal complexation with the ligand 1,10-diaza-18-crown-6 (DA18C6) in various solvents. In all cases only one resonance was observed. For solvents with high Gutmann donor numbers the shift is almost independent of ligand/metal ion ratio which is attributed to the formation of only a very weak complex. For solvents of low and medium solvating ability, the shift is significantly affected by addition of ligand.

Chapter 5

Experimental

5.1 Origin and Purification of Chemicals

5.1.1 Hydrated Metal Salts

Hydrated lanthanide perchlorate salts were prepared by reacting hot concentrated perchloric acid (Merck) with a slight excess of the corresponding oxide (Spex: Yb_2O_3, Tm_2O_3; Fluka: Er_2O_3, Ho_2O_3, Dy_2O_3, Tb_4O_7, Pr_6O_{11}). Excess oxide was filtered off and the resulting solution dried *in vacuo* over P_2O_5.

Hydrated lanthanide trifluoromethanesulphonate salts were prepared using a similar method using trifluoromethanesulphonic acid (Aldrich) instead of perchloric acid.

Hydrated dioxouranium(VI) perchlorate (G. Frederick Smith), NaSCN (Ajax), LiSCN (Fluka) and $Cd(SCN)_2$ (May and Baker) were used after drying *in vacuo* without further purification.

5.1.2 Dehydrating Agents

Triethylorthoformate (Fluka) was used without further purification. Linde 3A and 4A molecular sieves (B.D.H.) were activated by heating in a furnace for eight hours at 450 K. Phosphorous(V) pentoxide (Merck), used as supplied, was used to dry the atmosphere in glove-boxes and desiccators.

5.1.3 Ligands

The liquid tmu (Fluka) was vacuum distilled and dried over Linde 4A molecular sieves before use. The solids 1,1,3-trimethylurea (Alfa), 1,1-dimethylurea (Sigma) and 1,3-dimethylurea (Fluka) were dried over P_2O_5 *in vacuo*.

The solid 18-crown-6 (Aldrich) was purified and dried using the method of Gokel *et al.* [219]. The liquid 15-crown-5 (Aldrich) was used after drying over Linde 4A molecular sieves.

5.1.4 Solvents

The deuterated solvents d^6-dimethylsulphoxide (Aldrich, 99.9%D), d^3-acetonitrile (Aldrich, 99%D), d^6-acetone (Aldrich, 99.5%D) and d^2-dichloromethane (CEA, 99.4%D) were dried over Linde 3A or 4A molecular sieves. Other non-aqueous solvents were purified and dried by literature methods [220] and stored over Linde 4A molecular sieves. Anhydrous diethylether was prepared by drying analytical reagent grade diethylether (Ajax) with sodium wire.

5.2 Preparation of Metal Complexes

Hexakis(1,1,3,3-tetramethylurea)ytterbium(III) triperchlorate
Hexakis(1,1,3,3-tetramethylurea)thulium(III) triperchlorate
Hexakis(1,1,3,3-tetramethylurea)erbium(III) triperchlorate
Hexakis(1,1,3,3-tetramethylurea)holmium(III) triperchlorate
Hexakis(1,1,3,3-tetramethylurea)dysprosium(III) triperchlorate
Hexakis(1,1,3,3-tetramethylurea)terbium(III) triperchlorate
Hexakis(1,1,3,3-tetramethylurea)thulium(III) tri(trifluoromethanesulphonate)
Hexakis(1,1,3,3-tetramethylurea)ytterbium(III) tri(trifluoromethanesulphonate)

The above complexes were prepared using a procedure similar to that of van Leeuwen and Groeneveld [221]. The hydrated metal salt was dissolved in a five-fold excess of triethylorthoformate per mole of water and the solution heated at 330 K for 90 minutes. The solution was transferred to a dry nitrogen flushed glove-box where an excess of the ligand was introduced slowly. The complexes pre-

cipitated immediately and were filtered off and dried under a stream of dry nitrogen for several hours before drying under vacuum for 12 hours.

Pentakis(1,1,3-trimethylurea)dioxouranium(VI) diperchlorate

The complex was prepared by a similar method to that above except that the solid ligand was dissolved in a 10% solution by volume of ethanol in triethylorthoformate prior to introduction to the metal salt solution. Exposure to light of this and the other dioxouranium complexes and their solutions was kept to a minimum to avoid the possibility of decomposition or photochemically induced redox processes [222,223].

Pentakis(1,3-dimethylurea)dioxouranium(VI) diperchlorate

The hydrated salt was dissolved in a five-fold excess of triethylorthoformate and heated with stirring at 330 K for 90 minutes in a round bottomed flask fitted with a reflux condenser and a silica gel guard tube. A small excess of the solid ligand was finely ground and added. An oil precipitated from the solution and the mixture was subsequently heated for a further 90 minutes after which time the supernatent liquid was decanted off and the oil washed in anhydrous diethylether. The oil crystallised and the yellow crystals were filtered off, washed with diethylether and dried as for the complexes above.

Pentakis(1,1-dimethylurea)dioxouranium(VI) diperchlorate

Due to the insolubility of the ligand in neat triethylorthoformate, the hydrated salt was dissolved in a 25% solution by volume of ethanol in triethylorthoformate such that there was a five-fold excess of triethylorthoformate over the amount of water present. The solution was heated at 330 K for 90 minutes after which an excess of the finely divided solid ligand was added. The reaction mixture was heated for a further 90 minutes and cooled to room temperature in a dry atmosphere. The undissolved excess ligand was filtered off and diethylether was slowly added to the filtrate. An oil precipitated which crystallised after 48 hours under ether. The yellow crystals were filtered off and dried as for the complexes above.

Hexakis(1,1,3,3-tetramethylurea)praseodymium(III) triperchlorate

This complex was prepared as for the other analogous lanthanide complexes but

when the ligand was added, an oil and a solid precipitated out. The solid was decanted and filtered off and dried as for the other complexes.

Hexakis(1,1,3-trimethylurea)ytterbium(III) triperchlorate

Attempts to prepare a complex of stable coordination number failed, hence this avenue of research could not be pursued further.

Hexakis(1,1,3,3-tetramethylurea)scandium(III) triperchlorate
Hexakis(1,1,3,3-tetramethylurea)aluminium(III) triperchlorate

These complexes were prepared as for the lanthanide(III) perchlorates but a mixture of species was found to exist in solution (as evidenced by ^{1}H nmr in the first case and ^{27}Al in the latter case) rendering them unsuitable for study for kinetic purposes.

Tetrakis(1,1-dimethylurea)beryllium(II) diperchlorate
Tetrakis(1,3-dimethylurea)beryllium(II) diperchlorate

Attempts to make these complexes by similar methods to those above resulted in the production of an intractable oil in both cases which did not crystallise despite several washings and cooling.

CAUTION: Although no explosion hazard was encountered with these complexes, perchlorate salts are potentially explosive [57,58] and should be handled with care.

5.3 Elemental Analysis

For the perchlorate salts, analyses of carbon, nitrogen and hydrogen content were performed by the Australian Microanalytical Service, Melbourne. For the trifluoromethanesulphonate salts, these analyses were carried out by the Canadian Microanalytical Service, Vancouver. Metal ion content and stoichiometry for all complexes were determined using the method of Vogel [224]:

A known mass of anhydrous complex was dissolved in deionised water and eluted through a cation exchange column in the H^{+} form (Dowex 50W mesh). The eluate was titrated against a standard sodium hydroxide solution using bromothymol blue

as indicator.

The dioxouranium(VI) complexes were analysed in a similar way for the bipositive cation UO_2^{2+}. Analysis results are shown in Table 5.1.

5.4 Infrared Spectral Analysis

Infrared spectra were recorded on a Perkin-Elmer 683 infrared spectrophotometer as nujol mulls between dry sodium chloride plates. The mull was prepared in anhydrous conditions immediately prior to recording the spectrum. No absorption bands typical of O–H stretching modes (in the region 3200 – 3600 cm^{-1}) which would indicate the presence of water were observed. Only single bands were observed for the Cl–O asymmetric stretch and asymmetric bending modes of the perchlorate anion (ClO_4^-) consistent with the perchlorate anion retaining T_d symmetry indicating no coordinating perchlorate is present [225,23]. For the trifluoromethanesulphonate complexes, results were also consistent with non-coordinating anion in the solid state [55,24 (g)]. The reduction in C=O stretching frequency observed for the coordinated ligands compared to that for the free ligands is indicative of oxygen to metal bonding [25]. This should be accompanied by an increase in the carbon-nitrogen absorbance frequency but, in general, the overlapping of absorbances in the range 1400 – 1530 cm^{-1} precluded unequivocal frequency assignments.

5.5 Preparation of NMR Samples

Solutions of the lanthanide and dioxouranium complexes were prepared by addition of weighed quantities of complex and ligand such that approximately equimolar amounts of coordinated and free ligand were present into a 1 or 2 cm^3 volumetric flask which was then made up with inert deuterated diluent. About 0.7 cm^3 of each solution was degassed and sealed under vacuum in 5 mm o.d. nmr tubes (507-PP, Wilmad Glass Co.).

Samples of thiocyanate salts and crown ethers for study were prepared in the following manner. A stock solution of the salt was prepared by mass in a 10 cm^3

Table 5.1: Elemental Analysis Results

Complex		% M[1]	% C	% N	% H
$UO_2(1,1\text{-dmu})_5(ClO_4)_2$	found	30.13	19.58	15.32	4.16
	calc.	29.69	19.81	15.40	4.43
$UO_2(1,3\text{-dmu})_5(ClO_4)_2$	found	30.17	20.08	15.70	4.49
	calc.	29.69	19.81	15.40	4.43
$UO_2(trmu)_5(ClO_4)_2$	found	27.60	24.66	14.60	5.30
	calc.	27.56	24.52	14.30	5.14
$Yb(tmu)_6(ClO_4)_3$	found	15.11	30.73	14.73	6.29
	calc.	14.81	30.84	14.39	6.21
$Tm(tmu)_6(ClO_4)_3$	found	14.46	30.71	14.72	6.27
	calc.	14.51	30.95	14.44	6.23
$Er(tmu)_6(ClO_4)_3$	found	14.31	30.89	14.25	6.38
	calc.	14.39	31.00	14.46	6.24
$Ho(tmu)_6(ClO_4)_3$	found	14.43	31.13	14.82	6.29
	calc.	14.21	31.06	14.49	6.25
$Dy(tmu)_6(ClO_4)_3$	found	14.29	30.95	14.49	6.07
	calc.	14.03	31.12	14.52	6.27
$Tb(tmu)_6(ClO_4)_3$	found	13.79	31.10	14.64	6.29
	calc.	13.77	31.22	14.56	6.29
$Pr(tmu)_6(ClO_4)_3$	found	12.74	31.45	15.19	6.30
	calc.	12.40	31.71	14.79	6.39
$Tm(tmu)_6(CF_3SO_3)_3$	found	13.00	30.24	12.59	5.51
	calc.	12.87	30.19	12.80	5.53
$Er(tmu)_6(CF_3SO_3)_3$	found	12.80	29.78	12.53	5.42
	calc.	12.75	30.22	12.82	5.53
$Ho(tmu)_6(CF_3SO_3)_3$	found	12.62	30.14	12.80	5.48
	calc.	12.59	30.26	12.83	5.55

[1] % M = % metal ion or % UO_2^{2+} content.

volumetric flask and made up with the solvent of interest. The crown ether was weighed into a 1 or 2 cm^3 volumetric flask and then made up with the stock solution such the ratio of salt to crown was 2:1 giving approximately equimolar amounts of free and coordinated metal ion. About 0.7 cm^3 of each solution was degassed and sealed under vacuum in 5 mm o.d. nmr tubes. These were then inserted into 10 mm o.d. nmr tubes (513-1PP, Wilmad Glass Co.) containing either d^6-acetone or d^6-dimethylsulphoxide as lock solvent depending on the temperature under investigation.

All transfers were carried out in a dry nitrogen atmosphere and all glassware was dried at a temperature exceeding 400 K for at least 24 hours to ensure anhydrous conditions.

5.6 Instrumentation

For the ytterbium and thulium complexes, variable temperature 90 MHz ^1H nmr studies were carried out on a Bruker HX-90E spectrometer. Depending on the concentration and temperature of the sample, up to 1200 transients were collected and stored as 8192 datum point blocks prior to Fourier transformation and complete lineshape analysis (see Section 6.2) on a Nicolet BNC-12 computer.

For the other lanthanide systems, variable temperature 300.13 MHz ^1H nmr studies were carried out on a Bruker CXP-300 spectrometer and stored as 8192 datum point blocks prior to Fourier transformation and transfer to a Diablo disk system (using the Bruker program, SPECNET) for lineshape analysis on a Nicolet BNC-12 computer.

For UO_2(1,1-dmu)$_5$(ClO_4)$_2$ and UO_2(trmu)$_5$(ClO_4)$_2$ a similar method to that above was employed. For UO_2(1,3-dmu)$_5$(ClO_4)$_2$ the spectra were manually digitised and entered into program MATCH [226] on a Cyber 173 computer for lineshape analysis. Absolute chemical shifts, where quoted, were measured directly from the proton impurity resonance of the deuterated solvent and were then recalculated on the basis of the shift of this resonance from t.m.s..

In the case of the sodium thiocyanate/crown ether studies, ^{23}Na nmr spectra were

obtained at 79.39 MHz on a Bruker CXP-300 spectrometer. For each temperature studied, an average of 6000 transients were accumulated in a 2048 point data block prior to Fourier transformation and transfer to a BNC-12 computer for lineshape analysis. Similar methods were employed for the other thiocyanate salts studied, using the nmr frequency of the particular metal involved.

In all cases, sample temperature was controlled by a Bruker B-VT 1000 variable temperature unit to within $\pm$ 0.3 K calibrated with a copper-constantan thermocouple. The temperature unit was checked using the method of Van Geet [227,228] with standard methanol and ethylene glycol samples.

Chapter 6

Data Analysis

6.1 Kinetic Applications of NMR Spectroscopy

Nuclear magnetic resonance spectroscopy is a very useful method for observing rapid exchange processes in solution. Rates of exchange, activation parameters and mechanisms of exchange may all be derived (under favourable conditions) by observing the variation in nmr resonance lineshape with temperature. These methods have been used throughout this study, therefore it is now appropriate to describe the physical basis and mathematical description of the nmr experiments conducted in this work. This also forms the basis of the lineshaping (described in Section 6.2) from which the rates of exchange and consequently $\Delta H^{\ddagger}$ and $\Delta S^{\ddagger}$ were derived.

A magnetic field, $\vec{B}_0$, is applied to a sample and provides a directional reference (conventionally along the z axis). Individual nuclear magnetic moments precess about this axis with a frequency ω_0, the Larmor frequency for the particular nucleus under observation. Nuclei with a nuclear spin of $I = \frac{1}{2}$, such as hydrogen, may have two possible orientations corresponding to the spin quantum number m having values of $\pm\frac{1}{2}$. The lower energy state, with the nuclear spin aligned in the direction of the field, is favoured by the Boltzmann distribution leading to a net macroscopic magnetisation, $\vec{M}$, in the z direction ($\vec{M}_z$). There is no preference for either the x or y directions and so the components of $\vec{M}$ in these directions, $\vec{M}_x$ and $\vec{M}_y$, are zero.

The application of an additional radio frequency field, $\vec{B}_1$, of frequency ω with a magnetic vector rotating in the xy plane with angular frequency ω, provides

magnetic field components along the x and y axes:

$$\vec{B} = (B_1 \cos\omega t, -B_1 \sin\omega t, B_0) \tag{6.1}$$

and $\vec{M}$ is tipped away from the z axis. The time required for M_z to regain the equilibrium value M_0 is characterised by T_1, the spin-lattice or longitudinal relaxation time. The magnetisation in the xy plane takes a period T_2, the spin-spin or transverse relaxation time, to equilibrate to zero after a perturbation.

The time dependence of $\vec{M}$ in a stationary frame was described by Bloch [229] in a set of phenomenological equations:

$$\frac{dM_x}{dt} = \gamma(M_y B_0 + M_z B_1 \sin\omega t) - \frac{M_x}{T_2} \tag{6.2}$$

$$\frac{dM_y}{dt} = \gamma(-M_x B_0 + M_z B_1 \cos\omega t) - \frac{M_y}{T_2} \tag{6.3}$$

$$\frac{dM_z}{dt} = -\gamma(M_x B_1 \sin\omega t + M_y B_1 \cos\omega t) - \frac{(M_z - M_0)}{T_1} \tag{6.4}$$

where γ is the nuclear gyromagnetic ratio.

Taking a frame of reference rotating about the z axis with frequency ω and assigning the direction of $\vec{B}_1$ along the x' axis (the x axis of the rotating frame), the Bloch equations may be reformulated as [230]:

$$\frac{dM_{xy}}{dt} = -\alpha M_{xy} - i\gamma B_1 M_0 \tag{6.5}$$

$$\frac{dM_z}{dt} = \gamma v B_1 - \frac{(M_z - M_0)}{T_1} \tag{6.6}$$

where M_{xy} is the transverse relaxation, v is the component of M which is 90^o out of phase with B_1 in the rotating frame and $\alpha = \frac{1}{T_2} - i(\omega_0 - \omega)$. Thus the variation of M_z (and therefore the energy of the spin system) depends on v which therefore corresponds to the absorption mode of the nmr signal.

Nuclear magnetic resonance may be observed in a number of ways. The continuous wave (c.w.) slow passage experiment consists of slowly sweeping the radio frequency (r.f.) field applied to a sample in a fixed magnetic field or vice versa and observing the spectrum concurrently. On the other hand, pulse methods make use of short bursts of r.f. power at a discrete frequency with, in general, observation

of the nuclear spin system after the r.f. pulse is complete. The former method will be considered in detail, as it provides an easily visualised model for the nmr experiment and, as will be observed at the end of this section, the lineshape obtained under pulsed nmr conditions is equivalent to that obtained in the continuous wave experiment.

Under continuous wave slow passage conditions, ω is swept slowly through ω_0 such that dM_{xy}/dt and $dM_z/dt = 0$ and if B_1 is of low energy such that $M_z \approx M_0$ at all times and M_{xy} is small, the absorption mode (v) lineshape for the nmr signal is of the form given by the steady-state solution to the Bloch equations:

$$v = \frac{-\gamma B_1 T_2 M_0}{1 + T_2^2(\omega_0 - \omega)^2 + \gamma^2 B_1^2 T_1 T_2} \tag{6.7}$$

Generally B_1 is so small that

$$\gamma^2 B_1^2 T_1 T_2 \ll 1 + T_2^2(\omega_0 - \omega)^2$$

and the absorption mode lineshape becomes Lorentzian in character:

$$v = \frac{-\gamma B_1 T_2 M_0}{1 + T_2^2(\omega_0 - \omega)^2} \tag{6.8}$$

Gutowsky, McCall and Slichter [231] have shown how the classical Bloch equations may be modified to include certain fast reversible chemical exchange phenomena. These modifications apply to the case of slow passage nmr with no r.f. saturation, where the exchange of nuclear spins between sites induces transverse relaxation only (adiabatic exchange [232]) and where no spin-spin coupling occurs between exchanging nuclear spin. The Gutowsky, McCall and Slichter (GMS) treatment has been extended by several authors [233,234]. Alternative methods have been proposed by Kubo and Sack (KS) [235,236,237,238,239] and Hahn, Maxwell and McConnell (HMM) [240,241]. Although differing mathematically, the different approaches are kinetically identical. The Kubo-Sack method uses a matrix of exchanging sites and is convenient for complex systems (see Section 6.2). The HMM method is more easily understood on a physical basis and so is used in the following discussion.

The modifications due to chemical exchange may be introduced into the classical nmr lineshape equation through the mean lifetimes of the exchanging species in each of the chemical sites between which it exchanges. Consider a nucleus exchanging between two sites A and B at a rate $k_A\chi_A = \tau_A^{-1}\chi_A = k_B\chi_B = \tau_B^{-1}\chi_B$, where χ_A and χ_B are the relative populations (mole fractions) and τ_A and τ_B are the mean site lifetimes of nuclei in sites A and B respectively. The time required for a nuclear spin to transfer from site A to site B is assumed so small that no nuclear spin precession occurs in that time and the nucleus arrives at site B with its phase memory of site A intact, and vice versa. This causes dephasing at site B and results in an increase in M_{xyB}, the transverse magnetisation at site B, at a rate $k_A M_{xyA} = \tau_A^{-1} M_{xyA}$ and a decrease in M_{xyA} at the same rate. Similarly, transfer of a nuclear spin from site B to site A causes dephasing at site A and increases M_{xyA} at a rate $k_B M_{xyB} = \tau_B^{-1} M_{xyB}$ whilst decreasing M_{xyB} at the same rate:

$$\frac{dM_{xyA}}{dt} = \frac{M_{xyB}}{\tau_B} - \frac{M_{xyA}}{\tau_A} \tag{6.9}$$

$$\frac{dM_{xyB}}{dt} = \frac{M_{xyA}}{\tau_A} - \frac{M_{xyB}}{\tau_B} \tag{6.10}$$

Incorporation of this effect into the Bloch equation (6.5) yields:

$$\frac{dM_{xyA}}{dt} = -\alpha_A M_{xyA} - i\gamma B_1 M_{0A} + \frac{M_{xyB}}{\tau_B} - \frac{M_{xyA}}{\tau_A} \tag{6.11}$$

$$\frac{dM_{xyB}}{dt} = -\alpha_B M_{xyB} - i\gamma B_1 M_{0B} + \frac{M_{xyA}}{\tau_A} - \frac{M_{xyB}}{\tau_B} \tag{6.12}$$

where

$$\alpha_A = \frac{1}{T_{2A}} - i(\omega_{0A} - \omega)$$

$$\alpha_B = \frac{1}{T_{2B}} - i(\omega_{0B} - \omega)$$

which describe the rate of change of the transverse component of the magnetisation in the rotating frame incorporating effects due to chemical exchange.

(a) Under continuous wave slow passage conditions

Under these conditions, the M_z components are essentially unchanged from M_0 such that:

$$M_{zA} = M_{0A} = \chi_A M_0 \tag{6.13}$$

$$M_{zB} = M_{0B} = \chi_B M_0 \tag{6.14}$$

and

$$\frac{dM_{xyA}}{dt} = \frac{dM_{xyB}}{dt} = 0 \tag{6.15}$$

The total transverse magnetisation, $M_{xy} = M_{xyA} + M_{xyB}$ may now be expressed in terms of τ_A and τ_B [231,242]:

$$M_{xy} = \frac{-i\gamma B_1 M_0(\tau_A + \tau_B + \tau_A\tau_B(\alpha_A\chi_B + \alpha_B\chi_A))}{(1+\alpha_A\tau_A)(1+\alpha_B\tau_B) - 1} \tag{6.16}$$

The nmr absorption lineshape is proportional to the imaginary part of M_{xy} [230,243,244]:

$$v = \frac{-\gamma B_1 M_0[Y(1+\tau(\chi_B/T_{2A} + \chi_A/T_{2B})) + QR]}{Y^2 + R^2} \tag{6.17}$$

where

$$\begin{aligned}
\tau &= \chi_B\tau_A = \chi_A\tau_B \\
\Delta\omega &= \omega_{0A} - \omega_{0B} \\
\delta\omega &= \frac{1}{2} \mid \omega_{0A} - \omega_{0B} \mid - \omega \\
Y &= \tau\left[\frac{1}{T_{2A}T_{2B}} - \delta\omega^2 + \frac{\Delta\omega^2}{4}\right] + \frac{\chi_B}{T_{2B}} + \frac{\chi_A}{T_{2A}} \\
Q &= \tau\left[\delta\omega - \frac{\Delta\omega}{2}(\chi_A - \chi_B)\right] \\
R &= \delta\omega\left[1 + \tau\left(\frac{1}{T_{2A}} + \frac{1}{T_{2B}}\right)\right] + \frac{\Delta\omega}{2}\tau\left(\frac{1}{T_{2B}} - \frac{1}{T_{2A}}\right) + \frac{\Delta\omega}{2}(\chi_A + \chi_B)
\end{aligned}$$

Although the methods discussed are not applicable when there is coupling between exchanging nuclear spins, coupling within an exchanging group may be accommodated by separately applying equation 6.17 to each component of the multiplet and summing to produce the total lineshape. More complex systems may

be analysed using a more sophisticated treatment such as that involved in the intramolecular exchange of 1,3-dmu in $[UO_2(1,3\text{-dmu})_5]^{2+}$ described in Section 6.2.

The variation in nmr lineshape such as that seen in Chapters 2, 3 and 4, can be followed by considering equation 6.17 as the exchange rate is varied from "very slow" to "very fast" (by, for example, increasing the temperature):

(i) Very slow exchange limit

$$\tau_A^{-1}, \tau_B^{-1} \ll |\omega_{0A} - \omega_{0B}|, T_{2A}^{-1}, T_{2B}^{-1}$$

In this limit, equation 6.17 approximates to

$$v = \frac{-\gamma B_1 \chi_A M_0 T_{2A}^{-1}}{T_{2A}^{-2} + (\omega_{0A} - \omega)^2} + \frac{-\gamma B_1 \chi_B M_0 T_{2B}^{-1}}{T_{2B}^{-2} + (\omega_{0B} - \omega)^2} \tag{6.18}$$

which contains no chemical exchange parameters and describes two Lorentzian lineshapes centred at ω_{0A} and ω_{0B} with linewidths at half maximum amplitude, ignoring inhomogeneous field effects, of:

$$W_A = \frac{2}{T_{2A_{obs}}} = \frac{2}{T_{2A}}$$
$$\text{and } W_B = \frac{2}{T_{2B_{obs}}} = \frac{2}{T_{2B}}$$

where $T_{2A_{obs}}$ and $T_{2B_{obs}}$ are the observed transverse relaxation times of each lineshape.

(ii) Slow exchange

$$\tau_A^{-1}, \tau_B^{-1} \ll |\omega_{0A} - \omega_{0B}|$$
$$\text{with } \tau_A^{-1} \approx T_{2A}^{-1} \text{ and } \tau_B^{-1} \approx T_{2B}^{-1}$$

The absorption mode lineshape is

$$v = \frac{-\gamma B_1 \chi_A M_0 (T_{2A}^{-1} + \tau_A^{-1})}{(T_{2A}^{-1} + \tau_A^{-1})^2 + (\omega_{0A} - \omega)^2} + \frac{-\gamma B_1 \chi_B M_0 (T_{2B}^{-1} + \tau_B^{-1})}{(T_{2B}^{-1} + \tau_B^{-1})^2 + (\omega_{0B} - \omega)^2} \tag{6.19}$$

which again describes two Lorentzian lineshapes centred at ω_{0A} and ω_{0B}. The resonances are said to be "exchange broadened". The line widths at half maximum

amplitude are now:

$$W_A = \frac{2}{T_{2A_{obs}}} = \frac{2}{T_{2A}} + \frac{2}{\tau_A}$$
$$\text{and } W_B = \frac{2}{T_{2B_{obs}}} = \frac{2}{T_{2B}} + \frac{2}{\tau_B}$$

for A and B respectively.

(iii) Fast exchange

$$\tau_A^{-1}, \tau_B^{-1} \; > \; | \omega_{0A} - \omega_{0B} |$$

A single broad Lorentzian lineshape centred at $(\chi_A\omega_{0A} + \chi_B\omega_{0B})$ is observed. The line width observed is

$$W = \frac{2}{T_{2_{obs}}} = \frac{2\chi_A}{T_{2A}} + \frac{2\chi_B}{T_{2B}} + 2\chi_A^2\chi_B^2(\omega_{0A} - \omega_{0B})^2(\tau_A + \tau_B)$$

(iv) Very fast exchange limit

$$\tau_A^{-1}, \tau_B^{-1} \; \gg \; | \omega_{0A} - \omega_{0B} |, T_{2A}^{-1}, T_{2B}^{-1}$$

The absorption signal is now a single Lorentzian lineshape centred at $(\chi_A\omega_{0A} + \chi_B\omega_{0B})$ described by

$$v = \frac{-\gamma B_1 M_0(\chi_A T_{2A}^{-1} + \chi_B T_{2B}^{-1})}{(\chi_A T_{2A}^{-1} + \chi_B T_{2B}^{-1})^2 + (\chi_A\omega_{0A} + \chi_B\omega_{0B} - \omega)^2} \qquad (6.20)$$

with a width at half maximum amplitude of

$$W = \frac{2}{T_{2_{obs}}} = \frac{2\chi_A}{T_{2A}} + \frac{2\chi_B}{T_{2B}}$$

The rate of chemical exchange is now so fast that the exchanging nuclear spin experiences the weighted average of the environments A and B and no chemical exchange information is contained in the lineshape.

The above equations describe exchange between any two sites, A and B, without coupling between exchanging nuclear spins. For exchange caused by intramolecular rotation, such as that described for the 1,1-dmu ligands in $[UO_2(1,1\text{-dmu})_5]^{2+}$ (Section 3.2), the mole fractions in each site are equal ($\chi_A = \chi_B$) and the lifetimes in each site are equal ($\tau_A = \tau_B$). This reduces the above equations significantly as has been demonstrated for hindered internal rotation of amides [233].

(b) Under pulsed nmr conditions

In the frame (x', y', z), rotating about the z axis with angular velocity $\omega = \omega_0 = \gamma B_0$, a short ($10^{-6}$ – 10^{-4} s) r.f. pulse of high energy, $\vec{B}_1$, is directed along the x' axis, applying a torque to $\vec{M}$ (initially aligned with the z axis) which causes it to tilt towards the y' axis, generating a transverse component of $\vec{M}$. Immediately after the pulse, $\vec{M}$ begins to relax back to its equilibrium position aligned with the z axis. Transverse relaxation causes M_{xy} to undergo free induction decay (F.I.D.) to zero. Solving the differential equations 6.11 and 6.12 with $B_1 = 0$ gives the equation describing the F.I.D. [245]:

$$M_{xy} = C_1 e^{-\phi_+ t} + C_2 e^{-\phi_- t} \tag{6.21}$$

where C_1,C_2 are constants of integration and

$$2\phi_\pm = (\alpha_A + \tau_A^{-1} + \alpha_B + \tau_B^{-1}) \pm [(\alpha_A + \tau_A^{-1} - \alpha_B - \tau_B^{-1})^2 + 4\tau_A^{-1}\tau_B^{-1}]^{\frac{1}{2}} \tag{6.22}$$

The Fourier transform, S, of the F.I.D. is given by:

$$\begin{aligned} S &= \int_0^\infty M_0 e^{-i(\omega-\omega_1)t} dt \\ &= \frac{iM_0(\tau_A + \tau_B + \tau_A\tau_B(\alpha_A\chi_B + \alpha_B\chi_A))}{(1+\alpha_A\tau_A)(1+\alpha_B\tau_B) - 1} \end{aligned} \tag{6.23}$$

where

$$\begin{aligned} \alpha_A &= T_{2A}^{-1} + i(\omega_{0A} - \omega) \\ \alpha_B &= T_{2B}^{-1} + i(\omega_{0B} - \omega) \\ \omega &= \text{the variable frequency} \\ \omega_1 &= \text{the fixed pulse carrier frequency.} \end{aligned}$$

The absorption mode lineshape is derived from the imaginary part of equation 6.23 and is the same as that obtained in the continuous wave case. In general, the lineshape obtained for an uncoupled spin system undergoing chemical exchange from a pulsed Fourier transform experiment is equivalent to that derived from a continuous wave experiment [245,246,247,248,249].

A complete lineshape analysis (using an equation similar to 6.17) of the nmr spectra over the coalescence temperature range was employed to obtain kinetic parameters for the systems in this study.

6.2 Lineshape Analysis

All systems except for the UO_2(1,3-dimethylurea)$_5$(ClO_4)$_2$ one were analysed using an interactive program LINSHP based on the methods of Nakagawa [250], and Siddall, Stewart and Knight [251] and adapted for the BNC-12 computer of the HX-90E spectrometer by Williams [252]. The program involves visual comparison on a cathode ray oscilloscope of the experimental lineshape with a calculated theoretical spectrum generated from the input parameters.

The input parameters used to generate the theoretical spectrum are:

V_c, V_f the frequency of each resonance of a coalescing pair of peaks

W_c, W_f the width at half maximum height of each resonance in the absence of exchange

χ_c, χ_f the relative populations of each exchanging site

R the estimated rate of exchange $R = (\tau_c \chi_f)^{-1} = (\tau_f \chi_c)^{-1}$

where subscripts c and f refer to the coordinated and free ligand sites respectively, but in general, may refer to any two exchanging environments (e.g. in the case of intramolecular exchange).

The theoretical spectrum is generated by solving

$$M = \left| \frac{(1 + ar_c\chi_f + ar_f\chi_c)K + a(f + \chi_f - 1)L}{(K^2 + L^2)(\mid V_c - V_f \mid)} \right| \tag{6.24}$$

where

$$\begin{aligned}
M &= \text{the signal intensity at frequency } V \\
a &= \frac{2\pi \mid V_c - V_f \mid}{R} \\
f &= \frac{V - V_c}{V_f - V_c} \\
r_c &= \frac{W_c}{2 \mid V_c - V_f \mid} \\
r_f &= \frac{W_f}{2 \mid V_c - V_f \mid} \\
L &= f(1 + ar_c + ar_f) - (ar_c + \chi_f) \\
K &= r_c\chi_c + r_f\chi_f + a(r_c r_f - f(f-1)).
\end{aligned}$$

The estimated rate of exchange (R) is varied until the match is optimal. In this way, $k_{ex}(= R\chi_f = \tau_c^{-1})$ were obtained for a series of temperatures. The overall ligand exchange on an n-coordinate species is given by:

$$\text{exchange rate} = nk_{ex}[[M(L)_n]^{m+}] \tag{6.25}$$

where

$$k_{ex} = k_1 \text{ for a first order rate law} \tag{6.26}$$

$$k_{ex} = k_2[L] \text{ for a second order rate law} \tag{6.27}$$

$$k_{ex} = k_1 + k_2[L] \text{ for a two term rate law.} \tag{6.28}$$

Thus the order of the reaction may be determined by observing the variation of k_{ex} as the concentration of L is varied (see Section 1.2).

In order to minimise the introduction of systematic errors, the variation of the above parameters with temperature was obtained, where possible, in the region of very slow exchange and subsequently extrapolated into the region of coalescence. For all the systems lineshaped using this method little or no variation in the relative populations was observed. However, there were variations in chemical shift and linewidth and these were extrapolated from low temperature spectra, where available.

As the above method uses the method of coalescing doublets, it could not be used to solve the multi-site intramolecular exchange present in the UO_2(1,3-dimethylurea)$_5$(ClO_4)$_2$ system. The ligands in this complex have three possible isomers as shown in Figure 3.6. In this case, a non-interactive program [226], MATCH, on a Cyber 173 computer was used. The spectra were manually digitised and entered into the computer. The Kubo-Sack method of introducing chemical exchange into the classical lineshape equations [230] was used to generate theoretical spectra. If the NHMe protons of each 1,3-dmu ligand are designated as being in site 1 for isomer A, sites 2 and 3 for isomer B and site 4 for isomer C, the absorption mode lineshape, v, is given by:

$$v = \gamma B_1 M_0 Re(\chi_1, \chi_2, \chi_3, \chi_4) \times$$

$$\begin{bmatrix} -\alpha_1 - \frac{1}{\tau_1} & \frac{1}{2\tau_1} & \frac{1}{2\tau_1} & 0 \\ \frac{1}{2\tau_2} & -\alpha_2 - \frac{1}{\tau_2} & 0 & \frac{1}{2\tau_2} \\ \frac{1}{2\tau_3} & 0 & -\alpha_3 - \frac{1}{\tau_3} & \frac{1}{2\tau_3} \\ 0 & \frac{1}{2\tau_4} & \frac{1}{2\tau_4} & -\alpha_4 - \frac{1}{\tau_4} \end{bmatrix}^{-1} \cdot \begin{bmatrix} 1 \\ 1 \\ 1 \\ 1 \end{bmatrix} \tag{6.29}$$

where $\alpha_n = 1/(T_{2n}) - i(\omega_{0n} - \omega)$. χ_n , $1/T_{2n}$, ω_{0n} and τ_n are respectively the relative population, the transverse relaxation time, the Larmor frequency and the lifetime in site n. The site lifetimes are related through the following equation where the χ_n values are obtained as described in Section 3.3:

$$\frac{\tau_1}{\chi_1} = \frac{\tau_2}{\chi_2} = \frac{\tau_3}{\chi_3} = \frac{\tau_4}{\chi_4} \tag{6.30}$$

on this basis τ_1 and τ_4 are equal to τ_A and τ_C the lifetimes of isomers A and C respectively. The lifetime of isomer B, τ_B, is equal to τ_2 and τ_3.

6.3 Calculation of Activation Parameters

The Eyring equation [253,254] of the transition state theory expresses the dependence of k_{ex} on the activation parameters and temperature. When the observed rate constant consists only of a single elementary rate constant (a one term rate law, equations 6.26 and 6.27), the Eyring equation has the form:

$$k_{ex} = \frac{k_B T}{h} e^{\frac{-\Delta G^{\ddagger}}{RT}} = \frac{k_B T}{h} e^{\frac{-\Delta H^{\ddagger}}{RT}} e^{\frac{\Delta S^{\ddagger}}{R}} \tag{6.31}$$

where

$$\begin{aligned} k_B &= \text{Boltzmann's constant} \\ h &= \text{Planck's constant} \\ R &= \text{gas constant} \\ G^{\ddagger}, H^{\ddagger}, S^{\ddagger} &= \text{activation free energy, enthalpy and entropy} \\ T &= \text{temperature (K)} \end{aligned}$$

Substituting τ_c^{-1} for k_{ex} and taking logarithms gives the convenient linear form:

$$\ln(\tau_c T) = \left(\frac{-\Delta S^{\ddagger}}{R} + \ln\left(\frac{h}{k_B}\right) \right) + \frac{\Delta H^{\ddagger}}{RT}. \tag{6.32}$$

Thus, if $\ln(T\tau_c)$ is plotted against $\frac{1}{T}$, a straight line is obtained with intercept $\frac{-\Delta S^{\ddagger}}{R} + \ln(\frac{h}{k_B})$ and slope $\frac{\Delta H^{\ddagger}}{R}$.

When a two term rate law applies (equation 6.28), this relationship may not necessarily be linear due to the simultaneous contributions from the two pathways to the slope [255]. In this case, the appropriate form of the Eyring equation is:

$$k_{ex} = \frac{k_B T}{h}\left[e^{\frac{-\Delta H_1^{\ddagger}}{RT}} e^{\frac{\Delta S_1^{\ddagger}}{R}} + [L] e^{\frac{-\Delta H_2^{\ddagger}}{RT}} e^{\frac{S_2^{\ddagger}}{R}}\right]. \qquad (6.33)$$

A non-linear, weighted least squares method of fit was used by a computer program, DATAFIT [256], on a Cyber 173 or Vax 11-780 computer to fit the parameters k_{ex}, $[L]_{free}$ and temperature to the appropriate form of the Eyring equation. Utilising this model, values for the activation enthalpy and entropy were calculated. A modified form of the Eyring equation was used to obtain the elementary rate constants at a specified temperature.

DATAFIT minimises the residual differences in an n-dimensional sum of squares space between a calculated and an experimental surface (in the case of intramolecular exchange defined by k_{ex} and temperature and in the case of intermolecular exchange, also by $[L]_{free}$) using a method of Pitha and Jones [257]. The errors quoted for the activation parameters thus obtained are the standard deviations for each parameter in the sum of squares space. These values are also provided by DATAFIT, hence they only take into account the errors between the input parameters and not of other possible systematic errors arising from the estimation of the non-exchange modified half-widths and chemical shifts.

List of Publications

1. Stephen F. Lincoln, Alex White, "Proton Magnetic Resonance Study of Rotation about Carbon–Nitrogen Bonds in Pentakis(1,1-dimethylurea)dioxouranium(VI) and its 1,3-dimethylurea Analogue", *Inorg. Chim. Acta*, 1985, **110**, 107 – 112.

2. Stephen F. Lincoln, Alex White, "A Proton Magnetic Resonance Study of Ligand Exchange on Hexakis(1,1,3,3-tetramethylurea)thulium(III)", *Polyhedron*, 1986, **5**, 1351 – 1355.

3. Stephen F. Lincoln, Alex White, Andrea M. Hounslow, "Sodium Ion Exchange on the Sodium 18-crown-6 Cation in Several Solvents. A Sodium-23 Nuclear Magnetic Resonance Study", *J. Chem. Soc., Faraday*, accepted for publication.

4. Alex White, Stephen F. Lincoln, "Ligand Intra- and Intermolecular Exchange Processes on Dioxopentakis(1,1,3-trimethylurea)uranium(VI). A Proton Magnetic Resonance Study", *J. Chem. Soc., Dalton*, submitted for publication.

Bibliography

[1] H.S.Frank, W.-Y.Wen, *Discuss. Faraday Soc.*, 1957, **24**, 133.

[2] S.F.Lincoln, *Coord. Chem. Rev.*, 1971, **6**, 309.

[3] C.H.Langford, J.P.Tong, *Acc. Chem. Res.*, 1977, **10**, 258.

[4] C.H.Langford, H.B.Gray, *"Ligand Substitution Processes"*, 1966, W.A.Benjamin (New York).

[5] R.M.Fuoss, *J. Am. Chem. Soc.*, 1958, **80**, 5059; *J. Phys. Chem.*, 1978, **82**, 2427.

[6] M.Eigen, *Z. Physik. Chem. N.F.*, 1954, **1**, 176.

[7] A.J.Brown, O.W.Howarth, P.Moore, W.J.E.Parr, *J. Chem. Soc., Dalton*, 1978, 1776.

[8] C.Cossey, *Doctoral Thesis*, 1986, L'Université de Lausanne.

[9] D.L.Pisaniello, L.Helm, P.Meier, A.E.Merbach, *J. Am. Chem. Soc.*, 1983, **105**, 4528.

[10] G.J.Honan, S.F.Lincoln, E.H.Williams, *J. Chem. Soc., Dalton Trans.*, 1979, 320.

[11] R.D.Shannon, *Acta Cryst.*, 1976, **A32**, 751.

[12] S.F.Lincoln, *Adv. Inorg. Bioinorg. Mech.*, 1986, **4**, 217.

[13] C.K.Jørgensen, R.Reisfeld, *Topics in Current Chem.*, 1982, **100**, 127.

[14] S.S.Krishnamurthy, S.Soundararajan, *Can. J. Chem.*, 1969, **47**, 995.

[15] D.L.Pisaniello, A.E.Merbach, *Helv. Chim. Acta*, 1982, **65**, 573.

[16] L.N.Lugina, N.K.Davidenko, L.N.Zabotina, K.B.Yatsimirskii, *Z. Neorg. Khim.*, 1974, **19**, 2665.

[17] J.-C.G.Bünzli, J.-R.Yersin, *Helv. Chim. Acta*, 1982, **65**, 2498.

[18] J.-C.G.Bünzli, J.-R.Yersin, C.Mabillard, *Inorg. Chem.*, 1982, **21**, 1471.

[19] T.Moeller, G.Vicentini, *J. Inorg. Nucl. Chem.*, 1965, **27**, 1477.

[20] V.N.Krishnamurthy, S.Soundararajan, *J. Inorg. Nucl. Chem.*, 1967, **29**, 517.

[21] J.T.Donoghue, E.Fernandez, J.A.McMillan, D.A.Peters, *J. Inorg. Nucl. Chem.*, 1969, **31**, 1431.

[22] E.Giesbrecht, L.B.Zinner, *Inorg. Nucl. Chem. Lett.*, 1969, **5**, 575.

[23] R.P.Scholer, A.E.Merbach, *Inorg. Chim. Acta*, 1975, **15**, 15.

[24] (a) M.Perrier, G.Vicentini, *J. Inorg. Nucl. Chem.*, 1971, **33**, 2497;
(b) M.Perrier, G.Vicentini, *J. Inorg. Nucl. Chem.*, 1973, **35**, 555;
(c) M.Perrier, R.Najjar, G.Vicentini, *An. Acad. brasil. Ciênc.*, 1970, **42**, 439; (d) G.Vicentini, D.J.S.Nunes, *An. Acad. brasil. Ciênc.*, 1974, **46**, 5; (e) G.Vicentini, J.E.X.Mattos, *An. Acad. brasil. Ciênc.*, 1976, **48**, 701;
(f) G.Vicentini, R.Najjar, *Inorg. Nucl. Chem. Lett.*, 1970, **6**, 571;
(g) G.Vicentini, L.B.Zinner, *J. Inorg. Nucl. Chem.*, 1980, **42**, 1510;
(h) A.Seminara, A.Musumeci, A.Chisari, *J. Inorg. Nucl. Chem.*, 1978, **40**, 269.

[25] E.Giesbrecht, M.Kawashita, *J. Inorg. Nucl. Chem.*, 1970, **32**, 2461.

[26] S.M.Melo, J.M.C.Jatahy, E.E.Castellano, C.O.P.Santos, *Inorg. Chim. Acta*, 1985, **109**, 163.

[27] L.A.Aslanov, V.M.Ionov, S.S.Sotman, *Kristallografiya*, 1976, **21**, 1200.

[28] S.F.Lincoln, A.M.Hounslow, A.J.Jones, *Aust. J. Chem.*, 1982, **35**, 2393.

[29] D.L.Pisaniello, S.F.Lincoln, *J. Chem. Soc., Dalton*, 1980, 699.

[30] D.L.Pisaniello, S.F.Lincoln, E.H.Williams, A.J.Jones, *Aust. J. Chem.*, 1981, **34**, 495.

[31] R.V.Southwood-Jones, W.L.Earl, K.E.Newman, A.E.Merbach, *J. Phys. Chem.*, 1980, **73**, 5909.

[32] A.Hugi, *Doctoral Thesis*, 1986, L'Université de Lausanne.

[33] G.E.Glass, W.B.Schawabacher, R.S.Tobias, *Inorg. Chem.*, 1968, **7**, 2471.

[34] J.Mc.B.Harrowfield, D.L.Kepert, J.M.Patrick, A.H.White, *Aust. J. Chem.*, 1983, **36**, 483.

[35] D.L.Kepert, *"Inorganic Stereochemistry"*, Inorganic Chemistry Concepts, Vol. 6, 1982, Springer-Verlag (Berlin).

[36] M.C.Favas, D.L.Kepert, *Prog. Inorg. Chem.*, 1981, **28**, 309.

[37] S.P.Sinha, *Struct. Bond.*, 1976, **25**, 69.

[38] F.K.Meyer, K.E.Newman, A.E.Merbach, *J. Am. Chem. Soc.*, 1979, **101**, 5588.

[39] D.L.Pisaniello, P.J.Nichols, Y.Ducommun, A.E.Merbach, *Helv. Chim. Acta*, 1982, **65**, 1025.

[40] D.L.Pisaniello, L.Helm, D.Zbinden, A.E.Merbach, *Helv. Chim. Acta*, 1983, **66**, 1872.

[41] T.J.Swift, R.E.Connick, *J. Chem. Phys.*, 1962, **37**, 307; *J. Chem. Phys.*, 1964, **41**, 2553.

[42] A.E.Merbach, *Pure Appl. Chem.*, 1982, **54**, 1479.

[43] D.L.Pisaniello, S.F.Lincoln, E.H.Williams, *J. Chem. Soc., Dalton*, 1979, 1473.

[44] D.L.Pisaniello, S.F.Lincoln, *Inorg. Chim. Acta*, 1979, **36**, 85.

[45] D.L.Pisaniello, S.F.Lincoln, *Inorg. Chem.*, 1981, **20**, 3689.

[46] D.L.Pisaniello, S.F.Lincoln, *Aust. J. Chem.*, 1981, **34**, 1195.

[47] L.S.Frankel, E.R.Danielson, *Inorg. Chem.*, 1972, **11**, 1964.

[48] J.-J.Delpuech, M.R.Kaddar, A.A.Peguy, P.R.Rubini, *J. Am. Chem. Soc.*, 1975, **97**, 3373.

[49] L.Rodehüser, P.R.Rubini, J.-J.Delpuech, *Inorg. Chem.*, 1977, **11**, 2837.

[50] A.White, *Honours Report*, 1982, Department of Physical and Inorganic Chemistry, University of Adelaide.

[51] W.DeW.Horrocks Jr., in *"NMR of Paramagnetic Molecules"*, G.N.LaMar, W.DeW.Horrocks Jr., R.H.Holm eds., 1973, p. 479, Academic Press (London); R.D.Fischer, *ibid.*, p. 522.

[52] V.Gutmann, *"Coordination Chemistry in Nonaqueous Solutions"*, 1968, Springer-Verlag (Wien).

[53] D.R.Fitzwater, R.E.Rundle, *Z. Kristallogr. Kristallgeom. Kristallchem.*, 1959, **112**, 362.

[54] L.B.Zinner, G.Vicentini, *J. Inorg. Nucl. Chem.*, 1981, **43**, 193.

[55] A.Seminara, E.Rizzarelli, *Inorg. Chim. Acta*, 1980, **40**, 249.

[56] G.A.Lawrance, *Chem. Rev.*, 1986, *86*, 17.

[57] W.R.Robinson, *J. Chem. Ed.*, 1985, **62**, 1001.

[58] W.C.Wolsey, *J. Chem. Ed.*, 1973, **50**, A335.

[59] S.P.McGlynn, J.K.Smith, *J. Molec. Spect.*, 1961, **6**, 164.

[60] L.R.Nassimbeni, A.L.Rodgers, *Cryst. Struct. Commun.*, 1976, **5**, 301.

[61] N.W.Alcock, S.Esperas, *J. Chem. Soc., Dalton*, 1977, 893.

[62] N.W.Alcock, *J. Chem. Soc., Dalton*, 1973, 1616.

[63] H.T.Evans Jr., *Science*, 1963, **141**, 154.

[64] J.Mc.B.Harrowfield, D.L.Kepert, J.M.Patrick, A.H.White, S.F.Lincoln, *J. Chem. Soc., Dalton*, 1983, 393.

[65] N.K.Dalley, M.H.Mueller, S.H.Simonsen, *Inorg. Chem.*, 1972, **11**, 1840.

[66] G.Bombieri, G.De Paoli, in *"Handbook on the Physics and Chemistry of the Actinides"*, A.J.Freeman, C.Keller, eds., 1985, p. 75, Elsevier Scientific (Amsterdam).

[67] V.N.Serezhkin, *Z. Neorg. Khim.*, 1982, **27**, 1619.

[68] G.Gordon, H.Taube, *J. Inorg. Nucl. Chem.*, 1961 **16**, 272; *J. Inorg. Nucl. Chem.*, 1961, **19**, 189.

[69] S.W.Rabideau, *J. Phys. Chem.*, 1967, **71**, 2747.

[70] V.V.Yakshin, N.L.Khokhlova, *Koord. Khim.*, 1985, **11**, 1088.

[71] G.J.Honan, S.F.Lincoln, E.H.Williams, *Inorg. Chem.*, 1978, **17**, 1855.

[72] A.Fratiello, G.A.Vidulich, C.Cheng, V.Kubo, *J. Soln. Chem.*, 1972, **1**, 433.

[73] A.Fratiello, V.Kubo, R.E.Lee, R.E.Schuster, *J. Phys. Chem.*, 1970, **74**, 3726.

[74] A.Zalkin, H.Ruben, D.H.Templeton, *Inorg. Chem.*, 1979, **18**, 519.

[75] A.M.Hounslow, S.F.Lincoln, P.A.Marshall, E.H.Williams, *Aust. J. Chem.*, 1981, **32**, 2543.

[76] R.P.Bowen, S.F.Lincoln, E.H.Williams, *Inorg. Chem.*, 1976, **15**, 2126.

[77] R.P.Bowen, G.J.Honan, S.F.Lincoln, T.M.Spotswood, E.H.Williams, *Inorg. Chim. Acta*, 1979, **33**, 235.

[78] J.Crea, S.F.Lincoln, R.J.Williams, *Aust. J. Chem.*, 1976, **29**, 2183.

[79] G.J.Honan, S.F.Lincoln, E.H.Williams, *J. Soln. Chem.*, 1978, **7**, 443.

[80] G.J.Honan, S.F.Lincoln, E.H.Williams, *Aust. J. Chem.*, 1979, **32**, 1851.

[81] G.J.Honan, S.F.Lincoln, E.H.Williams, T.M.Spotswood, *J. Chem. Soc., Dalton*, 1979, 1220.

[82] J.Crea, R.Digiusto, S.F.Lincoln, E.H.Williams, *Inorg. Chem.*, 1977, **16**, 2825.

[83] A.E.Bakas, A.M.Hounslow, S.F.Lincoln, N.J.Maeji, *Aust. J. Chem.*, 1982, **35**, 1489.

[84] K.G.Rao, E.D.Becker, C.N.R.Rao, *J. Chem. Soc., Chem. Commun.*, 1977, 350.

[85] H.N.Cheng, H.S.Gutowsky, *J. Phys. Chem.*, 1980, **84**, 1039.

[86] W.E.Stewart, T.H.Siddall III, *Chem. Rev.*, 1970, **70**, 517.

[87] L.M.Jackman, in *"Dynamic Nuclear Magnetic Resonance Spectroscopy"*, L.M.Jackman, F.A.Cotton, eds., 1975, p. 203, Academic Press (London).

[88] K.Bokolo, J.-J.Delpuech, L.Rodehüser, P.R.Rubini, *Inorg. Chem.*, 1981, **20**, 992.

[89] Y.Ikeda, H.Tomiyashu, H.Fukutomi, *Inorg. Chem.*, 1984, **23**, 1356.

[90] L.Rodehüser, P.R.Rubini, K.Bokolo, J.-J.Delpuech, *Inorg. Chem.*, 1982, **21**, 1061.

[91] A.Vasilescu, T.Oncescu, *Rev. Roum. Chim.*, 1978, **23**, 1055.

[92] H.Fukutomi, Y.Ikeda, *Inorg. Chim. Acta*, 1986, **115**, 223.

[93] M.L.Martin, M.L.Filleux-Blanchard, G.J.Martin, *Org. Magn. Reson.*, 1980, **13**, 396.

[94] J.C.Eisenstein, M.H.L.Pryce, *Proc. Roy. Soc. (London)*, 1955, **A229**, 20.

[95] T.H.Siddall III, C.A.Prohaska, *Inorg. Chem.*, 1965, **4**, 783.

[96] H.Doine, Y.Ikeda, H.Tomiyashu, H.Fukutomi, *Bull. Chem. Soc. Jpn.*, 1983, **56**, 1989.

[97] Y.Ikeda, H.Tomiyashu, H.Fukutomi, *Bull. Chem. Soc. Jpn.*, 1983, **56**, 1060.

[98] A.M.Hounslow, personal communication.

[99] H.Kessler, M.Molter, *J. Am. Chem. Soc.*, 1976, **98**, 5969.

[100] C.E.F.Rickard, D.C.Woollard, *Aust. J. Chem.*, 1980, **33**, 1161.

[101] H.Aghabozorg, G.J.Palenik, R.C.Stoufer, J.Summers, *Inorg. Chem.*, 1982, **21**, 3903.

[102] M.L.Niven, J.R.Nassimbeni, G.Gafner, *Cryst. Struct. Commun.*, 1980, **9**, 1133.

[103] G.J.Honan, *Doctoral Thesis*, 1979, University of Adelaide.

[104] M.C.Mattos, E.Surcouf, J.-P.Mornon, *Acta Cryst.*, 1977, **B33**, 1855.

[105] J.Delaunay, C.Kappenstein, R.P.Hugel, *J. Chem. Soc., Chem. Commun.*, 1980, 679.

[106] J.G.H.du Preez, B.Zeelie, U.Casellato, R.Graziani, *Inorg. Chim. Acta*, 1986, **122**, 119.

[107] J.Sandström, in *"Dynamic NMR Spectroscopy"*, 1982, p. 106, Academic Press (London).

[108] W.H.Zachariasen, *Acta Cryst.*, 1954, **7**, 795.

[109] E.F.Caldin, H.P.Bennetto, *J. Soln. Chem.*, 1973, **2**, 217.

[110] P.Fischer, H.Hoffman, G.Platz, *Ber. Bunsenges. Phys. Chem.*, 1972, **76**, 1060.

[111] S.F.Lincoln, *Pure Appl. Chem.*, 1979, **51**, 2059.

[112] S.F.Lincoln, *Chem. Aust.*, 1979, **46**, 530.

[113] D.L.Pisaniello, S.F.Lincoln, *Aust. J. Chem.*, 1979, **32**, 715.

[114] J.P.Hunt, *Coord. Chem. Rev.*, 1971, **7**, 1.

[115] A.McAuley, J.Hill, *Q. Rev. Chem. Soc.*, 1969, **24**, 18.

[116] C.J.Pedersen, *J. Am. Chem. Soc.*, 1967, **89**, 7017; *J. Am. Chem. Soc.*, 1967, **89**, 2495.

[117] B.Dietrich, J.-M.Lehn, J.-P.Sauvage, *Tetrahedron Lett.*, 1969, 2885.

[118] J.R.Hartman, R.E.Wolf Jr., B.M.Foxman, S.R.Cooper, *J. Am. Chem. Soc.*, 1983, **105**, 131.

[119] J.S.Bradshaw, J.Y.Hui, B.L.Haymore, J.J.Christensen, R.M.Izatt, *J. Heterocyclic Chem.*, 1973, **10**, 1.

[120] W.-H.Lin, W.I.Bailey Jr., R.J.Lagow, *J. Chem. Soc., Chem. Commun.*, 1985, 1350.

[121] C.Moore, B.C.Pressman, *Biochem. Biophys. Res. Commun.*, 1964, **15**, 562.

[122] W.Simon, W.E.Morf, in *"Membranes - A Series of Advances"*, Vol. 2, G.Eisenman ed., 1973, Marcel Dekker (New York).

[123] W.Simon, W.E.Morf, P.Ch.Meier, *Struct. Bond.*, 1973, **16**, 114.

[124] A.Gliozzi, in *"Bioenergetics and Thermodynamics: Model Systems"*, A.Braibanti ed., 1980, p. 339, D.Reidel (Dordrecht, Holland).

[125] D.E.Fenton, *ibid.*, p. 275.

[126] D.E.Fenton, *ibid.*, p. 229.

[127] D.E.Fenton, *Chem. Soc. Rev.*, 1977, **6**, 325.

[128] M.M.Shemyakin, Yu.A.Ovchinnikov, V.T.Ivanov, V.K.Antonov, E.I.Vinogradova, A.M.Shkrob, G.G.Malenkov, A.V.Evstatov, E.A.Laine, E.I.Melnik, I.D.Ryabova, *T. Membrane Biol.*, 1969, **1**, 402.

[129] M.Dobler, *Helv. Chim. Acta*, 1972, **55**, 1371.

[130] M.Dobler, J.D.Dunitz, B.T.Kilbourn *Helv. Chim. Acta*, 1969, **52**, 2573.

[131] W.L.Duax, H.Hauptman, C.M.Weeks, D.A.Norton, *Science*, 1972, **176**, 911.

[132] D.A.Norton, *Science*, 1972, **176**, 911.

[133] A.Rodrigue, J.W.Bovenkamp, B.V.Lacroix, R.A.B.Bannard, G.W.Buchanan, *Can. J. Chem.*, 1986, **64**, 808.

[134] N.S.Poonia, M.R.Truter, *J. Chem. Soc., Dalton*, 1973, 2062.

[135] D.G.Parsons, M.R.Truter, J.N.Wingfield, *Inorg. Chim. Acta*, 1975, **14**, 45.

[136] M.Mercer, M.R.Truter, *J. Chem. Soc., Dalton*, 1973, 2469.

[137] D.L.Hughes, *J. Chem. Soc., Dalton*, 1975, 2374.

[138] M.E.Fraser, S.Fortier, A.Rodrigue, J.W.Bovenkamp, *Can. J. Chem.*, 1986, **64**, 816.

[139] J.-C.G.Bünzli, D.Wessner, *Coord. Chem. Rev.*, 1984, **60**, 191.

[140] J.-C.G.Bünzli, D.Wessner, *Isr. J. Chem.*, 1984, **24**, 313.

[141] J.-C.G.Bünzli, D.Wessner, *Helv. Chim. Acta*, 1978, **61**, 1454.

[142] J.-C.G.Bünzli, D.Wessner, *Helv. Chim. Acta*, 1981, **64**, 582.

[143] D.L.Tomaja, *Inorg. Chim. Acta*, 1977, **21**, L31.

[144] D.G.Parsons, M.R.Truter, J.N.Wingfield, *Inorg. Chim. Acta*, 1980, **47**, 81.

[145] E.Mason, H.A.Eick, *Acta Cryst.*, 1982, **B38**, 1821.

[146] H.-J.Buschmann, *Chem. Ber.*, 1985, **118**, 2746.

[147] H.-J.Buschmann, *Chem. Ber.*, 1985, **118**, 4297.

[148] H.-J.Buschmann, *J. Soln. Chem.*, 1986, **15**, 453.

[149] F.P.Boer, M.A.Neuman, F.P. van Remoortere, E.C.Steiner, *Inorg. Chem.*, 1974, **13**, 2826.

[150] F.P.van Remoortere, F.P.Boer, *Inorg. Chem.*, 1974, **13**, 2071.

[151] M.Dobler, J.D.Dunitz, P.Seiler, *Acta Cryst.*, 1974, **B30**, 2741.

[152] D.Live, S.I.Chan, *J. Am. Chem. Soc.*, 1976, **98**, 3769.

[153] M.A.Bush, M.R.Truter, *J. Chem. Soc., Chem. Commun.*, 1970, 1439; *J. Chem. Soc. (B)*, 1971, 1440.

[154] P.Groth, *Acta Chem. Scand.*, 1981, **A35**, 463.

[155] P.Groth, *Acta Chem. Scand.*, 1982, **A36**, 109.

[156] P.Groth, *Acta Chem. Scand.*, 1981, **A35**, 721.

[157] A.I.Gorbunov, P.A.Storozhenko, L.V.Ivakina, B.M.Bulychev, A.I.Gusev, *Doklady Akad. Nauk SSSR*, 1985, **285**, 129.

[158] D.Bright, M.R.Truter, *Nature*, 1970, **225**, 176; *J. Chem. Soc. (B)*, 1970, 1544.

[159] M.Mercer, M.R.Truter, *J. Chem. Soc., Dalton*, 1973, 2215.

[160] P.Seiler, M.Dobler, J.D.Dunitz, *Acta Cryst.*, 1974, **B30**, 2744.

[161] R.B.Dyer, R.G.Ghirardelli, R.A.Palmer, E.M.Holt, *Inorg. Chem.*, 1986, **25**, 3184.

[162] M.A.Bush, M.R.Truter, *J. Chem. Soc., Perkin II*, 1972, 345.

[163] M.Dobler, R.P.Phizackerley, *Acta Cryst.*, 1974, **B30**, 2746.

[164] M.Dobler, R.P.Phizackerley, *Acta Cryst.*, 1974, **B30**, 2748.

[165] P.P.North, E.C.Steiner, F.P.van Remoortere, F.P.Boer, *Acta Cryst.*, 1976, **B32**, 370.

[166] J.D.Dunitz, P.Seiler, *Acta Cryst.*, 1974, **B30**, 2750.

[167] C.R.Paige, M.F.Richardson, *Can. J. Chem.*, 1984, **62**, 332.

[168] Y.Kawasaki, Y.Matsuura, *Chem. Lett.*, 1984, 155.

[169] P.Lu, C.Shen, Y.Fan, S.Jin, S.Zhang, F.Yu, *Fenzi Kexue Yu Huaxue Yanjiu*, 1983, **3**, 77. (*Chem. Abs.*, 1983, **99**, 46322d).

[170] J.D.J.Backer-Dirks, J.E.Cooke, A.M.R.Galas, J.S.Ghotra, C.J.Gray, F.A.Hart, M.B.Hursthouse, *J. Chem. Soc., Dalton*, 1980, 2191.

[171] M.E.Harman, F.A.Hart, M.B.Hursthouse, G.P.Moss, P.R.Raithby, *J. Chem. Soc., Chem. Commun.*, 1976, 396.

[172] J.-C.G.Bünzli, B.Klein, D.Wessner, N.W.Alcock, *Inorg. Chim. Acta*, 1982, **59**, 269.

[173] J.-C.G.Bünzli, B.Klein, G.Chapuis, K.J.Schenk, *Inorg. Chem.*, 1982, **21**, 808.

[174] J.-C.G.Bünzli, G.A.Leonard, D.Plancherel, G.Chapuis, *Helv. Chim. Acta*, 1986, **69**, 288.

[175] M.Ciampolini, N.Nardi, R.Cini, S.Mangani, P.Orioli, *J. Chem. Soc., Dalton*, 1979, 1983.

[176] N.Armağan, *Acta Cryst.*, 1977, **B33**, 2281.

[177] G.Bombieri, G.De Paoli, A.Cassol, A.Immirzi, *Inorg. Chim. Acta*, 1976, **18**, L23.

[178] R.M.Izatt, J.S.Bradshaw, S.A.Nielsen, J.D.Lamb, J.L.Christensen, D.Sen, *Chem. Rev.*, 1985, **85**, 271.

[179] B.Dietrich, in *"Inclusion Compounds"*, Vol. 2, J.L.Atwood, J.E.D.Davies, D.D.MacNicol eds., 1984, p. 337, Academic Press (London).

[180] B.Dietrich, *J. Chem. Ed.*, 1985, **62**, 954.

[181] J.M.Lehn, *Struct. Bond.*, 1973, **16**, 1.

[182] E.Eyal, G.A.Rechnitz, *Anal. Chem.*, 1971, **43**, 1090.

[183] R.M.Izatt, D.J.Eatough, J.J.Christensen, *Struct. Bond.*, 1973, **16**, 161.

[184] B.K.J.Leong, *Chem. Eng. News*, Jan.27, 1975, 5.

[185] B.K.J.Leong, T.O.T.Ts'o, M.B.Chenoweth, *Toxicol. Appl. Pharmacol.*, 1974, **27**, 342.

[186] A.A.Casselman, H.G.Thompson, R.A.B.Bannard, *Gov. Rep. Announce. Index (U.S.A.)*, 1980, **80**, 1038.

[187] B.O.Strasser, K.Hellenga, A.I.Popov, *J. Am. Chem Soc.*, 1985, **107**, 789.

[188] E.Shchori, J.Jagur-Grodzinski, Z.Luz, M.Shporer, *J. Am. Chem. Soc.*, 1971, **93**, 7133.

[189] E.Shchori, J.Jagur-Grodzinski, M.Shporer, *J. Am. Chem. Soc.*, 1973, **95**, 3842.

[190] B.O.Strasser, A.I.Popov, *J. Am. Chem. Soc.*, 1985, **107**, 7921.

[191] E.Schmidt, A.I.Popov, *J. Am. Chem. Soc.*, 1983, **105**, 1873.

[192] P.B.Chock, *Proc. Natl. Acad. Sci. U.S.A.*, 1972, **69**, 1939.

[193] E.Grell, T.Funk, F.Eggers, in *"Membranes - A Series of Advances"*, Vol. 3, G.Eisenman, ed., 1975, Marcel Dekker (New York).

[194] H.Farber, S.Petrucci, *J. Phys. Chem.*, 1981, **85**, 1396.

[195] C.C.Chen, S.Petrucci, *J. Phys. Chem.*, 1982, **86**, 2601.

[196] K.G.Maynard, D.E.Irish, E.Eyring, S.Petrucci, *J. Phys. Chem.*, 1984, **88**, 729.

[197] W.Wallace, C.Chen, E.Eyring, S.Petrucci, *J. Phys. Chem.*, 1985, **89**, 1357.

[198] C.C.Chen, W.Wallace, E.Eyring, S.Petrucci, *J. Phys. Chem.*, 1984, **88**, 2541.

[199] P.A.Mosier-Boss, A.I.Popov, *J. Am. Chem. Soc.*, 1985, **107**, 6168.

[200] N.Ahmad, M.C.Day, *J. Am. Chem. Soc.*, 1977, **99**, 941.

[201] M.S.Greenberg, A.I.Popov, *Spectrochim. Acta*, 1975, **31A**, 697.

[202] A.Hourdakis, A.I.Popov, *J. Soln. Chem.*, 1977, **6**, 299.

[203] M.Shamsipur, A.I.Popov, *Inorg. Chim. Acta*, 1980, **43**, 243.

[204] E.Mei, A.I.Popov, J.L.Dye, *J. Phys. Chem.*, 1977, **81**, 1677.

[205] R.D.Boss, A.I.Popov, *Inorg. Chem.*, 1986, **25**, 1747.

[206] M.S.Greenberg, R.L.Bodner, A.I.Popov, *J. Phys. Chem.*, 1973, **77**, 2449.

[207] R.H.Erlich, E.Roach, A.I.Popov, *J. Am. Chem. Soc.*, 1970, **92**, 4989.

[208] B.G.Cox, J.Garcias-Rosas, H.Schneider, *J. Am. Chem. Soc.*, 1981, **103**, 1054.

[209] S.F.Lincoln, I.M.Brereton, T.M.Spotswood, (submitted for publication).

[210] G.W.Liesegang, M.M.Farrow, F.A.Vazquez, N.Purdie, E.M.Eyring, *J. Am. Chem. Soc.*, 1977, **99**, 3240.

[211] J.D.Lin, A.I.Popov, *J. Am. Chem. Soc.*, 1981, **103**, 3773.

[212] H.K.Frensdorff, *J. Am. Chem. Soc.*, 1971, **93**, 600.

[213] R.M.Izatt, R.E.Terry, B.L.Haymore, L.D.Hansen, N.K.Dalley, A.G.Avondet, J.J.Christensen, *J. Am. Chem. Soc.*, 1976, **98**, 7620.

[214] B.G.Cox, H.Schneider, J.Stroka, *J. Am. Chem. Soc.*, 1978, **100**, 4746.

[215] J.M.Ceraso, P.B.Smith, J.S.Landers, J.L.Dye, *J. Phys. Chem.*, 1977, **81**, 760.

[216] B.G.Cox, I.Schneider, H.Schneider, *Ber. Bunsenges. Phys. Chem.*, 1980, **84**, 470.

[217] J.M.Lehn, J.P.Sauvage, *J. Am. Chem. Soc.*, 1975, **97**, 6700.

[218] A.J.Smetana, A.I.Popov, *J. Soln. Chem.*, 1980, **9**, 183.

[219] G.W.Gokel, D.J.Cram, C.L.Liotta, H.P.Harris, F.L.Cook, *J. Org. Chem.*, 1974, **39**, 2445.

[220] D.D.Perrin, W.L.F.Aramaego, D.R.Perrin, *"Purification of Laboratory Chemicals"*, 2nd. ed., 1980, Pergammon (Oxford).

[221] P.W.N.M. van Leeuwen, W.L.Groeneveld, *Inorg. Nucl. Chem. Lett.*, 1967, **3**, 145.

[222] J.T.Bell, R.E.Biggers, *J. Molec. Spect.*, 1965, **18**, 247.

[223] H.D.Burrows, T.J.Kemp, *Chem. Soc. Rev.*, 1974, **3**, 139.

[224] A.I.Vogel, J.Bassett, R.C.Denney, G.H.Jeffery, J.Mendham, in *"A Textbook of Quantitative Inorganic Analysis"*, 4th. ed., 1978, p.165, Longman Group Ltd. (London).

[225] B.J.Hathaway, A.E.Underhill, *J. Chem. Soc.*, **1961**, 3091.

[226] J.Crea, *Doctoral Thesis*, 1976, University of Adelaide.

[227] D.S.Raiford, C.L.Fisk, E.D.Becker, *Anal. Chem.*, 1979, **51**, 2050.

[228] A.L.Van Geet, *Anal. Chem.*, 1970, **42**, 679; *Anal. Chem.*, 1968, **40**, 2227.

[229] F.Bloch, *Phys. Rev.*, 1946, **70**, 460.

[230] S.F.Lincoln, *Prog. React. Kinetics*, 1977, **9**, 1.

[231] H.S.Gutowsky, D.M.McCall, C.P.Slichter, *J. Chem. Phys.*, 1953, **21**, 279.

[232] A.Abragam, *"The Principles of Nuclear Magnetism"*, 1961, Oxford University Press (New York).

[233] H.S.Gutowsky, C.H.Holm, *J. Chem. Phys.*, 1956, **25**, 1228.

[234] H.M.McConnell, *J. Chem. Phys.*, 1958, **28**, 430.

[235] C.S.Johnson, *Adv. Magn. Reson.*, 1965, **1**, 33.

[236] C.S.Johnson, C.G.Moreland, *J. Chem. Ed.*, 1973, **50**, 477.

[237] R.Kubo, *J. Phys. Soc. Jpn.*, 1954, **9**, 935.

[238] R.Kubo, K.Tomita, *J. Phys. Soc. Jpn.*, 1954, **9**, 888.

[239] R.A.Sack, *J. Chem. Phys.*, 1953, **21**, 1688.

[240] E.L.Hahn, D.E.Maxwell, *Phys. Rev.*, 1952, **88**, 1070.

[241] H.M.McConnell, *J. Chem. Phys.*, 1958, **28**, 430.

[242] H.S.Gutowsky, A.Saika, *J. Chem. Phys.*, 1953, **21**, 1688.

[243] M.T.Rodgers, J.C.Woodbrey, *J. Phys. Chem.*, 1962, **66**, 540.

[244] I.O.Sutherland, *Ann. Rep. NMR Spect.*, 1971, **4**, 71.

[245] R.K.Gupta, T.P.Pitner, R.Wasyrishen, *J. Magn. Reson.*, 1974, **13**, 383.

[246] J.I.Kaplan, *J. Chem. Phys.*, 1972, **57**, 5615.

[247] R.R.Ernst, *J. Chem. Phys.*, 1973, **59**, 989.

[248] J.I.Kaplan, *J. Chem. Phys.*, 1973, **59**, 990.

[249] T.C.Farrer, E.D.Becker, *"Pulse and Fourier Transform NMR"*, 1971, Academic Press (New York).

[250] T.Nakagawa, *Bull. Chem. Soc. Jpn.*, 1966, **39**, 1006.

[251] T.H.Siddall III, W.E.Stewart, F.D.Knight, *J. Phys. Chem.*, 1970, **74**, 3580.

[252] E.H.Williams, *Doctoral Thesis*, 1980, University of Adelaide.

[253] W.F.K.Wynne-Jones, H.Eyring, *J. Chem. Phys.*, 1935, **3**, 492.

[254] S.Glasstone, K.J.Laidler, H.Eyring in *"Theory of Rate Processes"*, 1941, McGraw-Hill (New York).

[255] D.L.Pisaniello, S.F.Lincoln, T.Kurucsev, *Aust. J. Chem.*, 1982, **35**, 839.

[256] T.Kurucsev, unpublished material.

[257] J.Pitha, R.N.Jones, *Can. J. Chem.*, 1966, 44, 3031.